



ATLAS Note

ATL-COM-PHYS-2019-962

11th April 2021



Draft version 0.1

1

2 WZ + Heavy Flavor Production in pp collisions 3 at $\sqrt{s} = 13$ TeV

4 The ATLAS Collaboration¹, Aaron Webb^a, Peter Onyisi^a, Heather
5 Russell^b, Philip Sommer^c

6 ^a*Univ. of Texas at Austin*

7 ^b*McGill University*

8 ^c*Univ. of Sheffield*

9 A measurement of WZ produced with an associated heavy flavor jet is performed using 140
10 fb^{-1} of proton-proton collision data at $\sqrt{s} = 13 \text{ TeV}$ from the ATLAS experiment at the
11 LHC. The measurement is performed in the fully leptonic decay mode, $\text{WZ} \rightarrow \ell\nu\ell\bar{\nu}$. The
12 cross-section of $\text{WZ} + \text{b-jets}$ is measured to be $X \pm X \pm X$, while the cross-section of $\text{WZ} +$
13 charm is measured as X , with a correlation of X between the two processes.

© 2021 CERN for the benefit of the ATLAS Collaboration.
14 Reproduction of this article or parts of it is allowed as specified in the CC-BY-4.0 license.

15 **Contents**

16	1 Changes and outstanding items	5
17	1.1 Changelog	5
18	1.1.1 Changes relative to v7	5
19	1.1.2 Changes relative to v5	5
20	1.1.3 Changes relative to v4	6
21	1.1.4 Changes relative to v3	6
22	1.1.5 Changes relative to v2	7
23	1.1.6 Changes relative to v1	7
24	1.2 Outstanding Items	7
25	2 Executive Summary	8
26	3 Data and Monte Carlo Samples	9
27	3.1 Data Samples	9
28	3.2 Monte Carlo Samples	10
29	4 Object Reconstruction	11
30	4.1 Trigger	11
31	4.2 Light leptons	12
32	4.3 Jets	13
33	4.4 B-tagged Jets	13
34	4.5 Missing transverse energy	14
35	4.6 Overlap removal	14
36	5 Event Selection and Signal Region Definitions	15
37	5.1 Event Preselection	15
38	5.2 Fit Regions	19
39	5.3 Non-Prompt Lepton Estimation	35
40	5.3.1 $t\bar{t}$ Validation	35
41	5.3.2 Z+jets Validation	38
42	6 tZ Separation Multivariate Analysis	42
43	6.1 Top Mass Reconstruction	43
44	6.2 tZ BDT	43
45	7 Systematic Uncertainties	47
46	8 Results	54
47	8.1 Fit Procedure	54
48	8.2 Independent 1-jet and 2-jet Results	56
49	9 Conclusion	66

50	A Appendices	69
----	---------------------	-----------

51	Appendices	69
52	A.1 Non-prompt lepton MVA	69
53	A.2 Non-prompt CR Modelling	70
54	A.3 tZ Interference Studies	74
55	A.4 Inclusive 1+2 Jet Cross Check	77
56	A.5 Alternate tZ Inclusive Fit	80
57	A.5.1 tZ Inclusive Fit	80
58	A.5.2 Floating tZ	80
59	A.6 DSID list	81

60 List of contributions

Aaron Webb	Main analyser. Responsible for ntuple production, fits, and note writing.
Peter Onyisi	Advisor to Aaron Webb. Analysis design and implementation strategy.
Heather Russell	EWK group convener. Note editing, developing analysis strategy.
Philip Sommer	EWK group convener. Note editing, developing analysis strategy.

63 **1 Changes and outstanding items**

64 **1.1 Changelog**

65 This is version 8

66 **1.1.1 Changes relative to v7**

- 67 • Moved from LO to NLO tZ sample
- 68 • Add additional plots of Z+jets and ttbar CRs in Section A.2
- 69 • Clarified CDI file used, MC ptag, PFlow jet algorithm
- 70 • Included overlap removal procedure
- 71 • Included details on PLV
- 72 • Added plots of missing tZ BDT input features for each fit region
- 73 • Changed reference on PLV to recent ttH/ttW note
- 74 • Included alternate fits with WZ+1-2 jet inclusive, tZ floating

75 **1.1.2 Changes relative to v5**

- 76 • added list of DSIDs to an appendix
- 77 • included systematics on jet migrations
- 78 • Updated results section to include simultaneous fit over 1-jet and 2-jet bins, describe
- 79 • unfolding procedure
- 80 • Updated other sections to account for this change
- 81 • Included info about migrations in Section 5.2

82 **1.1.3 Changes relative to v4**

- 83 • Fixed various typos, clarified wording
 84 • Expanded info about JER uncertainties, electron systematics, theory uncertainties
 85 • removed a table on lepton selection, included information in the text instead
 86 • Plotted lepton Pt Z and W for Zjet CR, rather than lep 1 and 2
 87 • fixed binning in kinematic plots
 88 • Included prefit and postfit yield tables
 89 • added signal modelling systematics
 90 • included alternate fit studies with tZ included in signal

91 **1.1.4 Changes relative to v3**

- 92 • Merged introduction into executive summary, including unblinding details and list of
 93 SRs/CRs used
 94 • listed ptag used (p4133), and release (AB 21.2.127)
 95 • Included table reftab:xsecUnc listing x-sec uncertainties used
 96 • Removed selection criteria listed in table ?? (QMisID, AmbiguityType) that were removed
 97 from the analysis
 98 • specified variable used to make truth jet flavor determination (HadronConeExclTruthLa-
 99 belIID)
 100 • fixed bug in MtLepMet calculation, updated selection/fits to account for this
 101 • Included plots of MtLepMet and PtZ, swapped lep 1 and 2 p_T plots for lep W and lep Z
 102 plots
 103 • updated tZ BDT training to reduce overfitting, updated plots to include error bars, feature
 104 importance
 105 • updated table 8 to clarify selection, fix the tZ_BDT cut used
 106 • replace a few broken ntuples which included large weight events
 107 • include DL1r distribution for Z+jets and t \bar{t} VRs
 108 • Expanded section on fakes, included information on derived scale factors from VRs.
 109 • Changed the kinematic plots to include $p_T(Z)$ and $m_T(W)$, list lepton p_T based on W and
 110 Z candidates.

111 1.1.5 Changes relative to v2

- 112 • Added alternate VBS samples to include missing b-jet diagrams
113 • Included a section on tZ interference effects, ??.
114 • Updated to reflect changes for 2018, including the move to PFlow jets, DL1r, updated
115 trigger, and updated AnalysisBase version (now 21.2.127)
116 • Revised fit regions, using separate 1-jet and 2-jet fits, with all 2-j regions included
117 • updated plots for tZ BDT, added details about the model
118 • Included truth jet information

119 1.1.6 Changes relative to v1

- 120 • Added GRL list
121 • Fixed latex issue in line 92, typo in line 172
122 • Added tables 6 and ??, summarizing the event and object selection
123 • Added table 2, which includes the DSID of samples used
124 • Included reference to WZ inclusive paper in introduction

125 1.2 Outstanding Items

- 126 • Complete interference studies, apply any interference effects observed as a systematic
127 • Update results section with additional studies, possibly including:
128 – Truth jet migration studies
129 – Simultaneous fit over 1j and 2j
130 – Impact of allowing tZ to float
131 • Unblind, update plots and fits to include data
132 • Add cross-section, significance once unblinded

133 2 Executive Summary

134 The production of WZ in association with a heavy flavor jet represents an important background
 135 for many major analyses. This includes any process with leptons and b-jets in the final state,
 136 such as $t\bar{t}H$, $t\bar{t}W$, and $t\bar{t}Z$. While precise measurements have been made of WZ production
 137 [1], $WZ +$ heavy flavor remains poorly understood. This is largely because the QCD processes
 138 involved in the production of the b-jet make it difficult to simulate accurately. This introduces a
 139 large uncertainty for analyses that include this process as a background.

140 Motivated by its relevance to the $t\bar{t}H$ multilepton analysis, we perform a study of the fully
 141 leptonic decay mode of this channel; that is, events where both the W and Z decay leptonically.
 142 Because WZ has no associated jets at leading order, while the major backgrounds for this channel
 143 tend to have high jet multiplicity, events with more than two jets are rejected. This gives a final
 144 state signature of three leptons and one or two jets.

145 Events that meet this selection criteria are sorted into pseudo-continuous b-tagging regions based
 146 on the DL1r b-tag score of their associated jets. This is done to separate $WZ +$ b-jet events from
 147 $WZ +$ charm and $WZ +$ light jets. These regions are fit to data in order make a more accurate
 148 estimate of the contribution of $WZ +$ heavy-flavor, where heavy-flavor jets include b-jets and
 149 charm jets. The full Run-2 dataset collected by the ATLAS detector, representing 139 fb^{-1} of
 150 data from pp collisions at $\sqrt{s} = 13 \text{ TeV}$, is used for this study.

151 All backgrounds are accounted for using Monte Carlo, with the simulation of non-prompt lepton
 152 backgrounds - $Z+jets$ and $t\bar{t}$ - validated using non-prompt Validation Regions.

153 Section 3 details the data and Monte Carlo (MC) samples used in the analysis. The reconstruction
 154 of various physics objects is described in section 4. Section 5 describes the event selection applied
 155 to these samples, along the definitions of the various regions used in the fit. The multivariate
 156 analysis techniques used to separate the tZ background from $WZ +$ heavy flavor are described in
 157 section 6. Section 7 describes the various sources of systematic uncertainties considered in the
 158 fit. Finally, the results of the analysis are summarized in section 8, followed by a brief conclusion
 159 in section 9.

160 The analysis aims to report a cross-section measurement of $WZ+b$ and $WZ+charm$, along with
 161 their correlations, for both 1-jet and 2-jet exclusive regions. The proposed fiducial region for
 162 these measurements includes events with three leptons, where the invariant mass of at least one
 163 opposite charge, same flavor lepton pair falls within 10 GeV of 91.2 GeV , with 1 or 2 associated
 164 jets. An alternate version of the measurement is included in the appendix, which considers tZ as
 165 part of the $WZ+b$ signal.

166 The current state of the analysis shows blinded results for the full Run 2 dataset. Regions
 167 containing $>5\%$ $WZ+b$ events are blinded, and results are from Asimov, MC only fits. Expected
 168 significance and cross-section numbers are reported.

169 3 Data and Monte Carlo Samples

170 Both data and Monte Carlo samples used in this analysis were prepared in the `xAOD` format,
 171 which was used to produce a `DxAOD` sample in the `HIGG8D1` derivation framework. The `HIGG8D1`
 172 framework is designed for the $t\bar{t}H$ multi-lepton analysis, which targets events with multiple
 173 leptons as well as tau hadrons. This framework skims the dataset to remove unneeded variables
 174 as well as entire events. Events are removed from the derivations that do not meet the following
 175 selection:

- 176 • at least two light leptons within a range $|\eta| < 2.6$, with leading lepton $p_T > 15$ GeV and
 177 subleading lepton $p_T > 5$ GeV
- 178 • at least one light lepton with $p_T > 15$ GeV within a range $|\eta| < 2.6$, and at least two hadronic
 179 taus with $p_T > 15$ GeV.

180 Samples were then generated from these `HIGG8D1` derivations with `p-tag` of `p4134` for data
 181 and `p4133` for Monte Carlo using `AnalysisBase` version 21.2.127 modified to include custom
 182 variables.

183 3.1 Data Samples

184 The study uses a sample of proton-proton collision data collected by the ATLAS detector from
 185 2015 through 2018 at an energy of $\sqrt{s} = 13$ TeV, which represents an integrated luminosity of
 186 139 fb^{-1} . This data set was collected with a bunch crossing rate of 25 ns. All data used in this
 187 analysis was verified by data quality checks, having been included in the following Good Run
 188 Lists:

- 189 • `data15_13TeV.periodAllYear_DetStatus-v79-repro20-02_DQDefects-00-02-02`
 190 `_PHYS_StandardGRL_All_Good_25ns.xml`
- 191 • `data16_13TeV.periodAllYear_DetStatus-v88-pro20-21_DQDefects-00-02-04`
 192 `_PHYS_StandardGRL_All_Good_25ns.xml`
- 193 • `data17_13TeV.periodAllYear_DetStatus-v97-pro21-13_Unknown_PHYS_StandardGRL`
 194 `_All_Good_25ns_Triggerno17e33prim.xml`
- 195 • `data18_13TeV.periodAllYear_DetStatus-v102-pro22-04_Unknown_PHYS_StandardGRL`
 196 `_All_Good_25ns_Triggerno17e33prim.xml`

197 Runs included from the `AllYear` period containers are included.

198 3.2 Monte Carlo Samples

199 Several different generators were used to produce Monte Carlo simulations of the signal and
 200 background processes. For all samples, the response of the ATLAS detector is simulated using
 201 Geant4. The WZ signal samples are simulated using Sherpa 2.2.2 [2]. Specific information
 202 about the Monte Carlo samples being used can be found in Table 1. A list of the specific samples
 203 used by data set ID is shown in Table 2.

Table 1: The configurations used for event generation of signal and background processes, including the event generator, matrix element (ME) order, parton shower algorithm, and parton distribution function (PDF).

Process	Event generator	ME order	Parton Shower	PDF
WZ, VV	SHERPA 2.2.2	MEPS NLO	SHERPA	CT10
tZ	MG5_AMC	NLO	PYTHIA 8	CTEQ6L1
t̄W	MG5_AMC (SHERPA 2.1.1)	NLO (LO multileg)	PYTHIA 8 (SHERPA)	NNPDF 3.0 NLO (NNPDF 3.0 NLO)
t̄t(Z/γ* → ll)	MG5_AMC	NLO	PYTHIA 8	NNPDF 3.0 NLO
t̄tH	MG5_AMC (MG5_AMC)	NLO (NLO)	PYTHIA 8 (HERWIG++)	NNPDF 3.0 NLO [3] (CT10 [4])
tHqb	MG5_AMC	LO	PYTHIA 8	CT10
tHW	MG5_AMC (SHERPA 2.1.1)	NLO (LO multileg)	HERWIG++ (SHERPA)	CT10 (NNPDF 3.0 NLO)
tWZ	MG5_AMC	NLO	PYTHIA 8	NNPDF 2.3 LO
t̄t̄t, t̄t̄t̄t̄	MG5_AMC	LO	PYTHIA 8	NNPDF 2.3 LO
t̄tW+W-	MG5_AMC	LO	PYTHIA 8	NNPDF 2.3 LO
t̄t	POWHEG-BOX v2 [5]	NLO	PYTHIA 8	NNPDF 3.0 NLO
t̄t̄γ	MG5_AMC	LO	PYTHIA 8	NNPDF 2.3 LO
s-, t-channel, Wt single top	POWHEG-BOX v1 [6]	NLO	PYTHIA 6	CT10
qqVV, VVV				
Z → l+l-	SHERPA 2.2.1	MEPS NLO	SHERPA	NNPDF 3.0 NLO

Sample	DSID
WZ	364253, 364739-42
VV	364250, 364254, 364255, 363355-60, 364890
t̄W	410155
t̄Z	410156, 410157, 410218-20
low mass t̄Z	410276-8
Rare Top	410397, 410398, 410399
single Top	410658-9, 410644-5
three Top	304014
four Top	410080
t̄WW	410081
Z + jets	364100-41
low mass Z + jets	364198-215
W + jets	364156-97
Vγ	364500-35
tZ	412063
tW	410013-4
WtZ	410408
VVV	364242-9
VH	342284-5
WtH	341998
t̄tγ	410389
t̄t	410470
t̄tH	345873-5, 346343-5

Table 2: List of Monte Carlo samples by data set ID used in the analysis.

204 4 Object Reconstruction

205 All regions defined in this analysis share a common lepton, jet, and overall event preselection.
 206 The selection applied to each physics object is detailed here; the event preselection, and the
 207 selection used to define the various fit regions, is described in Section 5.

208 4.1 Trigger

209 Events are required to be selected by dilepton triggers, as summarized in Table 3.

Dilepton triggers (2015)	
$\mu\mu$ (asymm.)	HLT_mu18_mu8noL1
ee (symm.)	HLT_2e12_lhloose_L12EM10VH
$e\mu, \mu e$ (\sim symm.)	HLT_e17_lhloose_mu14
Dilepton triggers (2016)	
$\mu\mu$ (asymm.)	HLT_mu22_mu8noL1
ee (symm.)	HLT_2e17_lhvloose_nod0
$e\mu, \mu e$ (\sim symm.)	HLT_e17_lhloose_nod0_mu14
Dilepton triggers (2017)	
$\mu\mu$ (asymm.)	HLT_mu22_mu8noL1
ee (symm.)	HLT_2e24_lhvloose_nod0
$e\mu, \mu e$ (\sim symm.)	HLT_e17_lhloose_nod0_mu14
Dilepton triggers (2018)	
$\mu\mu$ (asymm.)	HLT_mu22_mu8noL1
ee (symm.)	HLT_2e24_lhvloose_nod0
$e\mu, \mu e$ (\sim symm.)	HLT_e17_lhloose_nod0_mu14

Table 3: List of lowest p_T -threshold, un-prescaled dilepton triggers used for 2015–2018 data taking.

210 **4.2 Light leptons**

- 211 Electron candidates are reconstructed from energy clusters in the electromagnetic calorimeter
 212 that are associated with charged particle tracks reconstructed in the inner detector [7]. Electron
 213 candidates are required to have $p_T > 10$ GeV and $|\eta_{\text{cluster}}| < 2.47$. Muon candidates are
 214 reconstructed by combining inner detector tracks with track segments or full tracks in the muon
 215 spectrometer [8]. Muon candidates are required to have $p_T > 10$ GeV and $|\eta| < 2.5$. Candidates
 216 in the transition region between different electromagnetic calorimeter components, $1.37 <$
 217 $|\eta_{\text{cluster}}| < 1.52$, are rejected. A multivariate likelihood discriminant combining shower shape
 218 and track information is used to distinguish real electrons from hadronic showers (fake electrons).
 219 To further reduce the non-prompt electron contribution, the track is required to be consistent
 220 with originating from the primary vertex; requirements are imposed on the transverse impact
 221 parameter significance ($|d_0|/\sigma_{d_0} < 5$) and the longitudinal impact parameter ($|\Delta z_0 \sin \theta_\ell| < 0.5$
 222 mm).
- 223 Muon candidates are reconstructed by combining inner detector tracks with track segments or
 224 full tracks in the muon spectrometer [8]. Muon candidates are required to have $p_T > 10$ GeV
 225 and $|\eta| < 2.5$. The longitudinal impact parameter is the same for both electrons and muons, while
 226 muons are required to pass a slightly tighter transverse impact parameter, $|d_0|/\sigma_{d_0} < 3$.

227 All leptons are required to be isolated, as defined through the standard PLVLoose working point
 228 supported by combined performance groups. Leptons are additionally required to pass a non-
 229 prompt BDT selection developed by the $t\bar{t}H$ multilepton/ $t\bar{t}W$ analysis group. This BDT is
 230 described in detail in [9]. Optimized working points and scale factors for this BDT are taken
 231 from that analysis.

232 4.3 Jets

233 Jets are reconstructed from calibrated topological clusters built from energy deposits in the
 234 calorimeters [10], using the anti- k_t algorithm with a radius parameter $R = 0.4$. Particle Flow,
 235 or PFlow, jets are used in the analysis. Jets with energy contributions likely arising from noise
 236 or detector effects are removed from consideration [11], and only jets satisfying $p_T > 25$ GeV
 237 and $|\eta| < 2.5$ are used in this analysis. For jets with $p_T < 60$ GeV and $|\eta| < 2.4$, a jet-track
 238 association algorithm is used to confirm that the jet originates from the selected primary vertex,
 239 in order to reject jets arising from pileup collisions [12].

240 4.4 B-tagged Jets

241 In order to make a measurement of $WZ +$ heavy flavor it is necessary to distinguish these events
 242 from $WZ +$ light jets. For this purpose, the DL1r b-tagging algorithm is used to distinguish
 243 heavy flavor jets from lighter ones. The DL1r algorithm uses jet kinematics, particularly jet
 244 vertex information, as input for a neural network which assigns each jet a score designed to
 245 reflect how likely that jet is to have originated from a b-quark.

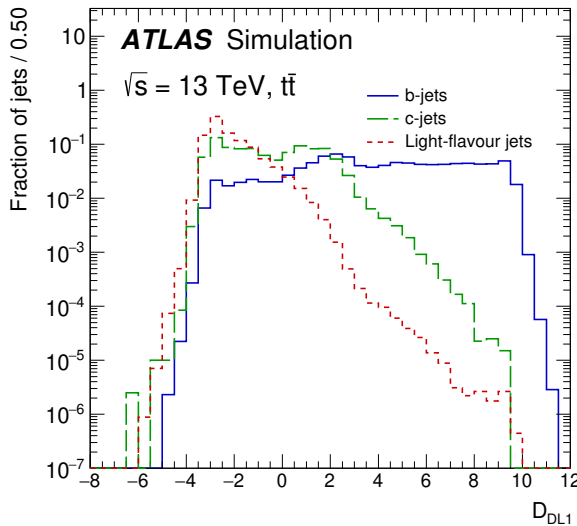


Figure 1: Output distribution of the DL1r algorithm for b-jets, charm jets, and light jets

246 From the output of the BDT, working points (WPs) are developed based on the efficiency of truth
 247 b-jets at particular values of the DL1r algorithm. These WPs are taken from the March 2020 CDI
 248 file, 2020-21-13TeV-MC16-CDI-2020-03-11_v2.root. The working points used in this analysis
 249 are summarized in Table 4.

WP	none	loose	medium	tight	tightest
b eff.	-	85%	77%	70%	60%

Table 4: B-tagging Working Points by tightness and b-jet efficiency

250 A tighter WP will accept fewer b-jets, but reject a higher fraction of charm and light jets.
 251 Generally, analyses that include b-jets will use a fixed working point, for example, requiring that
 252 a jet pass the 70% threshold. By instead treating these working point as bins, e.g. events with
 253 jets that fall between the 85% and 77% WPs fall into one bin, while events with jets passing the
 254 60% WP fall into another, and looking at the full psuedo-continuous DL1r spectrum of the jets,
 255 additional information can be gained. The psuedo-continuous b-tag spectrum is used in this case
 256 to separate out WZ + b, WZ + charm, and WZ + light.

257 4.5 Missing transverse energy

258 Missing transverse momentum (E_T^{miss}) is used as part of the event selection. The missing
 259 transverse momentum vector is defined as the inverse of the sum of the transverse momenta of
 260 all reconstructed physics objects as well as remaining unclustered energy, the latter of which is
 261 estimated from low- p_T tracks associated with the primary vertex but not assigned to a hard object,
 262 with object definitions taken from [13]. Light leptons considered in the E_T^{miss} reconstruction are
 263 required to have $p_T > 10$ GeV, while jets are required to have $p_T > 20$ GeV.

264 4.6 Overlap removal

265 To avoid double counting objects and remove leptons originating from decays of hadrons, overlap
 266 removal is performed in the following order: any electron candidate within $\Delta R = 0.1$ of another
 267 electron candidate with higher p_T is removed; any electron candidate within $\Delta R = 0.1$ of a muon
 268 candidate is removed; any jet within $\Delta R = 0.3$ of an electron candidate is removed; if a muon
 269 candidate and a jet lie within $\Delta R = \min(0.4, 0.04 + 10[\text{GeV}] / p_T(\text{muon}))$ of each other, the jet
 270 is kept and the muon is removed.

271 This algorithm is applied to the preselected objects. The overlap removal procedure is summarized
 272 in Table 5.

Keep	Remove	Cone size (ΔR)
electron	electron (low p_T)	0.1
muon	electron	0.1
electron	jet	0.3
jet	muon	$\min(0.4, 0.04 + 10[\text{GeV}]/p_T \text{ (muon)})$
electron	tau	0.2

Table 5: Summary of the overlap removal procedure between electrons, muons, and jets.

273 5 Event Selection and Signal Region Definitions

274 Event are required to pass a preselection described in Section 5.1 and summarized in Table 6.
 275 Those that pass this preselection are divided into various fit regions described in Section 5.2,
 276 based on the number of jets in the event, and the b-tag score of those jets.

277 **5.1 Event Preselection**

278 Events are required to include exactly three reconstructed light leptons passing the requirement
 279 described in 4.2, which have a total charge of ± 1 . As the opposite sign lepton is found to be
 280 prompt the vast majority of the time [14], it is required to be loose and isolated, as defined though
 281 the standard PLVLoose working point supported by combined performance groups. The same
 282 sign leptons are required to be very tightly isolated, as per the recommended PLVTight.

283 The leptons are ordered in the analysis code as 0, 1, and 2. Lepton 0 is the lepton whose charge
 284 is opposite the other two. Lepton 1 is the lepton closest to the opposite charge lepton, i.e. the
 285 smallest ΔR , leaving lepton 2 as the lepton further from the opposite charge lepton. Lepton 0
 286 is required to have $p_T > 10$ GeV, while the same sign leptons, 1 and 2, are required to have
 287 $p_T > 20$ GeV to reduce the contribution of non-prompt leptons.

288 The invariant mass of at least one pair of opposite sign, same flavor leptons is required to fall
 289 within 10 GeV of the mass of the Z boson, 91.2 GeV. Events where one of the opposite sign pairs
 290 have an invariant mass less than 12 GeV are rejected in order to suppress low mass resonances.

291 An additional requirement is placed on the missing transverse energy, $E_T^{\text{miss}} > 20$ GeV, and the
 292 transverse mass of the W candidate, $m(E_T^{\text{miss}} + l_{\text{other}}) > 30$ GeV, where E_T^{miss} is the missing
 293 transverse energy, and l_{other} is the lepton not included in the Z-candidate.

294 Events are required to have one or two reconstructed jets passing the selection described in
 295 Section 4.3. Events with more than two jets are rejected in order to reduce the contribution of
 296 backgrounds such as $t\bar{t}Z$ and $t\bar{t}W$, which tend to have higher jet multiplicity.

Event Selection
Exactly three leptons with charge ± 1
Two tight Iso, tight ID same-charge leptons with $p_T > 20 \text{ GeV}$
One loose Iso, medium ID opposite charge lepton with $p_T > 10 \text{ GeV}$
$m(l^+l^-)$ within 10 GeV of 91.2 GeV
Transverse mass of W-candidate, $m_T(E_T^{\text{miss}} + \text{lep}_{\text{other}}) > 30 \text{ GeV}$
Missing transverse energy, $E_T^{\text{miss}} > 20 \text{ GeV}$
One or two jets with $p_T > 25 \text{ GeV}$

Table 6: Summary of the selection applied to events for inclusion in the fit

297 The event yields in the preselection region for both data and Monte Carlo are summarized in
 298 Table 5.1, which shows good agreement between data and Monte Carlo, and demonstrates that
 299 this region consists primarily of WZ events. The WZ events are split into WZ + b, WZ + c, and
 300 WZ + l based on the truth flavor of the associated jet in the event. Specifically, this determination
 301 is made based on the HadronConeExclTruthLabelID of the jet, as recommended by the b-
 302 tagging working group [15]. In this ordering b-jet supersedes charm, which supersedes light. That
 303 is, WZ + l events contain no charm and no b jets at truth level, WZ + c contain at least one truth
 304 charm and no b-jets, and WZ + b contains at least one truth b-jet.

Process	Events
WZ + b	167.6 ± 6.5
WZ + c	1080 ± 40
WZ + l	7220 ± 310
Other VV	850 ± 140
t̄tW	16.8 ± 2.3
t̄tZ	115 ± 17
rare Top	2.2 ± 0.1
Single top	0.10 ± 0.45
Three top	0.01 ± 0.01
Four top	0.02 ± 0.01
t̄tWW	0.23 ± 0.05
Z + jets	600 ± 260
V + γ	37 ± 54
tZ	190 ± 70
tW	5.5 ± 1.2
WtZ	25.8 ± 1.1
VVV	26.2 ± 0.9
VH	94 ± 7
t̄t	108.68 ± 8
t̄tH	4.3 ± 0.5
Total	10600 ± 530
Data	10574

Table 7: Event yields in the preselection region at 139.0 fb^{-1}

305 Here Other VV represents diboson processes other than WZ, and consists predominantly of
 306 $ZZ \rightarrow ll\bar{l}\bar{l}$ events where one of the leptons is not reconstructed.

307 Simulations are further validated by comparing the kinematic distributions of the Monte Carlo
 308 with data, which are shown in Figure 2. Here, bins with 5% or more WZ+b are blinded.

WZ Fit Region - Inclusive

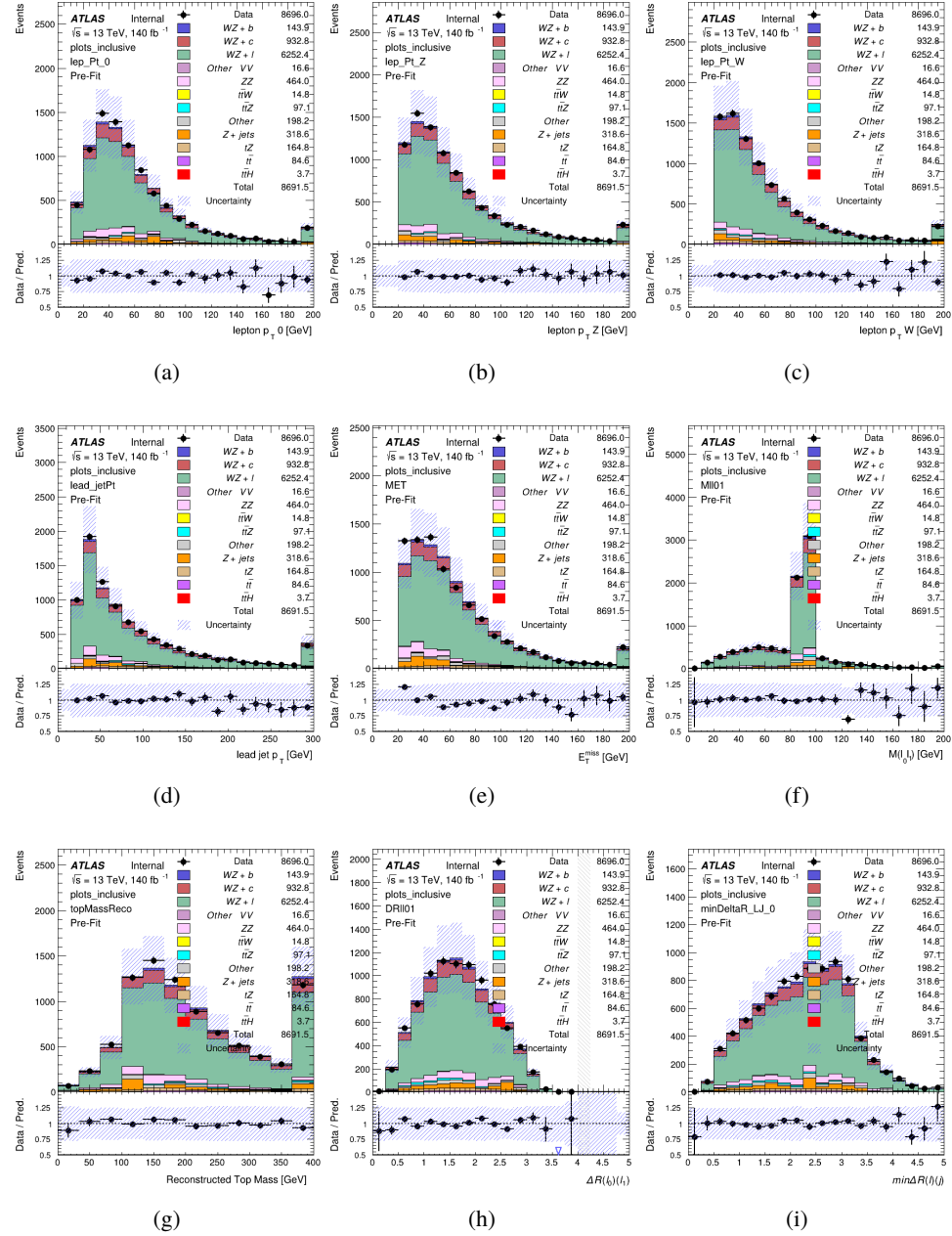


Figure 2: Comparisons between the data and MC distributions in the preselection region for (a) the p_T of the opposite sign lepton, (b) the p_T of the other lepton from the Z candidate, (c) the p_T of the lepton from the W candidate, (d) the leading jet p_T , (e) the E_T^{miss} , and (f) the invariant mass of leptons 0 and 1, (g) the reconstructed top mass, (h) $\Delta(R)$ between lepton 0 and 1, (i) the $\Delta(R)$ between the closest lepton and jet.

³⁰⁹ **5.2 Fit Regions**

³¹⁰ Once preselection has been applied, the remaining events are categorized into one of twelve
³¹¹ orthogonal regions. The regions used in the fit are summarized in Table 8.

Table 8: A list of the regions used in the fit and the selection used for each.

Region	Selection
1j, <85%	$N_{\text{jets}} = 1, n_{\text{Jets_DL1r_85}} = 0$
1j, 85%-77%	$N_{\text{jets}} = 1, n_{\text{Jets_DL1r_85}} = 1, n_{\text{Jets_DL1r_77}} = 0$
1j, 77%-70%	$N_{\text{jets}} = 1, n_{\text{Jets_DL1r_77}} = 1, n_{\text{Jets_DL1r_70}} = 0$
1j, 70%-60%	$N_{\text{jets}} = 1, n_{\text{Jets_DL1r_70}} = 1, n_{\text{Jets_DL1r_60}} = 0$
1j, >60%	$N_{\text{jets}} = 1, n_{\text{Jets_DL1r_60}} = 1, tZ \text{ BDT} > 0.725$
1j tZ CR	$N_{\text{jets}} = 1, n_{\text{Jets_DL1r_60}} = 1, tZ \text{ BDT} < 0.725$
2j, <85%	$N_{\text{jets}} = 2, n_{\text{Jets_DL1r_85}} = 0$
2j, 85%-77%	$N_{\text{jets}} = 2, n_{\text{Jets_DL1r_85}} \geq 1, n_{\text{Jets_DL1r_77}} = 0$
2j, 77%-70%	$N_{\text{jets}} = 2, n_{\text{Jets_DL1r_77}} \geq 1, n_{\text{Jets_DL1r_70}} = 0$
2j, 70%-60%	$N_{\text{jets}} = 2, n_{\text{Jets_DL1r_70}} \geq 1, n_{\text{Jets_DL1r_60}} = 0$
2j, >60%	$N_{\text{jets}} = 2, n_{\text{Jets_DL1r_60}} \geq 1, tZ \text{ BDT} > 0.725$
2j tZ CR	$N_{\text{jets}} = 2, n_{\text{Jets_DL1r_60}} \geq 1, tZ \text{ BDT} < 0.725$

³¹² The working points discussed in Section 4.4 are used to separate events into fit regions based on
³¹³ the highest working point reached by a jet in each event. Because the background composition
³¹⁴ differs significantly based on the number of b-jets, events are further subdivided into 1-jet and
³¹⁵ 2-jet regions in order to minimize the impact of background uncertainties.

³¹⁶ An unfolding procedure is performed to account for differences in the number of reconstructed
³¹⁷ jets compared to the number of truth jets in each event. The `AntiKt4TruthDressedWZJets`
³¹⁸ truth jet collection is used to make this determination. In order to account for migration of
³¹⁹ WZ+1-jet and WZ+2-jet events between the 1-jet and 2-jet bins at reco level, the signal samples
³²⁰ are separated based on the number of truth jets. Events with 0 jets or more than 3 jets at truth
³²¹ level, yet fall within one of the categories listed in Table 8, are categorized as WZ + other, and
³²² treated as a background. The migration matrix in the number of jets at truth level versus reco
³²³ level is shown in Figure 3. The composition of the number of truth jets in each reco jet bin is
³²⁴ taken from MC, with uncertainties in these estimates described in detail in Section 7.

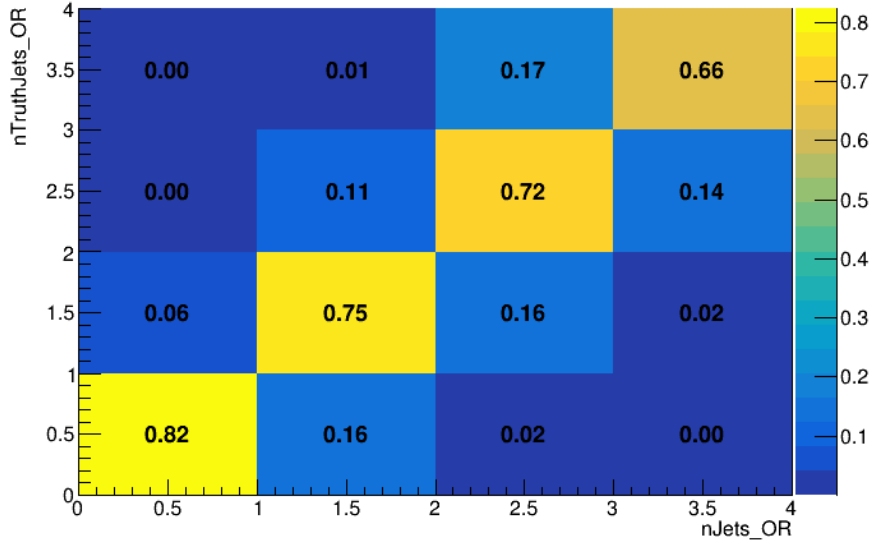


Figure 3: Number of truth jets compared to the number of reconstructed jets in each WZ event falling in the preselection region. Each row is normalized to unity.

325 An additional tZ control region is created based on the BDT described in Section 6. The region
 326 with 1-jet passing the 60% working point is split in two - a signal enriched region of events with
 327 a BDT score greater than 0.03, and a tZ control region including events with less than 0.03. This
 328 cutoff is arrived at by performing an Asimov fit with a variety of cutoffs, and selecting the value
 329 that produces the highest significance for the measurement of WZ + b.

330 The modeling in each region is validated by comparing data and MC predictions for various
 331 kinematic distributions. These plot are shown in Figures 4-17.

WZ Fit Region - 1j Inclusive

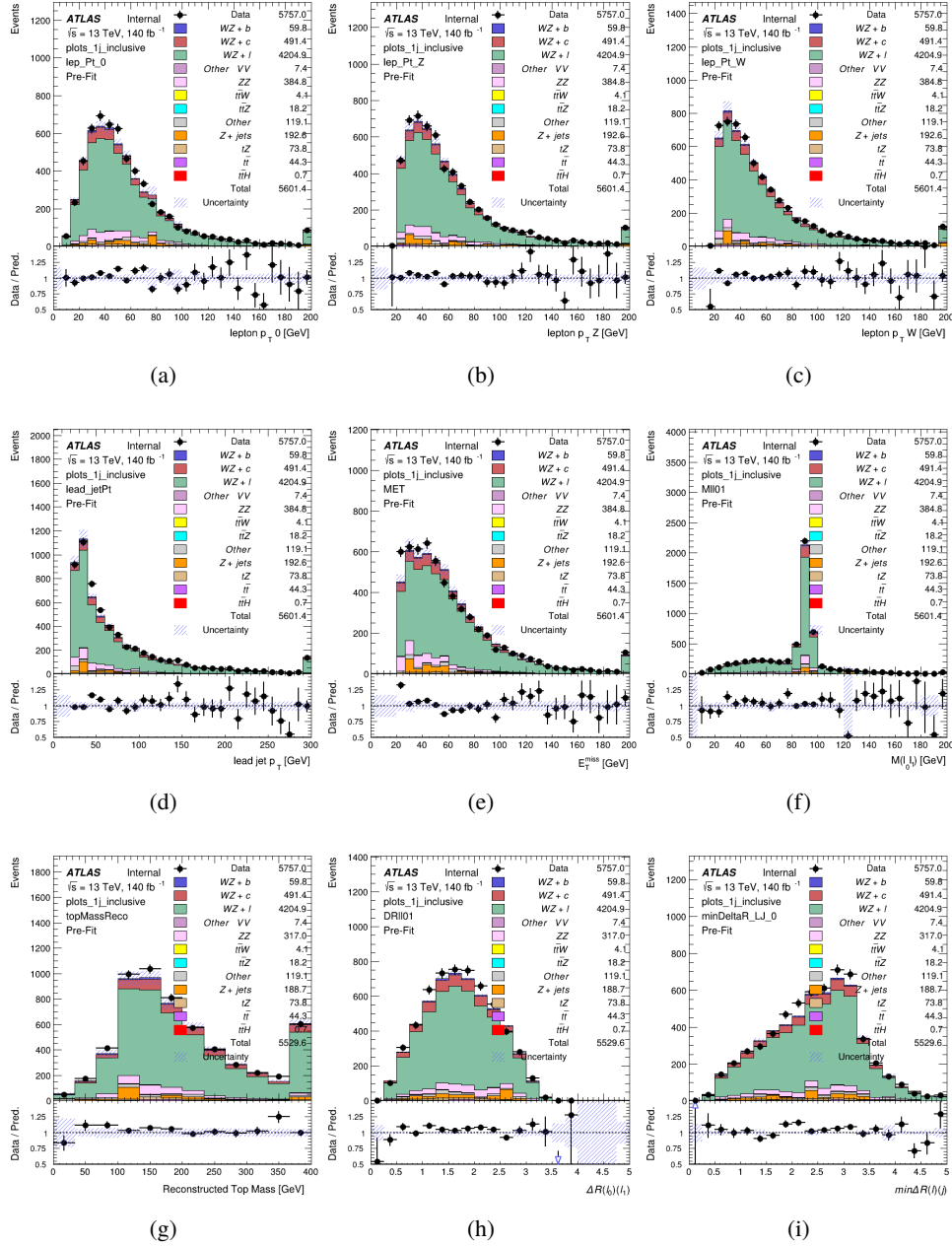


Figure 4: Comparisons between the data and MC distributions in the preselection region for (a) the p_T of the opposite sign lepton, (b) the p_T of the other lepton from the Z candidate, (c) the p_T of the lepton from the W candidate, (d) the leading jet p_T , (e) the E_T^{miss} , and (f) the invariant mass of leptons 0 and 1, (g) the reconstructed top mass, (h) $\Delta(R)$ between lepton 0 and 1, (i) the $\Delta(R)$ between the closest lepton and jet.

WZ Fit Region - 1j < 85% WP

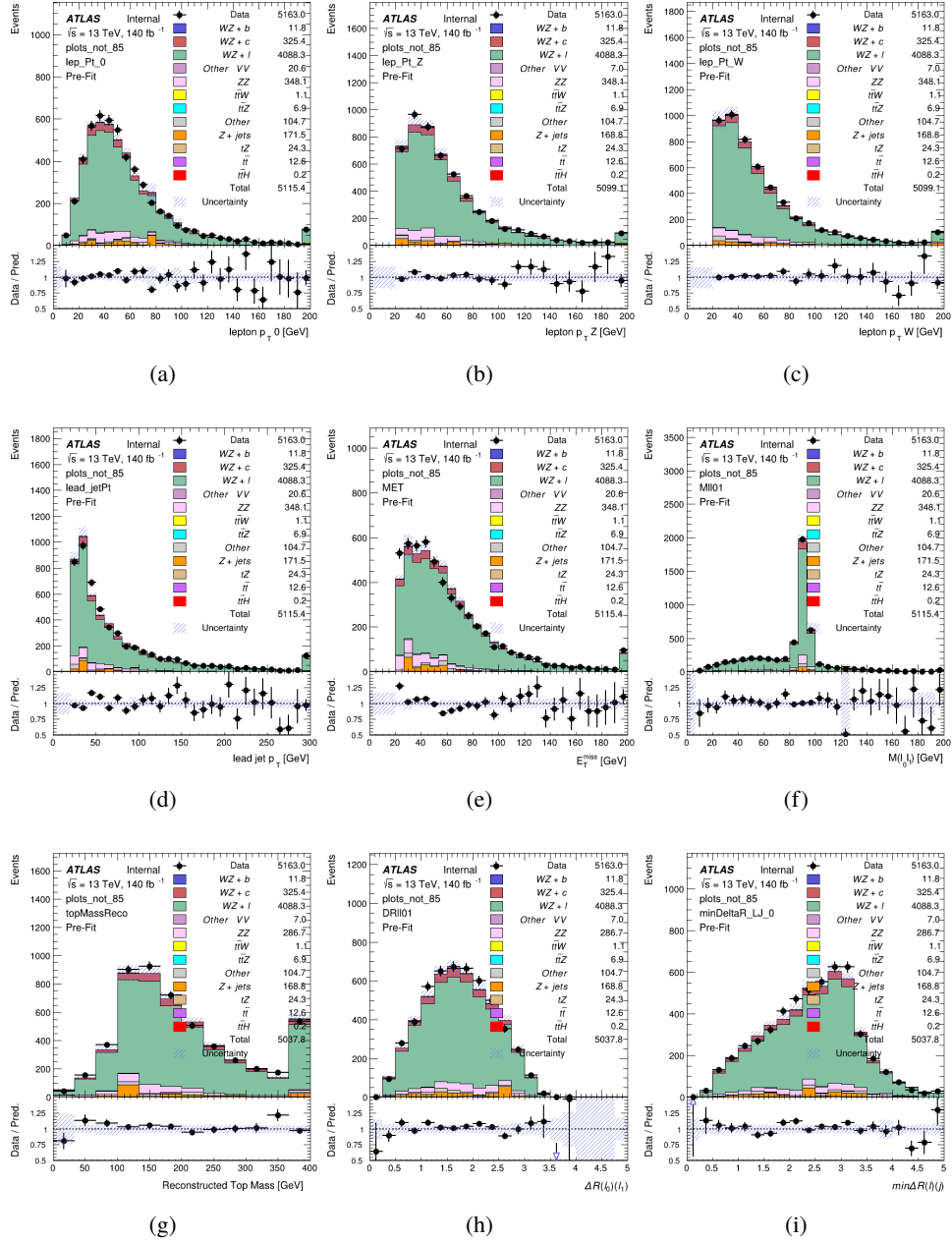


Figure 5: Comparisons between the data and MC distributions in the preselection region for (a) the p_T of the opposite sign lepton, (b) the p_T of the other lepton from the Z candidate, (c) the p_T of the lepton from the W candidate, (d) the leading jet p_T , (e) the E_T^{miss} , and (f) the invariant mass of leptons 0 and 1, (g) the reconstructed top mass, (h) $\Delta(R)$ between lepton 0 and 1, (i) the $\Delta(R)$ between the closest lepton and jet.

WZ Fit Region - 1j 77-85% WP

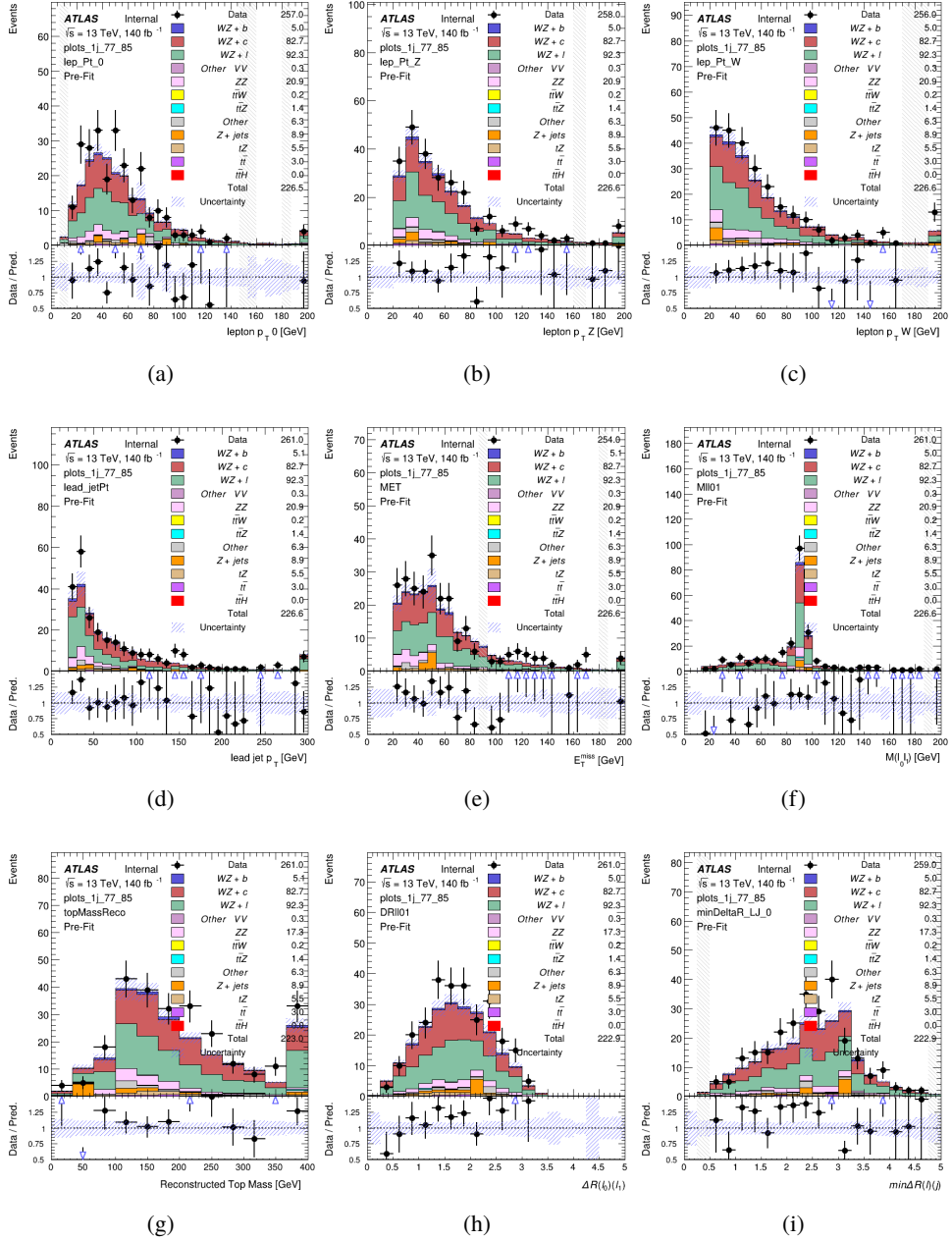


Figure 6: Comparisons between the data and MC distributions in the preselection region for (a) the p_T of the opposite sign lepton, (b) the p_T of the other lepton from the Z candidate, (c) the p_T of the lepton from the W candidate, (d) the leading jet p_T , (e) the E_T^{miss} , and (f) the invariant mass of leptons 0 and 1, (g) the reconstructed top mass, (h) $\Delta(R)$ between lepton 0 and 1, (i) the $\Delta(R)$ between the closest lepton and jet.

WZ Fit Region - 1j 70-77% WP

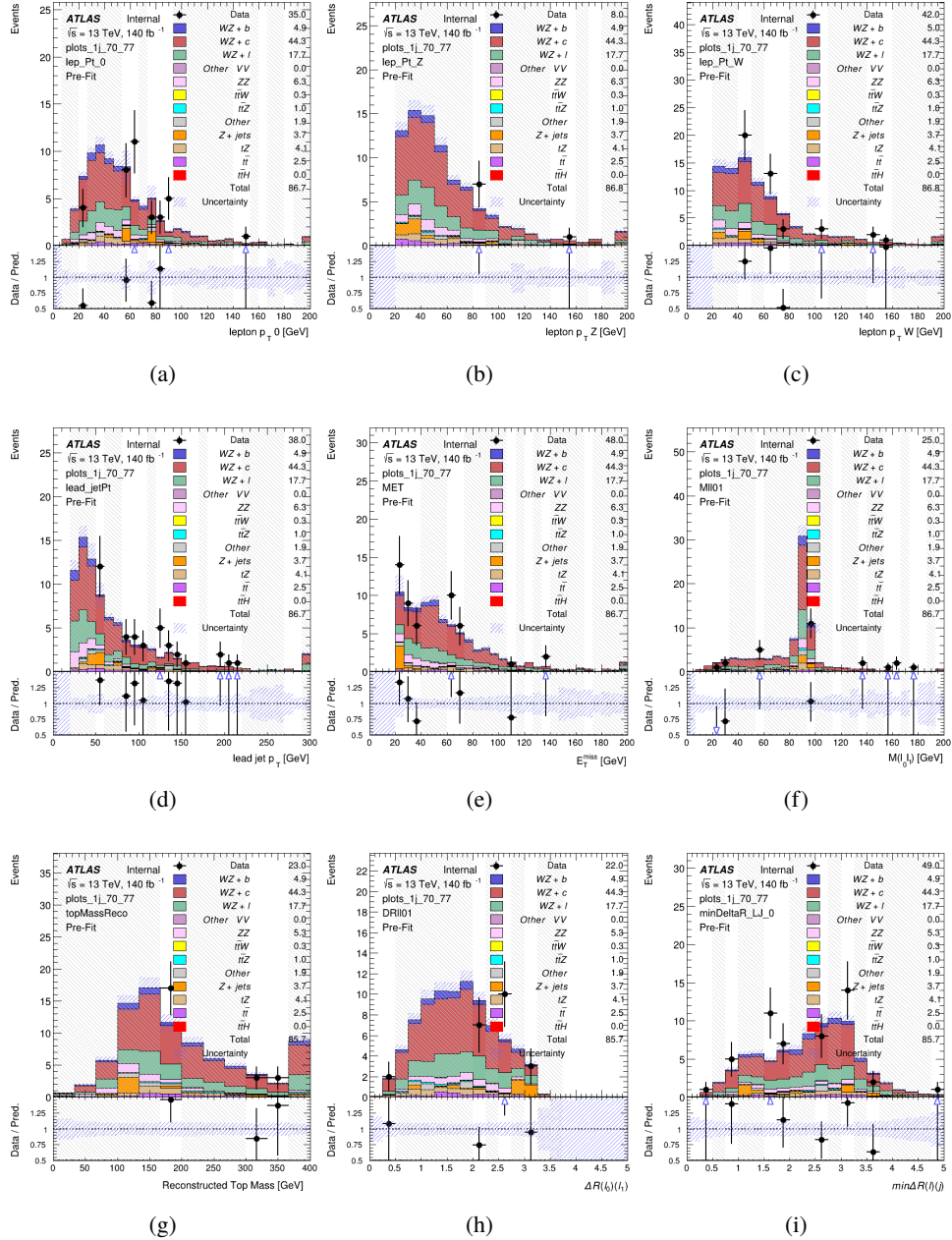


Figure 7: Comparisons between the data and MC distributions in the preselection region for (a) the p_T of the opposite sign lepton, (b) the p_T of the other lepton from the Z candidate, (c) the p_T of the lepton from the W candidate, (d) the leading jet p_T , (e) the E_T^{miss} , and (f) the invariant mass of leptons 0 and 1, (g) the reconstructed top mass, (h) $\Delta(R)$ between lepton 0 and 1, (i) the $\Delta(R)$ between the closest lepton and jet.

WZ Fit Region - 1j 60-70% WP

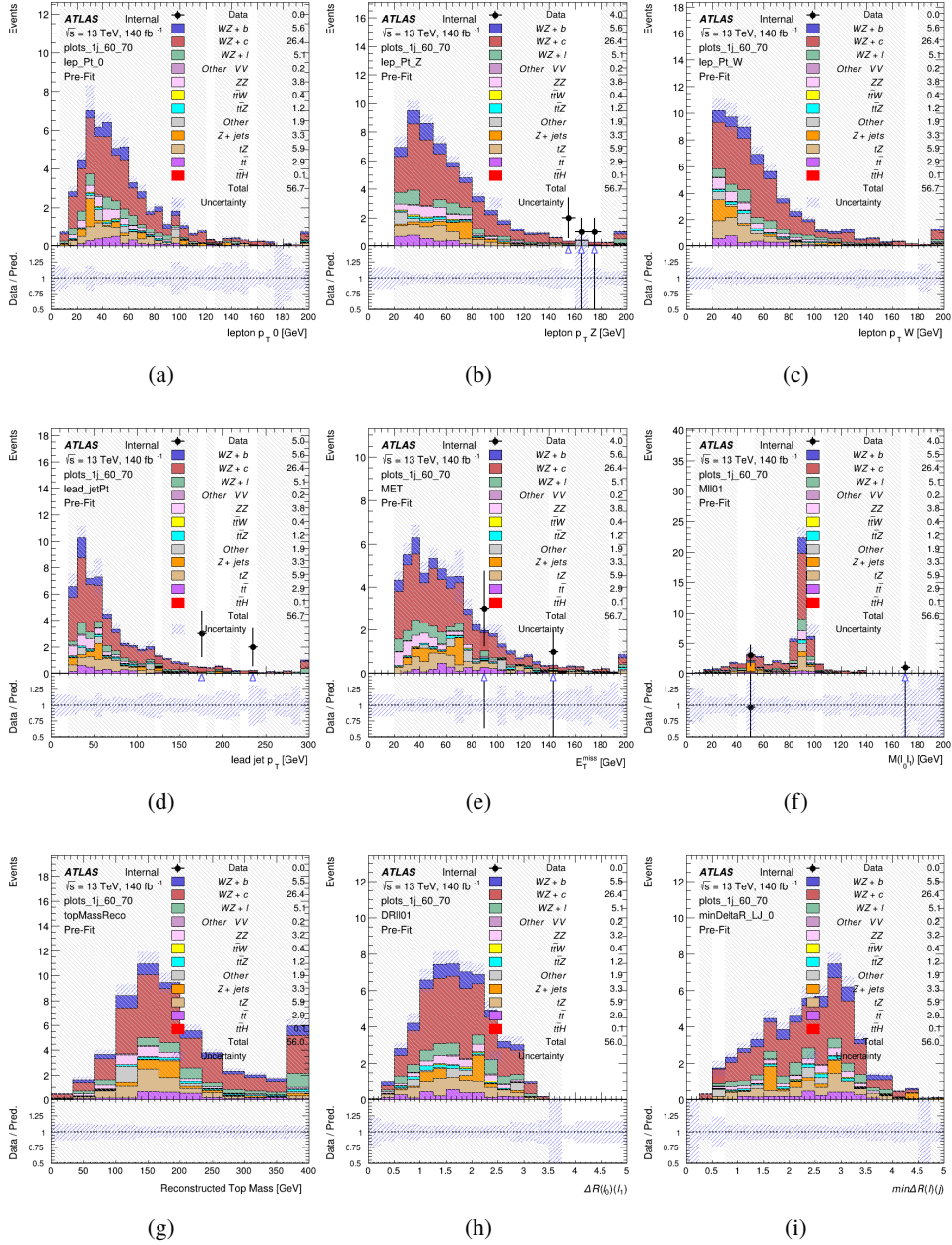


Figure 8: Comparisons between the data and MC distributions in the preselection region for (a) the p_T of the opposite sign lepton, (b) the p_T of the other lepton from the Z candidate, (c) the p_T of the lepton from the W candidate, (d) the leading jet p_T , (e) the E_T^{miss} , and (f) the invariant mass of leptons 0 and 1, (g) the reconstructed top mass, (h) $\Delta(R)$ between lepton 0 and 1, (i) the $\Delta(R)$ between the closest lepton and jet.

WZ Fit Region - 1j 60% WP

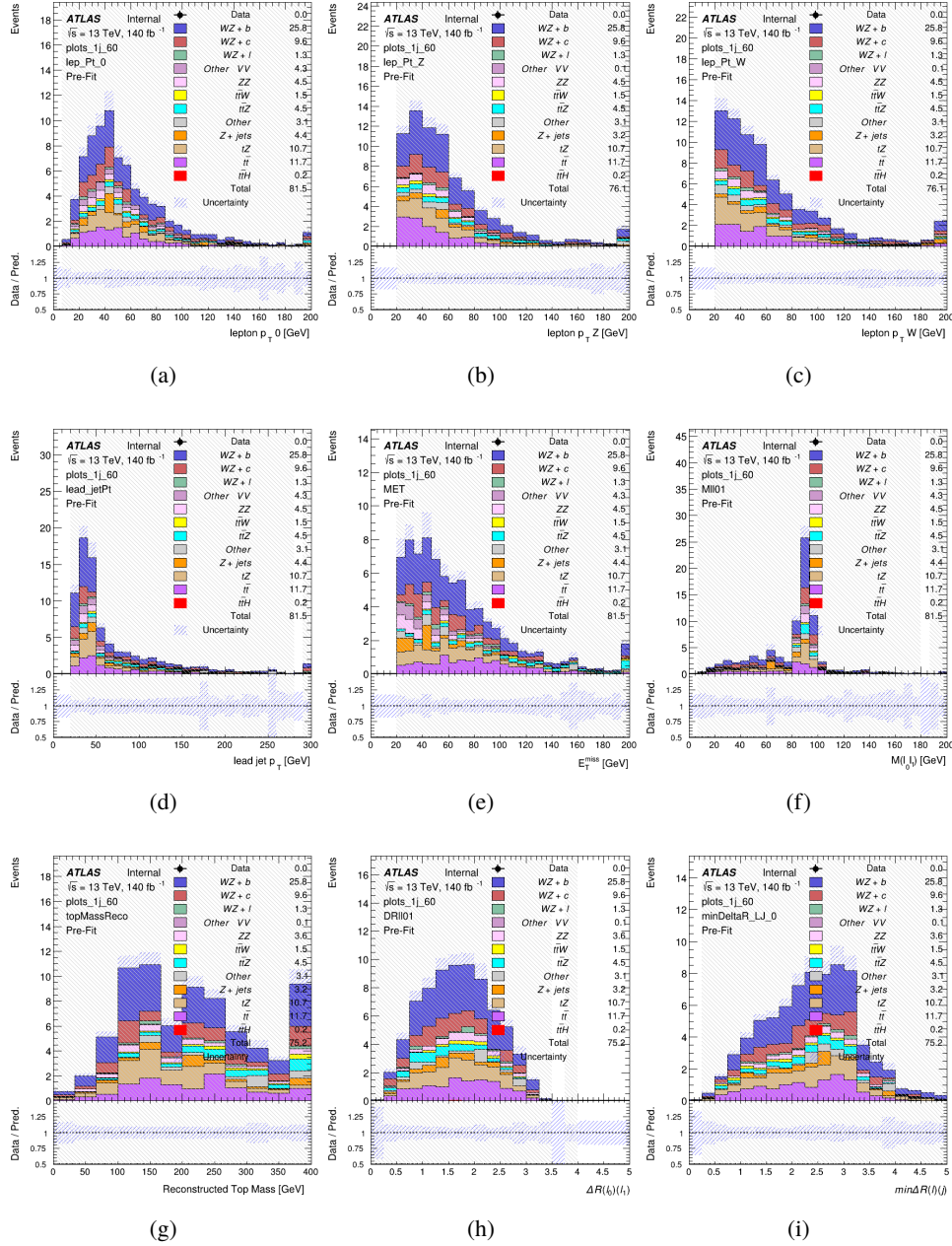


Figure 9: Comparisons between the data and MC distributions in the preselection region for (a) the p_T of the opposite sign lepton, (b) the p_T of the other lepton from the Z candidate, (c) the p_T of the lepton from the W candidate, (d) the leading jet p_T , (e) the E_T^{miss} , and (f) the invariant mass of leptons 0 and 1, (g) the reconstructed top mass, (h) $\Delta(R)$ between lepton 0 and 1, (i) the $\Delta(R)$ between the closest lepton and jet.

WZ Fit Region - tZ-CR

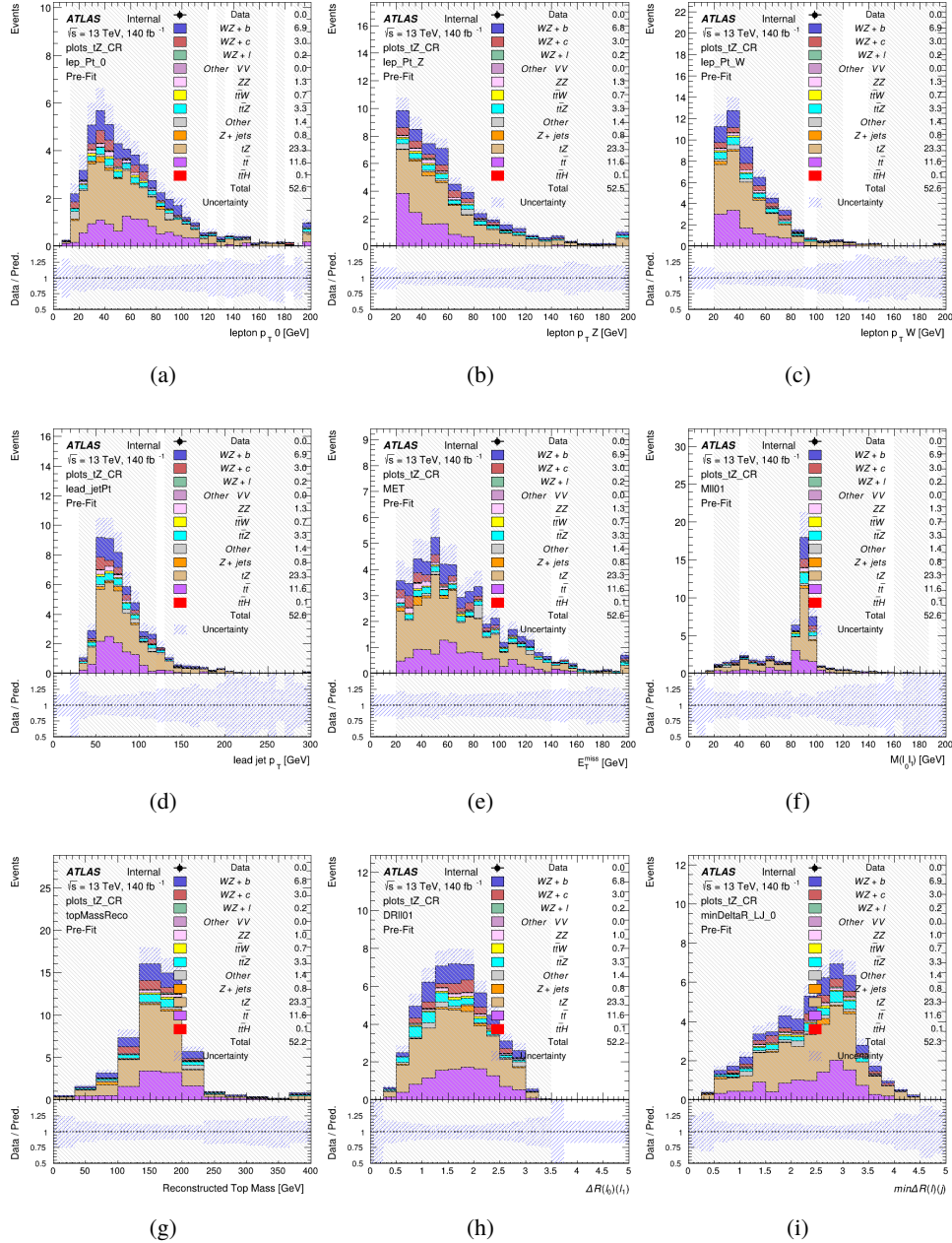


Figure 10: Comparisons between the data and MC distributions in the preselection region for (a) the p_T of the opposite sign lepton, (b) the p_T of the other lepton from the Z candidate, (c) the p_T of the lepton from the W candidate, (d) the leading jet p_T , (e) the E_T^{miss} , and (f) the invariant mass of leptons 0 and 1, (g) the reconstructed top mass, (h) $\Delta(R)$ between lepton 0 and 1, (i) the $\Delta(R)$ between the closest lepton and jet.

WZ Fit Region - 2j Inclusive

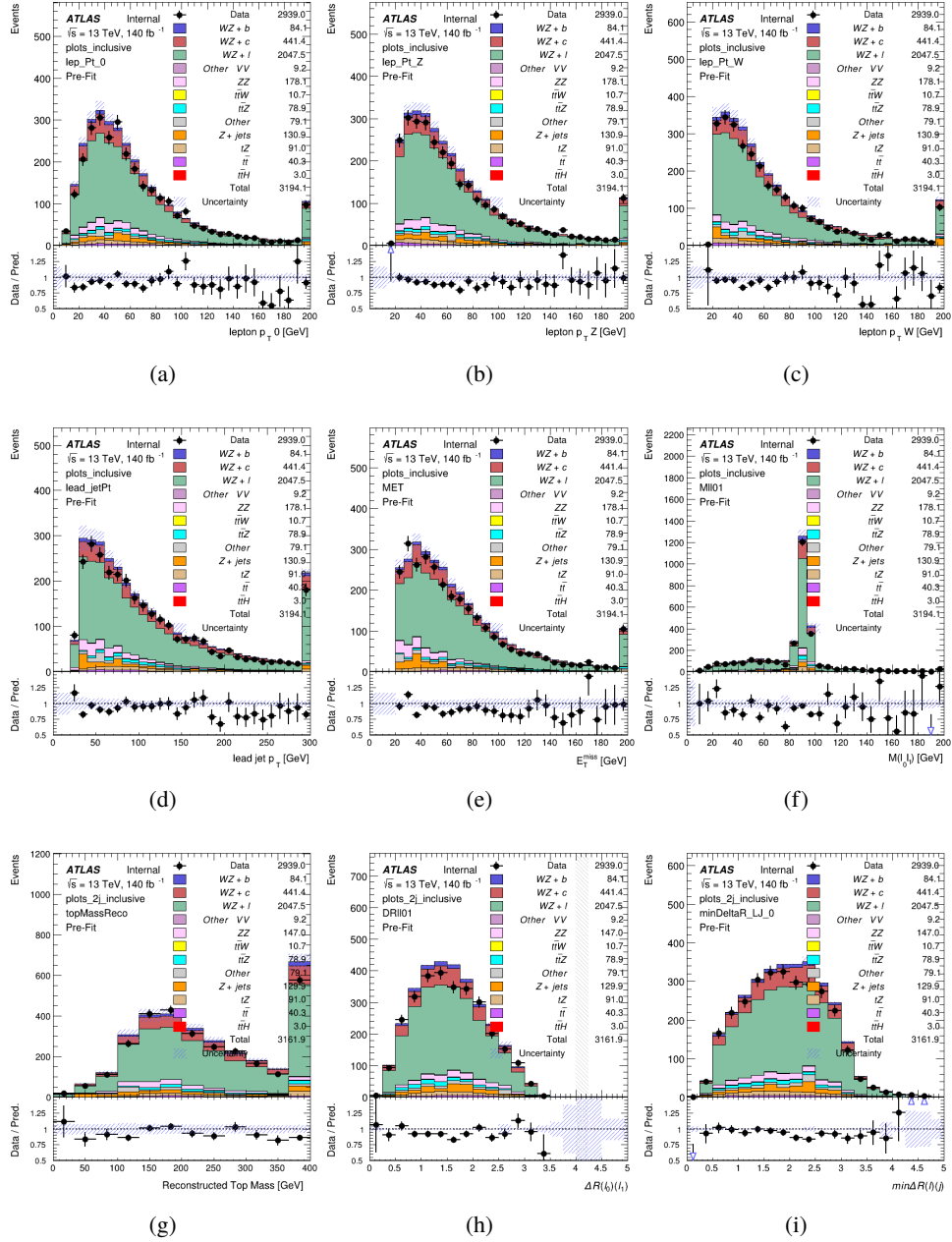


Figure 11: Comparisons between the data and MC distributions in the preselection region for (a) the p_T of the opposite sign lepton, (b) the p_T of the other lepton from the Z candidate, (c) the p_T of the lepton from the W candidate, (d) the leading jet p_T , (e) the E_T^{miss} , and (f) the invariant mass of leptons 0 and 1, (g) the reconstructed top mass, (h) $\Delta(R)$ between lepton 0 and 1, (i) the $\Delta(R)$ between the closest lepton and jet.

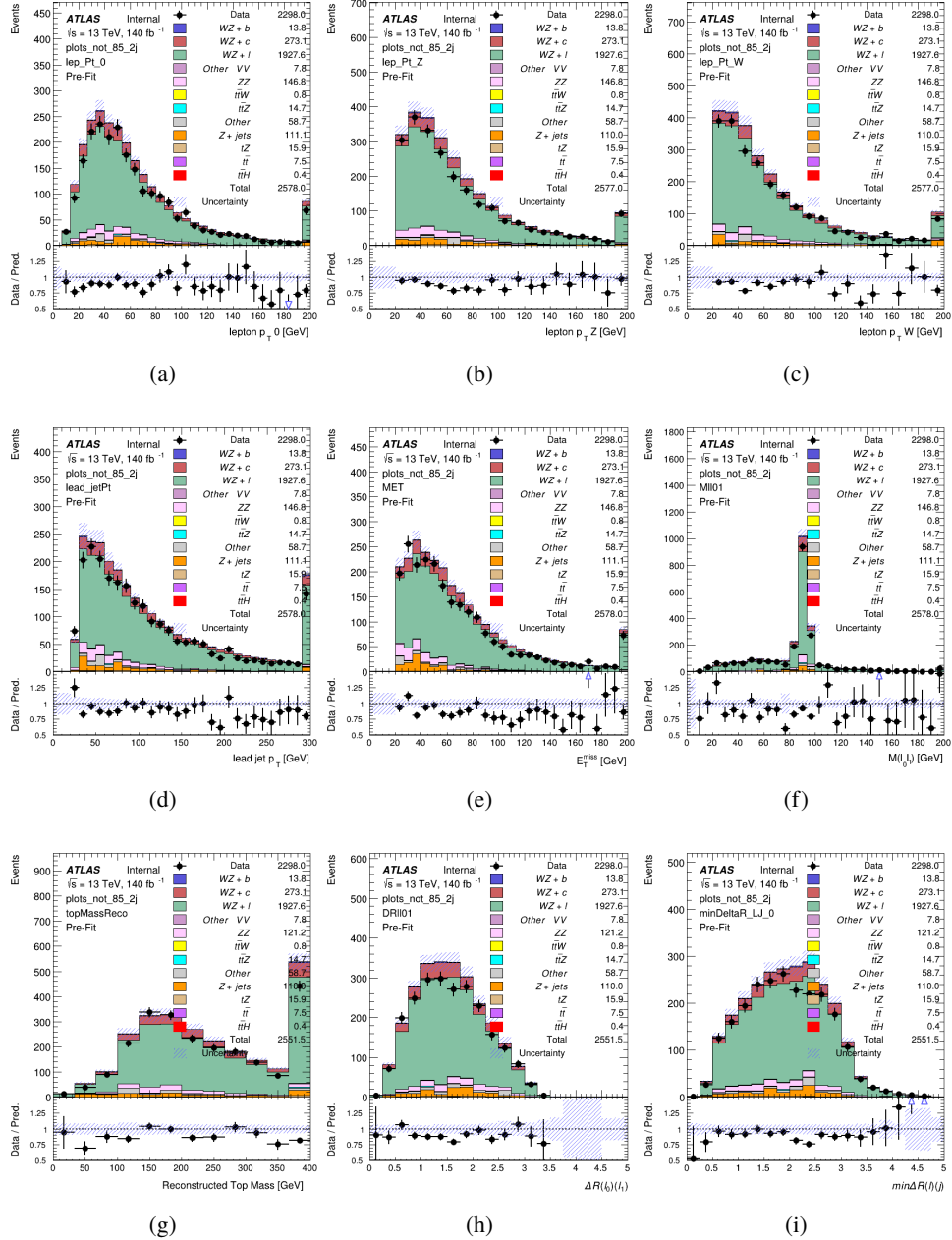
WZ Fit Region - $2j < 85\%$ WP

Figure 12: Comparisons between the data and MC distributions in the preselection region for (a) the p_T of the opposite sign lepton, (b) the p_T of the other lepton from the Z candidate, (c) the p_T of the lepton from the W candidate, (d) the leading jet p_T , (e) the E_T^{miss} , and (f) the invariant mass of leptons 0 and 1, (g) the reconstructed top mass, (h) $\Delta(R)$ between lepton 0 and 1, (i) the $\Delta(R)$ between the closest lepton and jet.

WZ Fit Region - 2j 77-85% WP

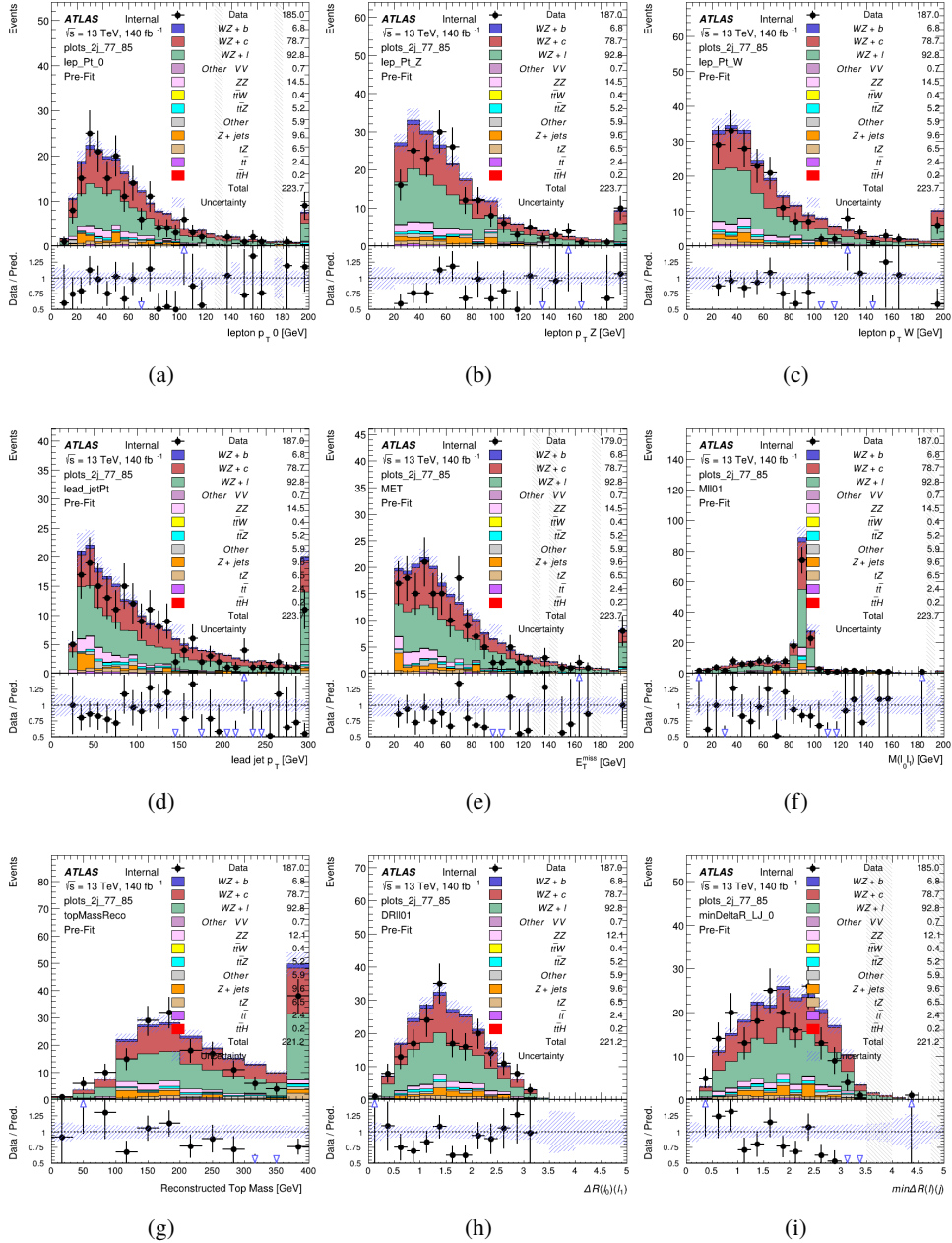


Figure 13: Comparisons between the data and MC distributions in the preselection region for (a) the p_T of the opposite sign lepton, (b) the p_T of the other lepton from the Z candidate, (c) the p_T of the lepton from the W candidate, (d) the leading jet p_T , (e) the E_T^{miss} , and (f) the invariant mass of leptons 0 and 1, (g) the reconstructed top mass, (h) $\Delta(R)$ between lepton 0 and 1, (i) the $\Delta(R)$ between the closest lepton and jet.

WZ Fit Region - 2j 70-77% WP

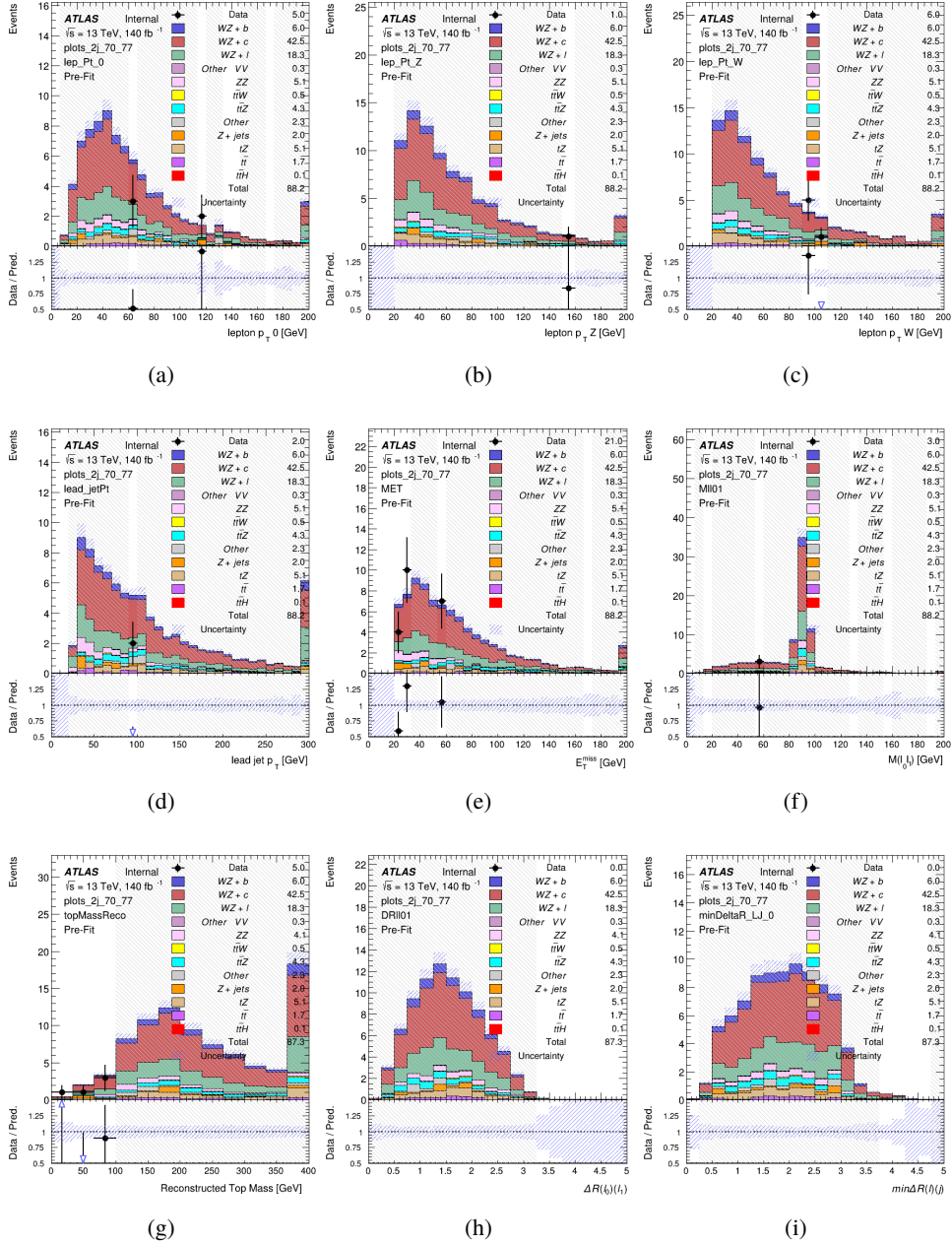


Figure 14: Comparisons between the data and MC distributions in the preselection region for (a) the p_T of the opposite sign lepton, (b) the p_T of the other lepton from the Z candidate, (c) the p_T of the lepton from the W candidate, (d) the leading jet p_T , (e) the E_T^{miss} , and (f) the invariant mass of leptons 0 and 1, (g) the reconstructed top mass, (h) $\Delta(R)$ between lepton 0 and 1, (i) the $\Delta(R)$ between the closest lepton and jet.

WZ Fit Region - 2j 60-70% WP

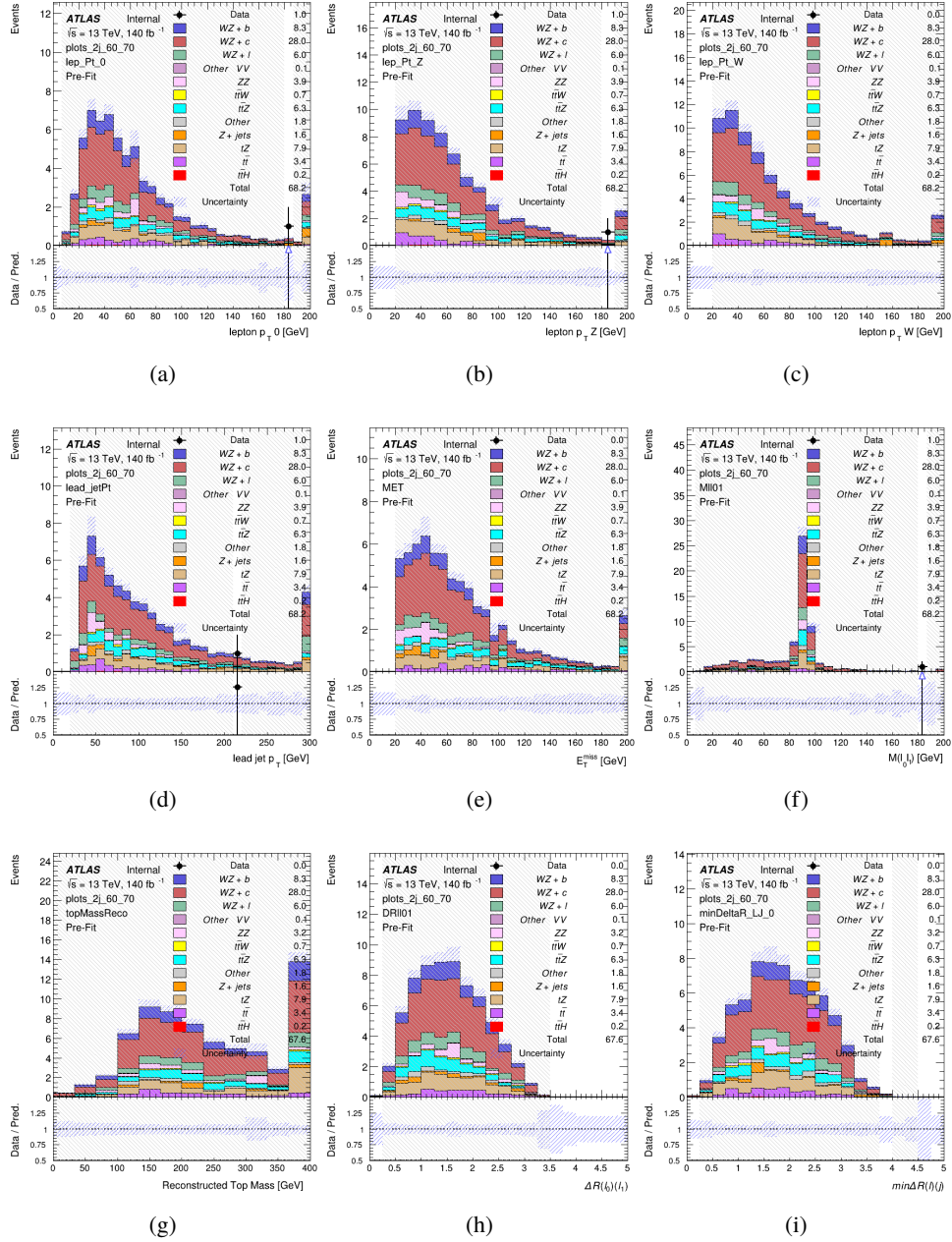


Figure 15: Comparisons between the data and MC distributions in the preselection region for (a) the p_T of the opposite sign lepton, (b) the p_T of the other lepton from the Z candidate, (c) the p_T of the lepton from the W candidate, (d) the leading jet p_T , (e) the E_T^{miss} , and (f) the invariant mass of leptons 0 and 1, (g) the reconstructed top mass, (h) $\Delta(R)$ between lepton 0 and 1, (i) the $\Delta(R)$ between the closest lepton and jet.

WZ Fit Region - 2j 60% WP

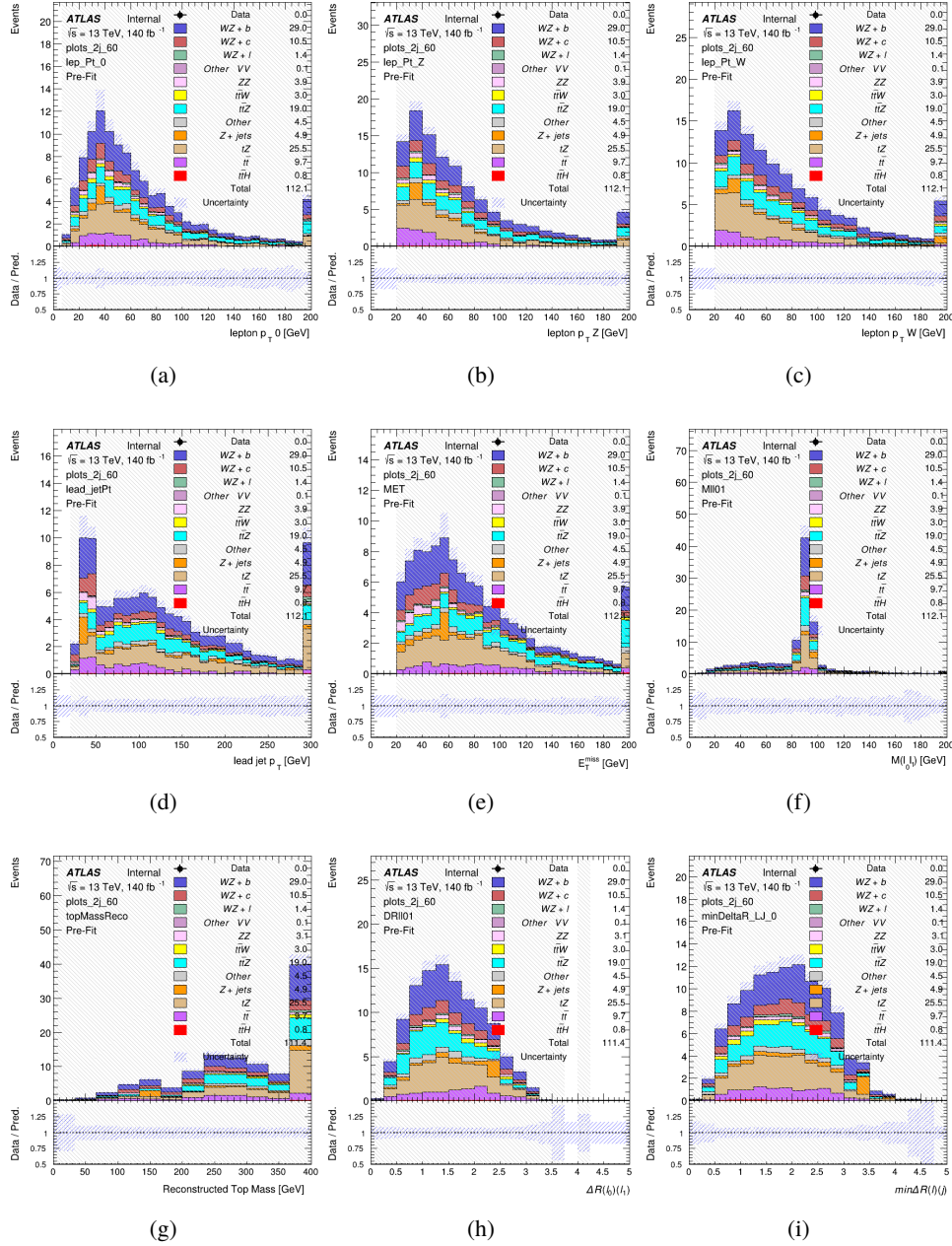


Figure 16: Comparisons between the data and MC distributions in the preselection region for (a) the p_T of the opposite sign lepton, (b) the p_T of the other lepton from the Z candidate, (c) the p_T of the lepton from the W candidate, (d) the leading jet p_T , (e) the E_T^{miss} , and (f) the invariant mass of leptons 0 and 1, (g) the reconstructed top mass, (h) $\Delta(R)$ between lepton 0 and 1, (i) the $\Delta(R)$ between the closest lepton and jet.

WZ Fit Region - tZ-CR-2j

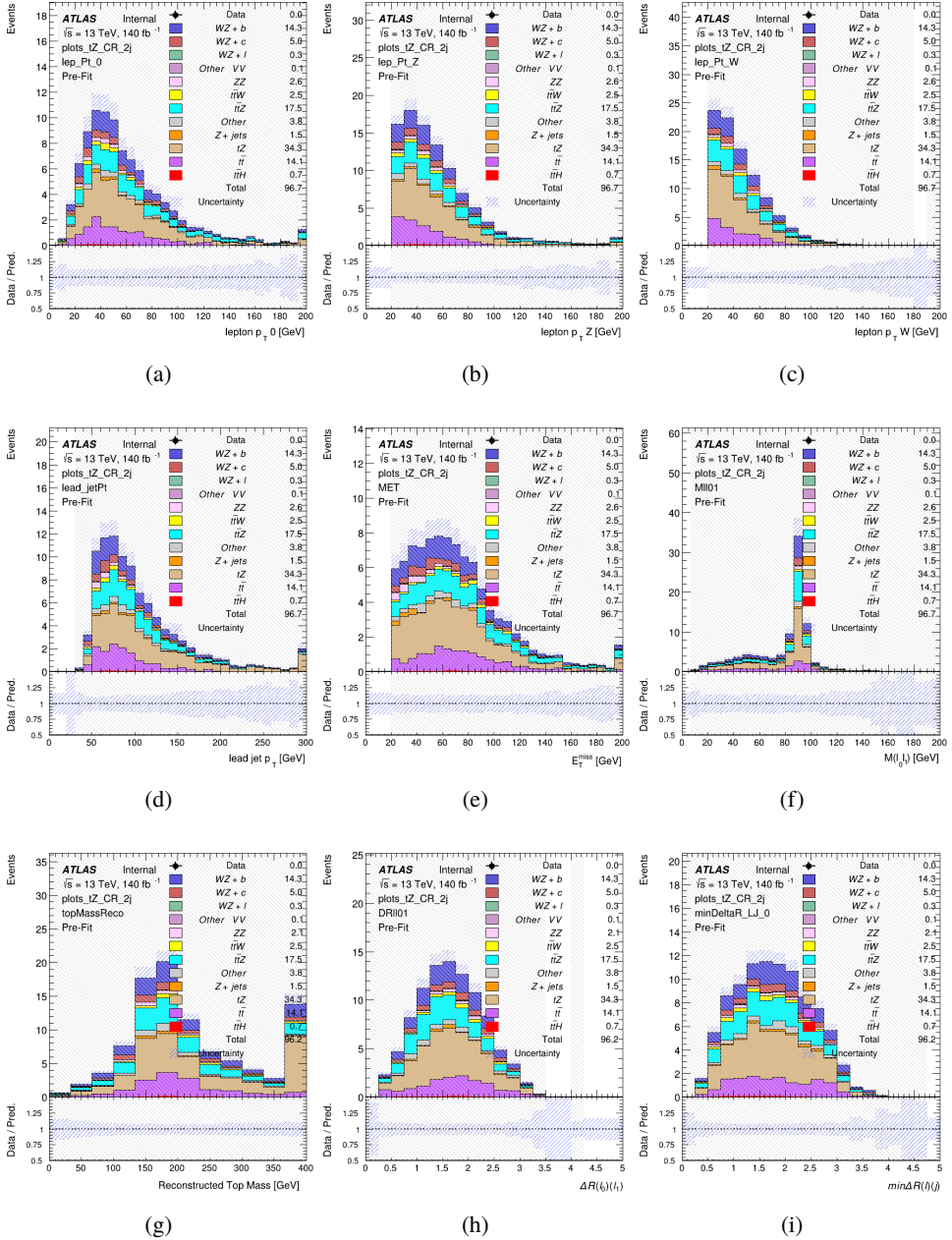


Figure 17: Comparisons between the data and MC distributions in the preselection region for (a) the p_T of the opposite sign lepton, (b) the p_T of the other lepton from the Z candidate, (c) the p_T of the lepton from the W candidate, (d) the leading jet p_T , (e) the E_T^{miss} , and (f) the invariant mass of leptons 0 and 1, (g) the reconstructed top mass, (h) $\Delta(R)$ between lepton 0 and 1, (i) the $\Delta(R)$ between the closest lepton and jet.

332 **5.3 Non-Prompt Lepton Estimation**

333 Two processes act as sources of non-prompt leptons appear in the analysis: $t\bar{t}$ and $Z+jet$
334 production both produce two prompt leptons, and each contribute to the 31 region when an
335 additional non-prompt lepton appears in the event. The contribution of these processes is
336 estimated with Monte Carlo simulations, which are validated using enriched control regions.

337 **5.3.1 $t\bar{t}$ Validation**

338 $t\bar{t}$ events can produce two prompt leptons from the decay of each of the tops. These top decays
339 produce two b-quarks, the decay of which can produce additional non-prompt leptons, which
340 occasionally pass the event preselection. In order to validate that the Monte Carlo accurately
341 simulates this process accurately, the MC prediction in a non-prompt $t\bar{t}$ enriched control region
342 is compared to data.

343 The $t\bar{t}$ control region is similar to the preselection region - three leptons meeting the criteria
344 described in Section 5 are required, and the requirements on E_T^{miss} remain the same. However,
345 the selection requiring a lepton pair form a Z-candidate are reversed. Events where the invariant
346 mass of any two opposite sign, same flavor leptons falls within 10 GeV of 91.2 GeV are rejected.
347 This ensures the $t\bar{t}$ control region is orthogonal to the preselection region.

348 Further, because the jet multiplicity of $t\bar{t}$ events tends to be higher than WZ, the number of jets
349 in each event is required to be greater than 1. As b-jets are almost invariably produced from top
350 decays, at least one b-tagged jet passing the 70% DL1r WP in each event is required. Various
351 kinematic plots of this region are shown in Figure 18.

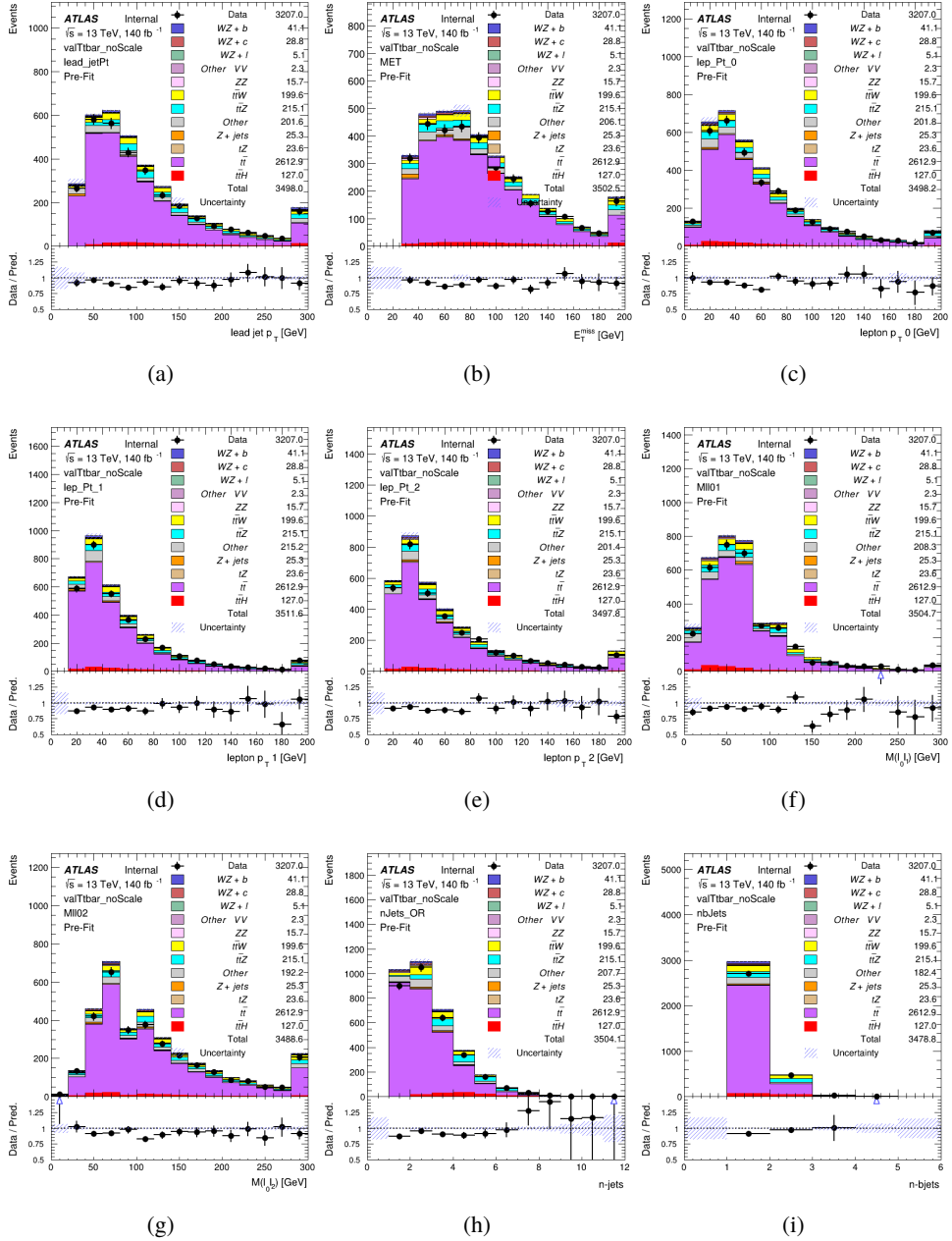


Figure 18: Comparisons between the data and MC distributions in the $t\bar{t}$ control region for (a) the p_T of the leading jet, (b) the missing transverse energy, (c) the p_T of lepton 0, (d) p_T of lepton 1, (e) p_T of lepton 2, (f) the invariant mass of leptons 0 and 1, (g) the invariant mass of leptons 0 and 2, (h) the number of jets, (i) the number of b-tagged jets.

352 The shape of each distribution agrees quite well between data and MC, with a constant offset
 353 between the two. This is accounted for by applying a constant correction factor of 0.883 to the $t\bar{t}$

354 MC prediction. Plots showing the kinematics of the $t\bar{t}$ VR after this correction factor has been
 355 applied are shown in Figure 19.

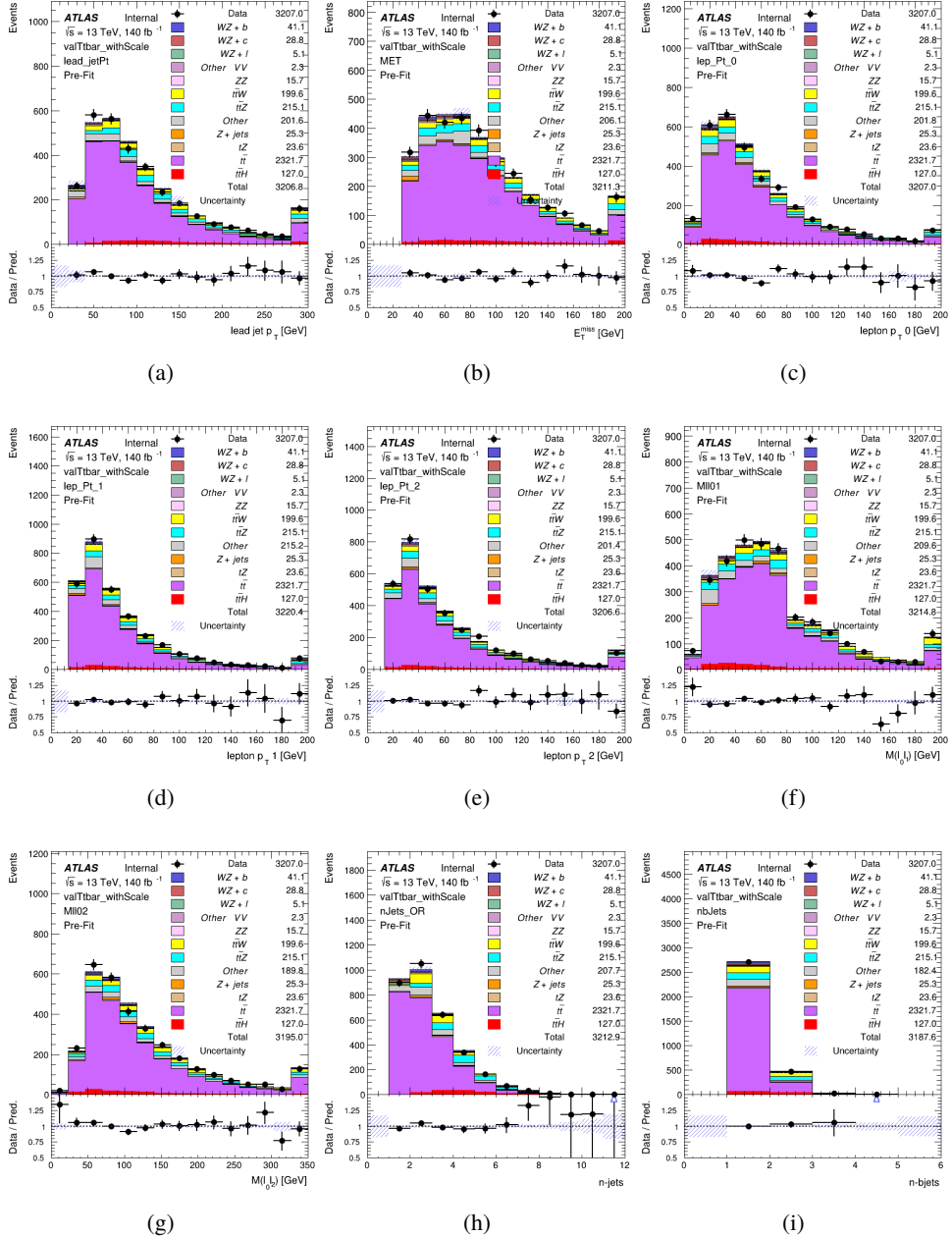


Figure 19: Comparisons between the data and MC distributions in the $t\bar{t}$ control region after the correction factor has been applied for (a) the p_T of the leading jet, (b) the missing transverse energy, (c) the p_T of lepton 0, (d) p_T of lepton 1, (e) p_T of lepton 2, (f) the invariant mass of leptons 0 and 1, (g) the invariant mass of leptons 0 and 2, (h) the number of jets, (i) the number of b-tagged jets.

356 The modeling is further validated by looking at the yield in the $t\bar{t}$ VR for each DL1r WP, giving
 357 a clearer correspondence to the signal regions used in the fit. Each region shown in Figure 20
 358 requires one or more jets pass the listed WP, with no jets passing the next highest WP.

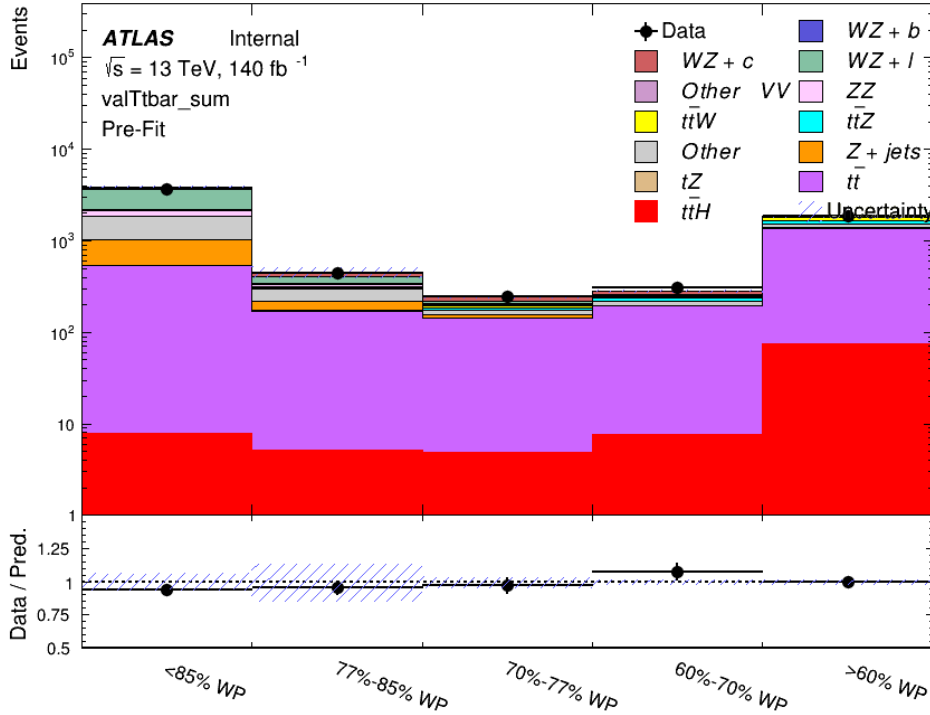


Figure 20: Data and MC comparisons for each DL1r WP for both 1-jet and 2-jet regions, after the $t\bar{t}$ VR selection and correction factor have been applied

359 As data and MC are found to agree within 20% for each of these working points, a 20% systematic
 360 uncertainty on the $t\bar{t}$ prediction is included for the analysis.

361 5.3.2 Z+jets Validation

362 Similar to $t\bar{t}$, a non-prompt Z+jets control region is produced in order to validate the MC
 363 predictions. The lepton requirements remain the same as the preselection region. Because no
 364 neutrinos are present for this process, the E_T^{miss} cut is reversed, requiring $E_T^{\text{miss}} < 30 \text{ GeV}$. This
 365 also ensures this control region is orthogonal to the preselection region. Further, the number of
 366 jets in each event is required to be greater than or equal to one. Various kinematic plots of this
 367 region are shown below. The general agreement between data and MC in each of these suggests
 368 that the non-prompt contribution of Z+jets is well modeled by Monte Carlo.

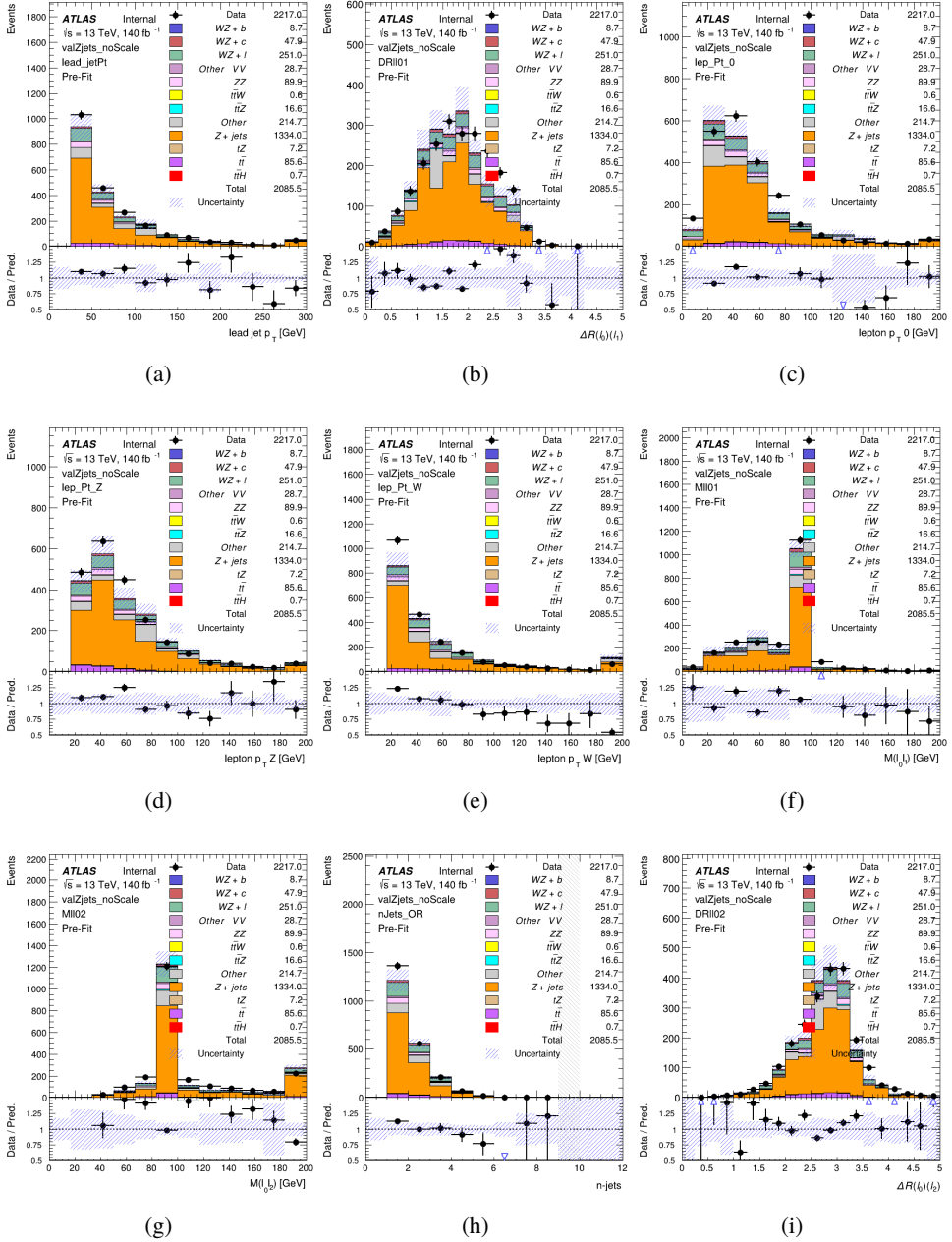


Figure 21: Comparisons between the data and MC distributions in the Z+jets control region for (a) the p_T of the leading jet, (b) ΔR between leptons 0 and 1, (c) the p_T of lepton 0, (d) p_T of SS lepton from the Z candidate, (e) p_T of the SS lepton from the W candidate, (f) the invariant mass of leptons 0 and 1, (g) the invariant mass of leptons 0 and 2, (h) the number of jets, (i) ΔR between leptons 0 and 2. Includes only statistical uncertainties

369 While there is general agreement between data and MC within statistical uncertainty, the shape

³⁷⁰ of the p_T spectrum of the lepton from the W is found to differ. To account for this discrepancy,
³⁷¹ a variable correction factor is applied to Z+jets. χ^2 minimization of the lepton 2 p_T spectrum
³⁷² is performed to derive a correction factor of $1.53 - 6.6 * 10^{-6}(\text{lep}_\ell \text{Pt}_W)$. Kinematic plots of
³⁷³ the Z + jets control region after this correction factor has been applied are shown in Figure 22.

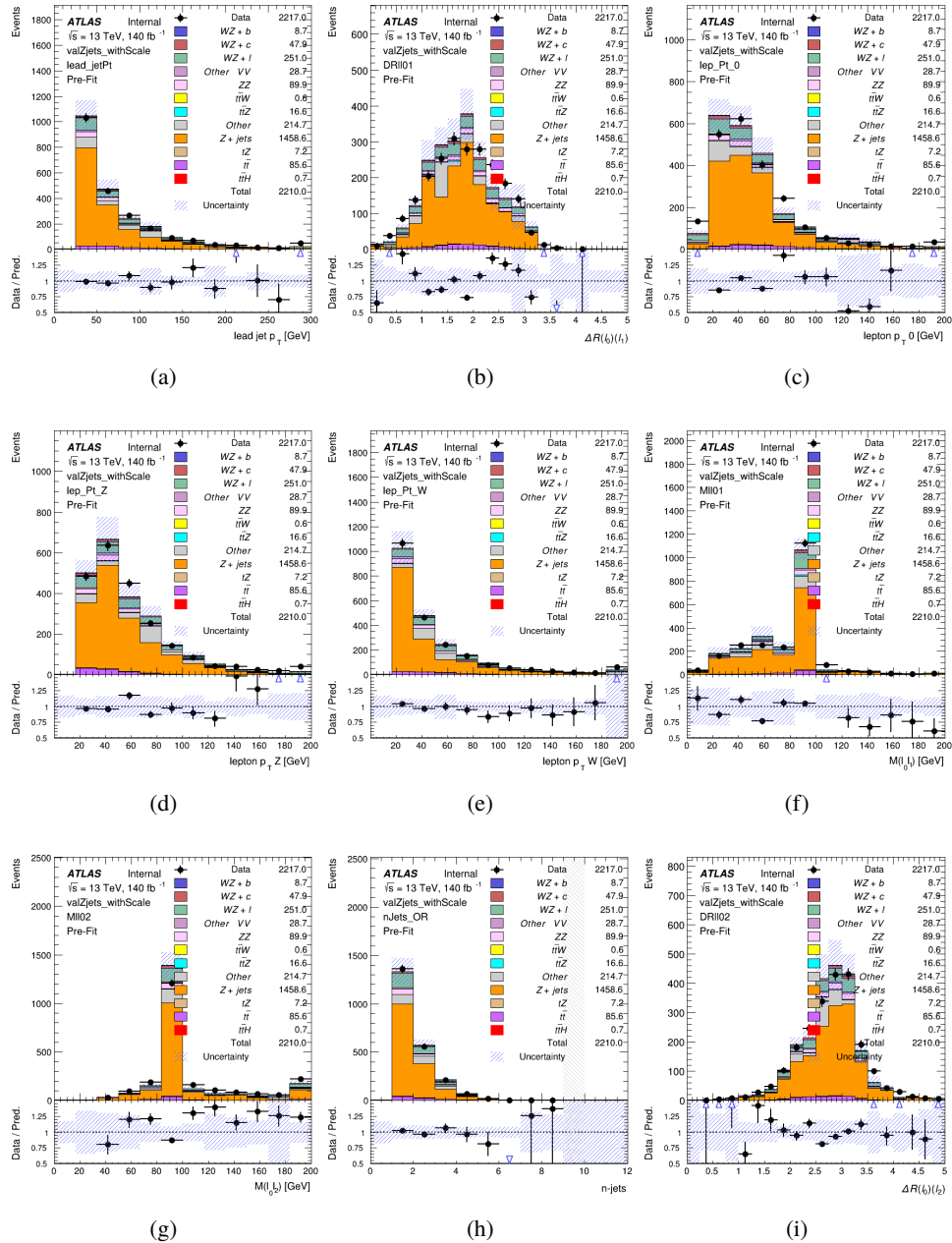


Figure 22: Comparisons between the data and MC distributions in the Z+jets control region after the correction factor has been applied for (a) the p_T of the leading jet, (b) ΔR between leptons 0 and 1, (c) the p_T of lepton 0, (d) p_T of SS lepton from the Z candidate, (e) p_T of the SS lepton from the W candidate, (f) the invariant mass of leptons 0 and 1, (g) the invariant mass of leptons 0 and 2, (h) the number of jets, (i) ΔR between leptons 0 and 2

374 The modeling is further validated by looking at the yield in the Z+jets VR for each DL1r WP,

375 giving a clearer correspondence to the signal regions used in the fit. Each region shown in Figure
 376 23 requires one or more jets pass the listed WP, with no jets passing the next highest WP.

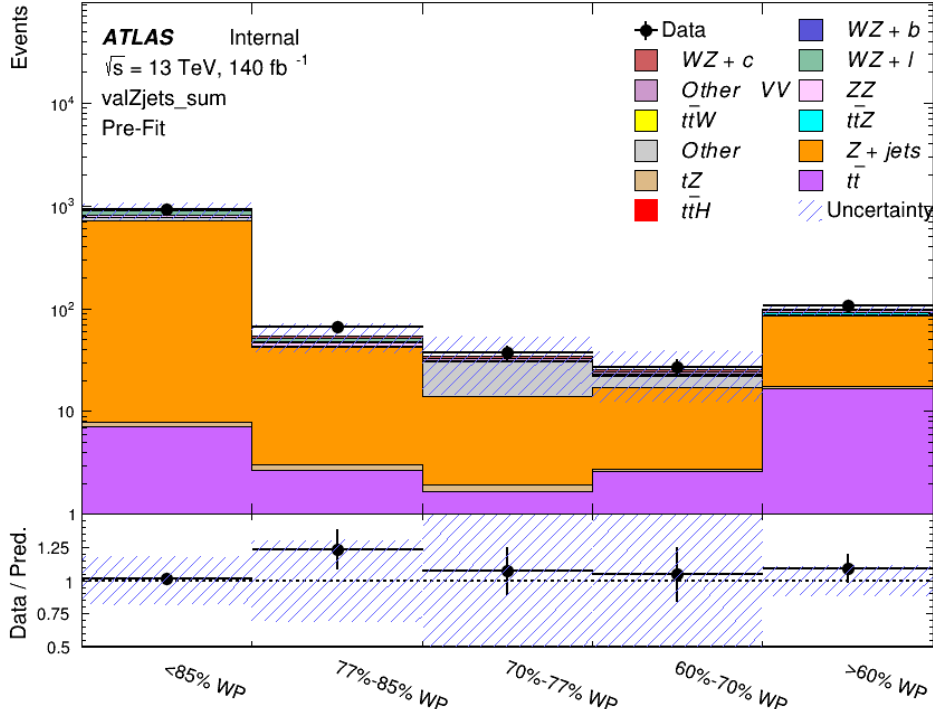


Figure 23: Data and MC comparisons for each DL1r WP for both 1-jet and 2-jet regions, after the Z+jets VR selection and correction factor have been applied

377 For each of the b-tagging working points considered, the data falls within 25% of the MC
 378 prediction once this correction factor has been applied. Therefore, a 25% systematic uncertainty
 379 is applied to Z + jets in the analysis.

380 6 tZ Separation Multivariate Analysis

381 Because tZ produces a final state identical to signal, it represents a predominant background in
 382 the most signal enriched regions. That is, the region with one jet passing the 60% DL1r WP.
 383 Therefore, a boosted decision tree (BDT) algorithm is trained using TMVA [16] to separate WZ
 384 + heavy flavor from tZ.

385 Separation between tZ and WZ + heavy flavor is achieved in part by reconstructing the invariant
 386 mass of the top candidate, which clusters more closely to the top mass for tZ than WZ + heavy
 387 flavor.

388 The result of this BDT is used to create a tZ enriched region in the fit, reducing its impact on the
 389 measurement of WZ + heavy flavor.

390 **6.1 Top Mass Reconstruction**

391 The reconstruction of the top mass follows the procedure described in detail in section 6.1 of
 392 [17]. The mass of the top quark candidate is reconstructed from the jet, the lepton not included
 393 in the Z-candidate, and a reconstructed neutrino. In the case that there is one jet in the event,
 394 there is only possible b-jet candidate. For events with two jets, the jet with the highest DL1r
 395 score is used.

396 The neutrino from the W decay is expected to be the only source of E_T^{miss} . Therefore, the E_T
 397 and ϕ of the neutrino are taken from the E_T^{miss} measurement. This leaves the z-component of
 398 the neutrino momentum, $p_{\nu z}$ as the only unknown.

399 This unknown is solved for by taking the combined invariant mass of the lepton and neutrino to
 400 give the invariant mass of the W boson:

$$401 \quad (p_l + p_\nu)^2 = m_W^2$$

402 Expanding this out into components, this equation gives:

$$403 \quad \sqrt{p_{T\nu}^2 + p_{z\nu}^2} E_l = \frac{m_w^2 - m_l^2}{2} + p_{T\nu}(p_{lx}\cos\phi_\nu + p_{ly}\sin\phi_\nu) + p_{lz}p_{\nu z}$$

404 This equation gives two solutions for $p_{\nu z}$. For cases where only one of these solutions is real,
 405 that is taken as the value of $p_{\nu z}$. For instances with two real solutions, the one which is shown
 406 to be correct in the largest fraction of simulations is taken. For cases when no real solution is
 407 found, often because of detector effects, the value of E_T^{miss} is varied in decreasing increments of
 408 100 MeV until a real solution is found.

409 The reconstructed top mass distribution for tZ and WZ + b can be seen in figure 24.

410 **6.2 tZ BDT**

411 A Boosted Decision Tree (BDT), specifically XGBoost [18], is used to provide separation between
 412 tZ and WZ+b. The following kinematic variables are used as inputs:

- 413 • The invariant mass of the reconstructed top candidate
- 414 • p_T of each of the leptons, jet
- 415 • The invariant mass of each combination of lepton pairs, $M(l\bar{l})$
- 416 • E_T^{miss}

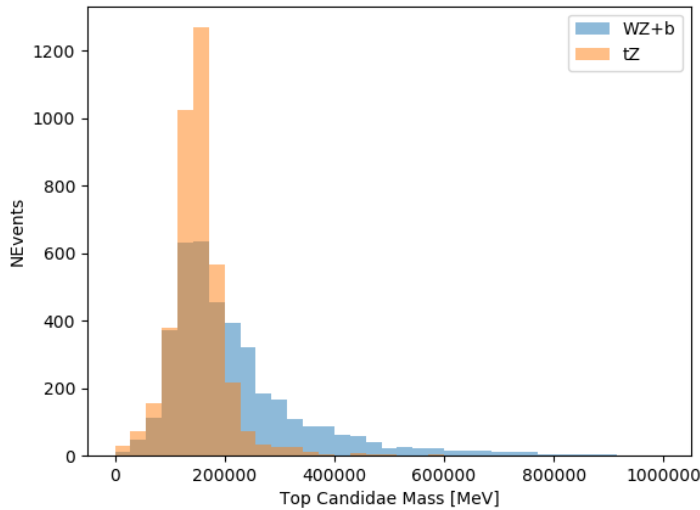


Figure 24: Reconstructed top mass distributions for tZ and WZ + b, measured in MeV.

- Distance between each combination of leptons, $\Delta R(ll)$
 - Distance between each lepton and the jet, $\Delta R(lj)$
- The training samples included only events meeting the requirements of the 1-jet, >60% region, i.e. passing all the selection described in section 5 and having exactly one jet which passes the tightest (60%) DL1r working point.
- The distributions of a few of these features for both signal and background is shown in figure 25.

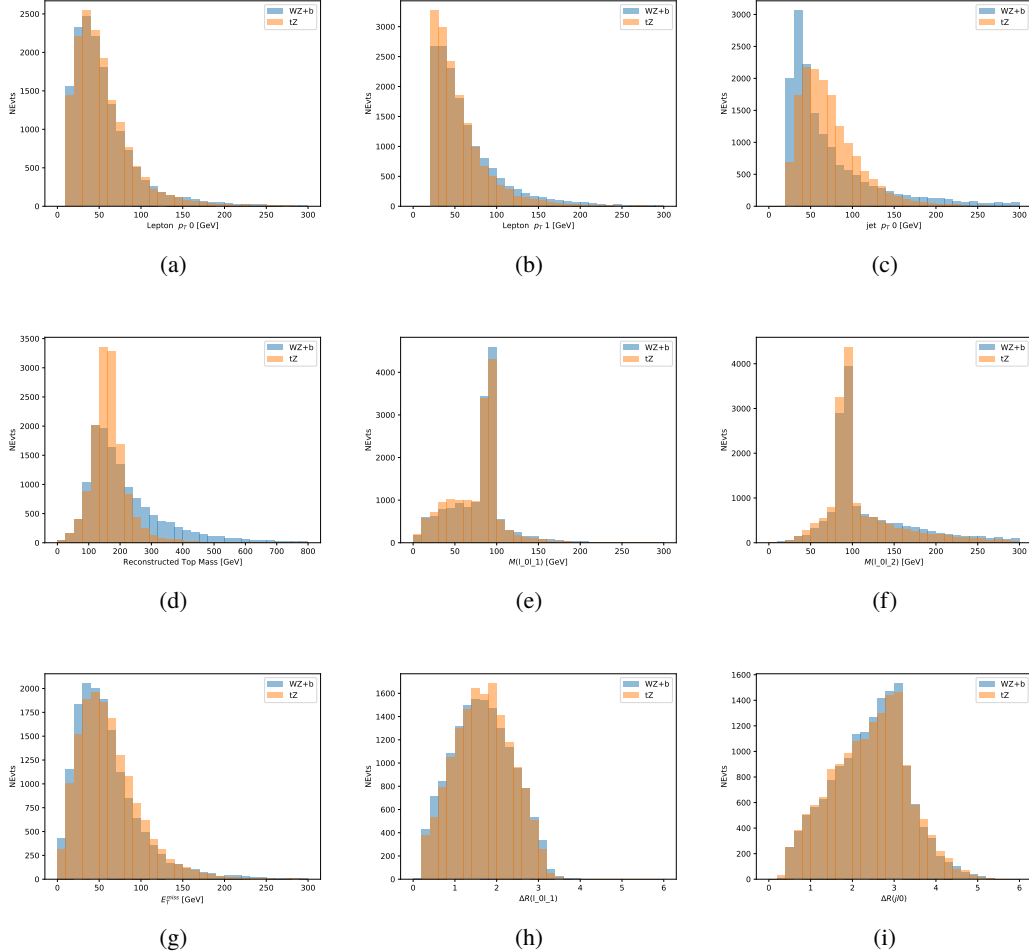


Figure 25: Distribution of input features of the BDT for signal (WZ) and background (tZ). Both are scaled to an equal number of events. (a), (b) and (c) show the p_T of lepton 0, lepton 1, and the jet, (d) show the reconstructed top mass, (e) and (f) show the invariant mass of leptons 0 and 1, leptons 0 and 2. (g) shows the E_T^{miss} of each event. (h) and (i) show the ΔR between lepton 0 and lepton 1, and the jet.

424 A sample of 20,000 background (tZ) and signal (WZ+b) Monte Carlo events are used to train
 425 the BDT. And additional 5,000 events are reserved for testing the model, in order to prevent
 426 over-fitting. A total of 750 decision trees with a maximum depth of 6 branches are used to build
 427 the model. These parameters are chosen empirically, by training several models with different
 428 parameters and selecting the one that gave the best separation for the test sample.

429 The results of the BDT training are shown in figure 26. The output scores for both signal and
 430 background events is shown on the left. The right shows the receiving operating characteristic
 431 (ROC) curve that results from the MVA. The ROC curve represents the background rejection
 432 as a function of signal efficiency, where each point on the curve represents a different response

433 score. The ROC curve of the BDT is compared to the performance of using an optimal set of flat
 434 selections on the same set of input variables.

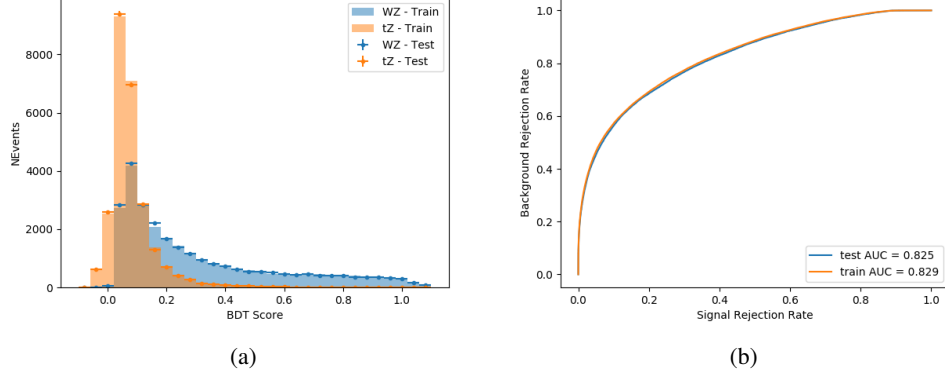


Figure 26: Distribution of the BDT response for signal and background events on the left, the ROC curve for the BDT on the right.

435 The relative important of each input feature in the model, measured by how often they appeared
 436 in the decision trees, is shown in figure 27.

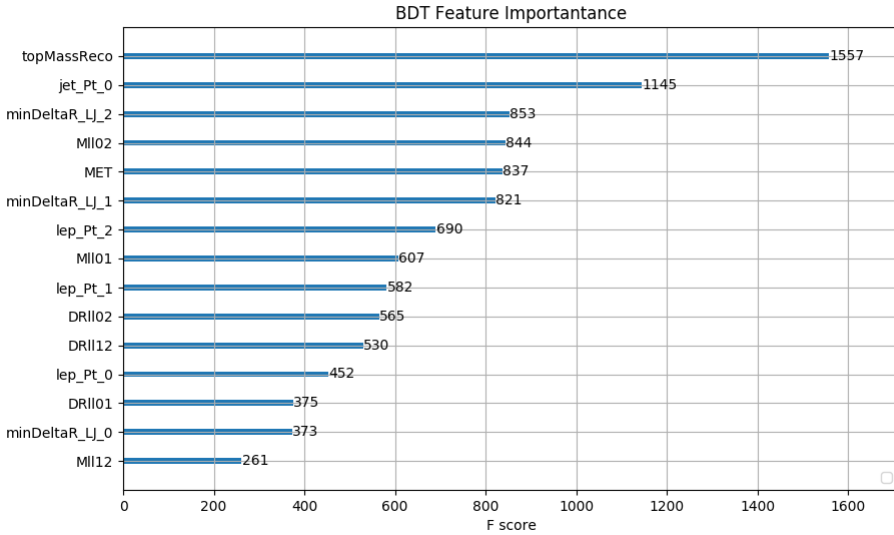


Figure 27: Relative importance of each input feature in the model.

437 These results suggest that some amount of separation can be achieved between these two pro-
 438 cesses, with a high BDT score selecting a set of events that is pure in WZ + b. A BDT score

439 of 0.725 is selected as a cutoff, where events with scores higher than this form a signal enriched
 440 region, and events with scores lower than this form a tZ control region. This cutoff is selected by
 441 varying the value of this cutoff in stat-only Asimov fits, and selecting the value that minimizes
 442 the statistical uncertainty on WZ + b.

443 7 Systematic Uncertainties

444 The systematic uncertainties that are considered are summarized in Table 9. These are imple-
 445 mented in the fit either as a normalization factors or as a shape variation or both in the signal
 446 and background estimations. The numerical impact of each of these uncertainties is outlined in
 447 Section 8.

Table 9: Sources of systematic uncertainty considered in the analysis.

Systematic uncertainty	Components
Luminosity	1
Pileup reweighting	1
Physics Objects	
Electron	6
Muon	15
Jet energy scale	28
Jet energy resolution	8
Jet vertex fraction	1
Jet flavor tagging	131
E_T^{miss}	3
Total (Experimental)	194
Signal Modeling	
Shape modelling	3
Renormalization and factorization scales	5
nJet Migration	4
Background Modeling	
Cross section	15
Renormalization and factorization scales	12
Total (Signal and background modeling)	35
Total (Overall)	229

448 The uncertainty in the combined integrated luminosity is derived from a calibration of the
 449 luminosity scale performed for 13 TeV proton-proton collisions [19], [20].

450 The experimental uncertainties are related to the reconstruction and identification of light
451 leptons and b-tagging of jets, and to the reconstruction of E_T^{miss} . The TOTAL electron ID
452 correlation model is used, corresponding to 1 electron ID systematic. Electron ID is found to be
453 a subleading systematic that is unconstrained by the fit, making it an appropriate choice for this
454 analysis.

455 The sources which contribute to the uncertainty in the jet energy scale (JES) [21] are decom-
456 posed into uncorrelated components and treated as independent sources in the analysis. The
457 CategoryReduction model is used to account for JES uncertainties, which decomposes the uncer-
458 tainties into 30 nuisance parameters included in the fit. The SimpleJER model is used to account
459 for jet energy resolution (JER) uncertainties, and 8 JER uncertainty components unclued as
460 NPs in the fit.

461 The uncertainties in the b-tagging efficiencies measured in dedicated calibration analyses
462 [22] are also decomposed into uncorrelated components. The large number of components for
463 b-tagging is due to the calibration of the distribution of the MVA discriminant.

464 The full list of systematic uncertainties considered in the analysis is summarized in Tables 10,
465 11 and 12.

466

Experimental Systematics on Leptons and E_T^{miss}			
Type	Description	Systematics Name	Application
Trigger			
Scale Factors	Trigger Efficiency	lepSFTrigTight_MU(EL)_SF_Trigger_STAT(SYST)	Event Weight
Muons			
Efficiencies	Reconstruction and Identification	lepSFObjTight_MU_SF_ID_STAT(SYST)	Event Weight
	Isolation	lepSFObjTight_MU_SF_Isol_STAT(SYST)	Event Weight
	Track To Vertex Association	lepSFObjTight_MU_SF_TTVA_STAT(SYST)	Event Weight
p_T Scale	p_T Scale	MUONS_SCALE	p_T Correction
Resolution	Inner Detector Energy Resolution	MUONS_ID	p_T Correction
	Muon Spectrometer Energy Resolution	MUONS_MS	p_T Correction
Electrons			
Efficiencies	Reconstruction	lepSFObjTight_EL_SF_ID	Event Weight
	Identification	lepSFObjTight_EL_SF_Reco	Event Weight
	Isolation	lepSFObjTight_EL_SF_Isol	Event Weight
Scale Factor	Energy Scale	EG_SCALE_ALL	Energy Correction
Resolution	Energy Resolution	EG_RESOLUTION_ALL	Energy Correction
E_T^{miss}			
Soft Tracks Terms	Resolution	MET_SoftTrk_ResoPerp	p_T Correction
	Resolution	MET_SoftTrk_ResoPara	p_T Correction
	Scale	MET_SoftTrk_ScaleUp	p_T Correction
	Scale	MET_SoftTrk_ScaleDown	p_T Correction

Table 10: Summary of experimental systematics considered for leptons and E_T^{miss} . Includes type, description, name of systematic as used in the fit, and mode of application. The mode of application indicates the systematic evaluation, e.g. as an overall event re-weighting (Event Weight) or rescaling (p_T Correction).

Experimental Systematics on Jets			
Type	Origin	Systematics Name	Application
Jet Vertex Tagger		JVT	Event Weight
Energy Scale	Calibration Method	JET_21NP_ JET_EffectiveNP_1-19	p_T Correction p_T Correction
	η inter-calibration	JET_EtaIntercalibration_Modelling JET_EtaIntercalibration_NonClosure JET_EtaIntercalibration_TotalStat	p_T Correction p_T Correction p_T Correction
	High p_T jets	JET_SingleParticle_HighPt	p_T Correction
	Pile-Up	JET_Pileup_OffsetNPV JET_Pileup_OffsetMu JET_Pileup_PtTerm JET_Pileup_RhoTopology	p_T Correction p_T Correction p_T Correction p_T Correction
	Non Closure	JET_PunchThrough_MC15	p_T Correction
	Flavour	JET_Flavor_Response JET_BJES_Response JET_Flavor_Composition	p_T Correction p_T Correction p_T Correction
Resolution		JET_JER_SINGLE_NP	Event Weight

Table 11: Jet systematics take into account effects of jets calibration method, η inter-calibration, high p_T jets, pile-up, and flavor response. They are all diagonalised into effective parameters.

Experimental Systematics on b-tagging		
Type	Origin	Systematic Name
Scale Factors	DL1r b-tagger efficiency on b originated jets in bins of η	DL1r_Continuous_EventWeight_B0-29
	DL1r b-tagger efficiency on c originated jets in bins of η	DL1r_Continuous_EventWeight_C0-19
	DL1r b-tagger efficiency on light flavoured originated jets in bins of η and p_T	DL1r_Continuous_EventWeight_Light0-79
	DL1r b-tagger extrapolation efficiency	DL1r_Continuous_EventWeight_extrapolation DL1r_Continuous_EventWeight_extrapolation_from_charm

Table 12: Summary of experimental systematics to be included for b-tagging of jets in the analysis, using the continuous DL1r tagging algorithm. All of the b-tagging related systematics are applied as event weights. From left: type, description, and the name of systematic used in the fit.

467 Theoretical uncertainties applied to MC predictions, including cross section, PDF, and scale
 468 uncertainties are taken from theory calculations, with the exception of non-prompt and diboson
 469 backgrounds. The cross-section uncertainty on tZ is taken from [23]. Derivation of the non-
 470 prompt background uncertainties, Z+jets and tt}, are explained in detail in Section 5.3. These
 471 normalization uncertainties are chosen so as to account for the complete uncertainty in the
 472 non-prompt contribution, and therefore no additional modelling uncertainties are considered for
 473 Z+jets and tt}.

474 The other VV + heavy flavor processes (namely VV+b and VV+charm, which primarily consist
 475 of ZZ events) are also poorly understood, because these processes involve the same physics as
 476 WZ + heavy flavor, and have also not been measured. Therefore, a conservative 50% uncertainty
 477 is applied to those samples. While this uncertainty is large, it is found to have little impact on
 478 the significance of the final result.

479 The theory uncertainties applied to the predominate background estimates are summarized in
 480 Table 13.

Process	X-section [%]
tZ	X-sec: ± 15.2 QCD Scale: $^{+5.2}_{-1.3}$ PDF($+\alpha_S$): ± 1.2
t <bar>t} H (aMC@NLO+Pythia8)</bar>	QCD Scale: $^{+5.8}_{-9.2}$ PDF($+\alpha_S$): ± 3.6
t <bar>t} Z (aMC@NLO+Pythia8)</bar>	QCD Scale: $^{+9.6}_{-11.3}$ PDF($+\alpha_S$): ± 4
t <bar>t} W (aMC@NLO+Pythia8)</bar>	QCD Scale: $^{+12.9}_{-11.5}$ PDF($+\alpha_S$): ± 3.4
VV + b/charm (Sherpa 2.2.1)	± 50
VV + light (Sherpa 2.2.1)	± 6
t <bar>t}</bar>	± 20
Z + jets	± 25
Others	± 50

Table 13: Summary of theoretical uncertainties for MC predictions in the analysis.

481 Additional signal uncertainties are estimated by comparing estimates from the nominal Sherpa
 482 WZ samples with alternate WZ samples generated with Powheg+PYTHIA8 (DSID 361601).
 483 MC/MC scale factors are applied to make these comparisons. The shape of the templates used
 484 in the fit are compared between these two samples for WZ + b, WZ + charm and WZ + light,
 485 as shown in Figures 28 and 29. Each of these plots are normalized to unity in order to capture
 486 differences in shape.

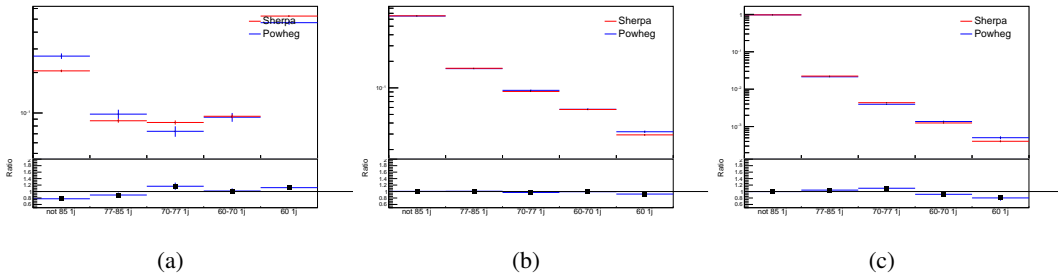


Figure 28: Comparison between Sherpa and Powheg predictions of the distribution of (a) WZ + b, (b) WZ + charm, and (c) WZ + light among the various b-tag WPs used in the 1-jet fit.

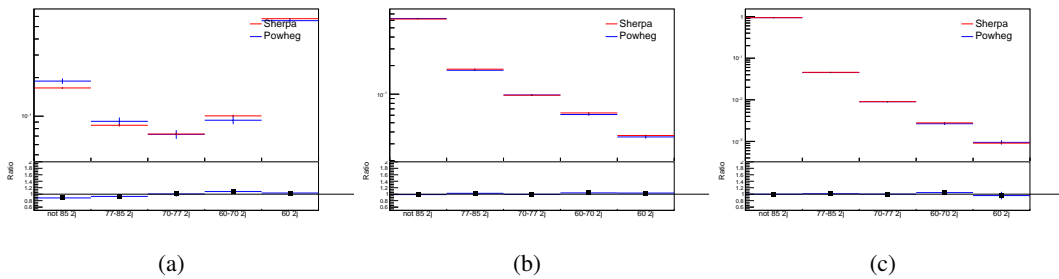


Figure 29: Comparison between Sherpa and Powheg predictions of the distribution of (a) WZ + b, (b) WZ + charm, and (c) WZ + light among the various b-tag WPs used in the 2-jet fit.

⁴⁸⁷ Separate systematics are included in the fit for WZ + b, WZ + charm and WZ + light, where
⁴⁸⁸ the distribution among each of the fit regions is varied based on the prediction of the Powheg
⁴⁸⁹ sample.

490 A similar approach is taken to account for uncertainties in migrations between the number of
491 reco and truth jets. The fraction of events with 1 truth jet which fall into the 1 jet bin versus the
492 2 jet bin at reco level is compared for Sherpa and Powheg. The same is done for events with 2
493 truth jets. This comparison is shown in figure 30.

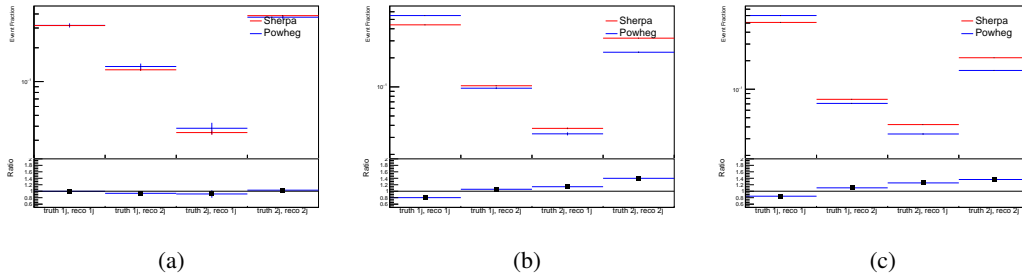


Figure 30: Comparison between Sherpa and Powheg predictions for truth jet migrations between the 1 and 2 jet reco bins for (a) WZ + b, (b) WZ + charm, and (c) WZ + light

494 A systematic is included where events are shifted between the 1-jet and 2-jet regions based on
495 the differences between these two shapes. This is done independently for each of the WZ + b,
496 WZ + charm, and WZ + light templates.

Additional systematics are included to account for the uncertainty in the contamination of 0 jet and 3 or more jet events (at truth level) in the 1 and 2 reco jet bins. Because these events fall outside the scope of this measurement, these events are included as a background. As such, a normalization, rather than a shape, uncertainty is applied for this background.

501 The number of WZ events with 0-jets and ≥ 3 -jets in the reconstructed 1-jet and 2-jet regions
 502 are compared for Sherpa and Powheg, as seen in figure 31. These differences are taken as separate
 503 normalization systematics on the yield of WZ+0-jet and WZ+ ≥ 3 -jet events.

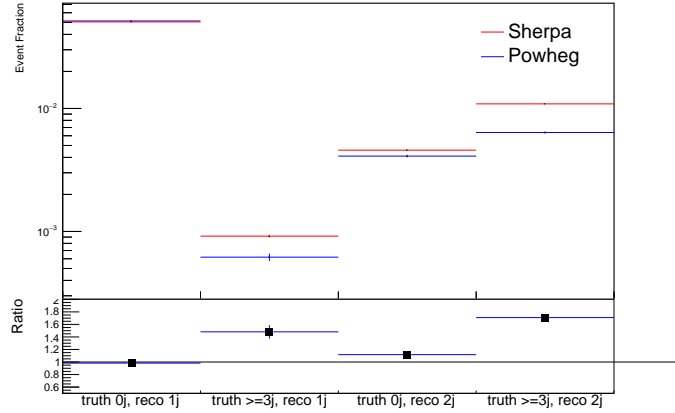


Figure 31: Comparison between Sherpa and Powheg predictions for 0 and ≥ 3 truth jet contributions in the 1 and 2 jet reco bins

504 8 Results

505 8.1 Fit Procedure

506 A maximum-likelihood fit is performed over the various fit regions described in Section 5 in
 507 order to extract the best-fit value of the WZ + b-jet and WZ + charm jet contributions for events
 508 with both 1 and 2 associated jets.

509 Because the fit regions are defined by the number of associated jets at reco-level, an unfolding
 510 procedure is applied to the signal in order to account for differences in the number of truth jets
 511 compared to the number of reco-jets. The WZ + b, WZ + charm and WZ + light contributions
 512 are separated into independent samples based on the number of truth jets in each event. WZ + 1
 513 truth-jet and WZ + 2 truth-jets are treated as signal samples, while WZ + 0 truth-jets and WZ +
 514 ≥ 3 truth-jets are treated as an additional background.

515 A maximum likelihood fit to data is performed simultaneously in the regions described in Section
 516 5, summarized in figure 32. The six signal templates, which include WZ+b 1-jet, WZ+c 1-jet,
 517 WZ+l 1-jet, WZ+b 2-jets, WZ+c 2-jets, WZ+l 2-jets, are allowed to float, while the remaining
 518 background contributions are held fixed. The parameters $\mu_{WZ+b-1-jet}$, $\mu_{WZ+charm1-jet}$,
 519 $\mu_{WZ+light-1-jet}$, $\mu_{WZ+b-2-jet}$, $\mu_{WZ+charm2-jet}$, $\mu_{WZ+light-2-jet}$, where $\mu = \sigma_{\text{observed}}/\sigma_{\text{SM}}$,
 520 are extracted from the fit. A simultaneous fit is performed over all 1-jet and 2-jet regions.

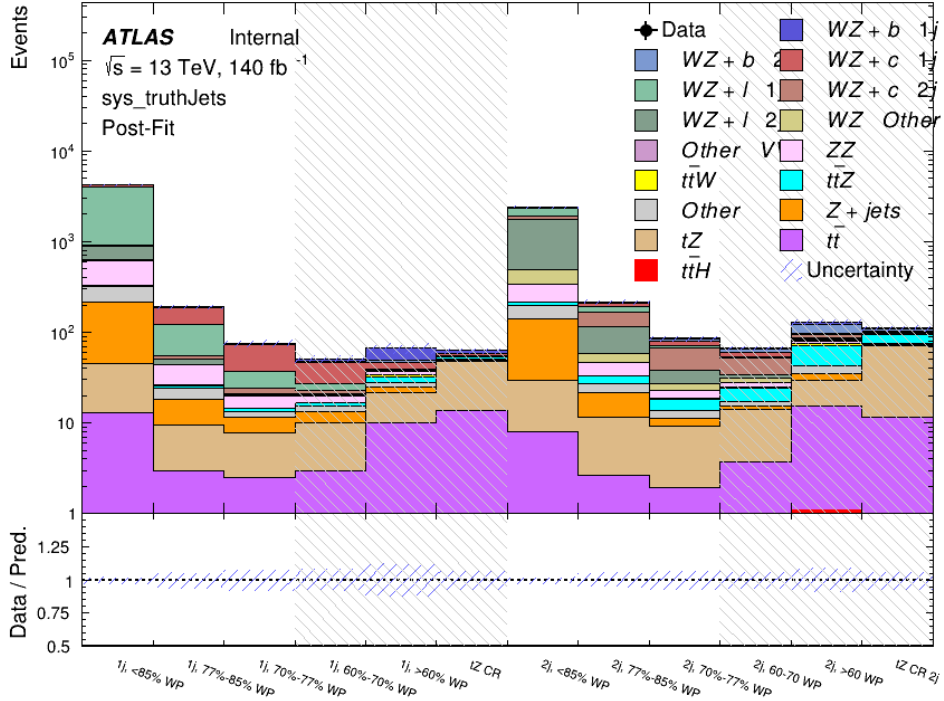


Figure 32: Post-fit summary of the fit regions.

As described in Section 7, there are 229 systematic uncertainties that are considered as NPs in the fit. These NPs are constrained by Gaussian or log-normal probability density functions. The latter are used for normalisation factors to ensure that they are always positive. The expected number of signal and background events are functions of the likelihood. The prior for each NP is added as a penalty term, decreasing the likelihood as it is shifted away from its nominal value. The correlations between these nuisance parameters are summarized in Figure 33.

The result of the fit is used to extract the cross-section of $WZ +$ heavy-flavor production in the fiducial region defined below:

- Three light leptons with total charge ± 1
- One OSSF lepton pair with $|M(l\bar{l}) - 91.2 \text{ GeV}| < 10 \text{ GeV}$
- One or two associated jets with $p_T > 25 \text{ GeV}$

Several alternate fit strategies are documented in Appendices A.4-A.5.1. These include a measurement of $WZ + 1$ or 2 jets inclusively, a fit where tZ is allowed to float, and a case where tZ is included as part of the signal.

535 **8.2 Independent 1-jet and 2-jet Results**

536 The Asimov fit for 1-jet events gives an expected μ value of $1.00^{+0.47}_{-0.43}(\text{stat})^{+0.30}_{-0.27}(\text{sys})$ for WZ
 537 + b. The fitted cross-section modifiers for WZ + charm and WZ + light are $1.00 \pm 0.17 \pm 0.17$
 538 and $1.00 \pm 0.06 \pm 0.14$, respectively.

539 The expected cross-section of WZ+b with 1-jet is $1.74^{+0.82}_{-0.75}(\text{stat})^{+0.53}_{-0.48}(\text{sys})$ fb, and $14.6 \pm$
 540 $2.5(\text{stat}) \pm 2.3(\text{sys})$ fb for WZ + charm, with a correlation of -0.15 between them. An expected
 541 significance of 2.0 is observed for WZ + b in this region.

542 For 2-jet events, the fit gives an expected μ value of $1.00^{+0.53}_{-0.51}(\text{stat})^{+0.39}_{-0.34}(\text{sys})$ for WZ + b.
 543 The fitted cross-section modifiers for WZ + charm and WZ + light are $1.00 \pm 0.25 \pm 0.21$ and
 544 $1.00 \pm 0.06 \pm 0.16$, respectively.

545 The expected WZ + b cross-section in the 2-jet region is $2.5^{+1.3}_{-1.3}(\text{stat})^{+0.95}_{-0.83}(\text{sys})$ fb with an
 546 expected significance of 1.7σ . The 2-jet expected cross-section of WZ + charm is $12.7 \pm$
 547 $3.2(\text{stat}) \pm 2.7(\text{sys})$ fb, and the correlation between WZ + charm and WZ + b is -0.22.

548 A summary of the correlation between the various WZ components is summarized in Table 14.

549

	WZ + b - 1-jet	WZ + c - 1-jet	WZ + l - 1-jet	WZ + b - 2-jet	WZ + c - 2-jet	WZ + l - 2-jet
WZ + b - 1-jet	1.00	-0.15	0.28	-0.13	-0.22	0.17
WZ + c - 1-jet	-	1.00	0.36	0.13	-0.14	-0.16
WZ + l - 1-jet	-	-	1.00	0.10	-0.20	-0.39
WZ + b - 2-jet	-	-	-	1.00	-0.22	0.17
WZ + c - 2-jet	-	-	-	-	1.00	0.23
WZ + l - 2-jet	-	-	-	-	-	1.00

Table 14: Correlations between the various components of WZ

550 The correlations between the all of the nuisance parameters considered in the fit are summarized
 551 in Figure 33.a

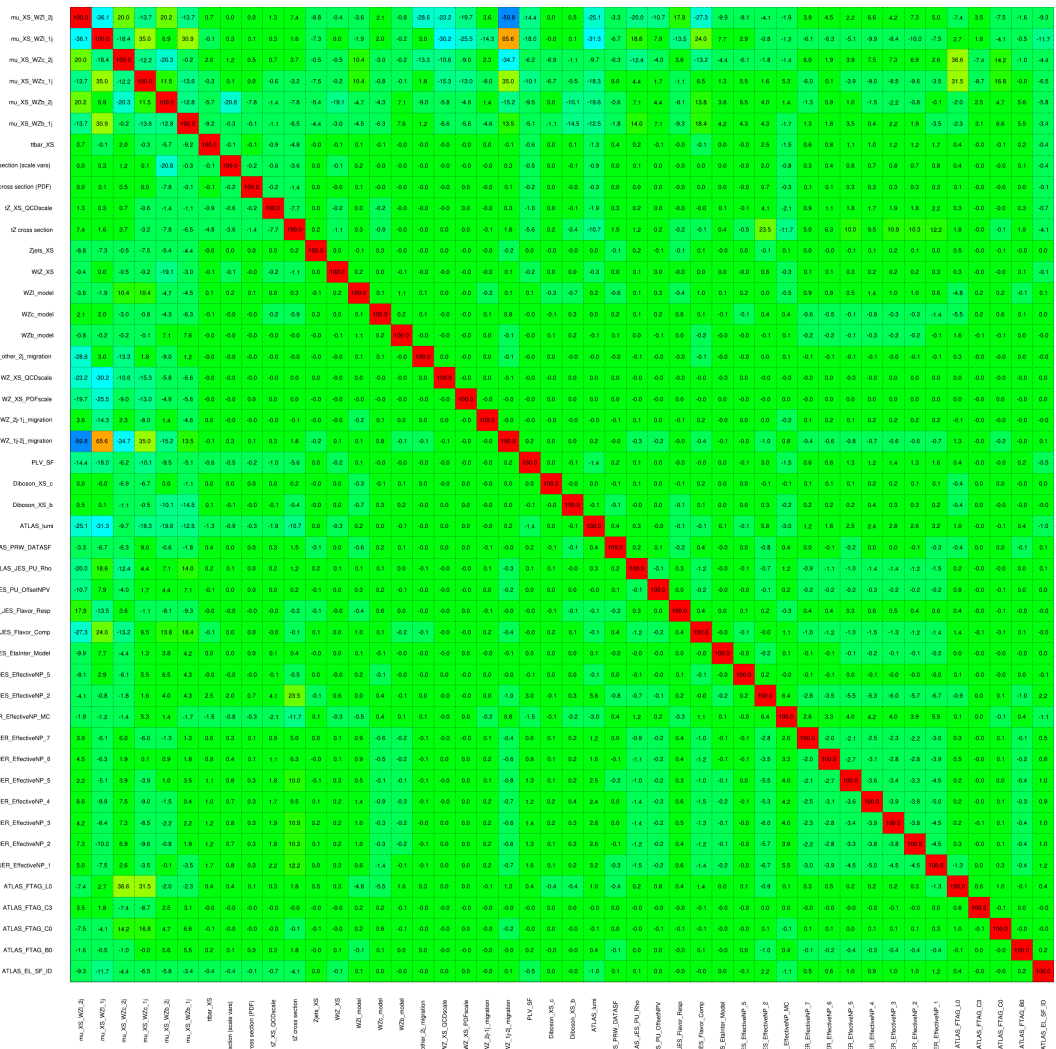


Figure 33: Correlations between nuisance parameters

552 The pre-fit yields in each of the 1-jet regions used in the fit are shown in Table 8.2.

Sample	1j, <85% WP	1j, 77%-85% WP	1j, 70%-77% WP	1j, 60%-70% WP	1j, >60% WP	tZ CR
WZ + b – 1j	8.1 ± 1.6	4.7 ± 0.5	4.6 ± 0.4	5.1 ± 0.4	18.1 ± 2.4	5.0 ± 0.6
WZ + c – 1j	260 ± 22	81 ± 6	43.1 ± 3.6	25.8 ± 2.6	9.4 ± 1.8	2.9 ± 0.6
WZ + l – 1j	3090 ± 250	91 ± 13	17 ± 3	4.9 ± 1.6	1.3 ± 0.4	0.2 ± 0.1
WZ + b – 2j	1.10 ± 0.37	0.44 ± 0.11	0.39 ± 0.06	0.62 ± 0.14	2.1 ± 0.5	0.59 ± 0.14
WZ + c – 2j	21 ± 5	5.6 ± 1.2	3.0 ± 0.7	2.0 ± 0.5	0.70 ± 0.20	0.30 ± 0.08
WZ + l – 2j	250 ± 60	5.7 ± 1.6	0.73 ± 0.53	0.31 ± 0.15	0.07 ± 0.06	0.01 ± 0.01
WZ – Other	13 ± 5	1.4 ± 0.4	0.42 ± 0.08	0.2 ± 0.01	0.30 ± 0.05	0.67 ± 0.15
Other VV	6.2 ± 0.6	0.2 ± 0.4	0.2 ± 0.04	0.07 ± 0.1	0.1 ± 0.1	0.1 ± 0.2
ZZ	336 ± 26	17.8 ± 2.1	4.3 ± 0.6	1.7 ± 0.5	0.36 ± 0.08	0.10 ± 0.03
t <bar>t>W</bar>	1.1 ± 0.2	0.2 ± 0.1	0.3 ± 0.1	0.4 ± 0.1	1.5 ± 0.3	0.7 ± 0.2
t <bar>t>Z</bar>	6.8 ± 1.2	1.4 ± 0.3	1.0 ± 0.2	1.2 ± 0.2	4.4 ± 0.8	3.2 ± 0.6
Z + jets	169 ± 38	8.9 ± 1.9	3.7 ± 0.8	3.3 ± 0.7	3.2 ± 0.7	0.8 ± 0.17
V + γ	45 ± 28	1.9 ± 2.4	0.1 ± 0.1	0.02 ± 0.01	1.0 ± 0.9	0.02 ± 0.03
tZ	31.8 ± 4.3	6.4 ± 1.1	5.3 ± 0.8	7.2 ± 1.1	11.8 ± 2.0	33.9 ± 4.5
tW	1.4 ± 0.8	0.2 ± 0.5	0.0 ± 0.2	0.7 ± 0.6	0.26 ± 0.42	0.39 ± 0.41
WtZ	2.3 ± 1.2	0.6 ± 0.3	0.3 ± 0.21	0.27 ± 0.2	1.1 ± 0.7	0.6 ± 0.5
VVV	12.4 ± 0.5	0.93 ± 0.06	0.35 ± 0.03	0.13 ± 0.02	0.14 ± 0.03	0.02 ± 0.01
VH	40 ± 6	2.6 ± 1.4	0.9 ± 0.8	0.7 ± 0.8	0.5 ± 0.6	0.0 ± 0.0
t <bar>t></bar>	12.1 ± 1.6	2.9 ± 0.6	2.5 ± 0.5	2.8 ± 0.5	11.2 ± 1.4	10.9 ± 1.5
t <bar>t>H</bar>	0.24 ± 0.03	0.05 ± 0.01	0.04 ± 0.01	0.06 ± 0.01	0.20 ± 0.03	0.13 ± 0.02
Total	5010 ± 260	227 ± 24	88 ± 12	57 ± 8	76 ± 16	53 ± 8

Table 15: Pre-fit yields in each of the 1-jet regions.

⁵⁵⁴ The post-fit yields in each region are summarized in Figure 8.2.

⁵⁵⁵

	1j, <85% WP	1j, 77%-85% WP	1j, 70%-77% WP	1j, 60%-70% WP	1j, >60% WP	tZ CR
WZ + b – 1j	8.1 ± 4.9	4.7 ± 2.0	4.6 ± 2.0	5.1 ± 2.1	18 ± 10	5.0 ± 2.5
WZ + c – 1j	260 ± 60	80 ± 14	43 ± 7	26 ± 5	7.4 ± 2.3	2.1 ± 0.7
WZ + l – 1j	3090 ± 130	90 ± 11	17.3 ± 2.8	4.9 ± 1.6	1.3 ± 0.4	0.23 ± 0.13
WZ + b – 2j	1.10 ± 0.37	0.44 ± 0.11	0.39 ± 0.06	0.62 ± 0.14	2.1 ± 0.5	0.59 ± 0.14
WZ + c – 2j	21 ± 5	5.6 ± 1.2	3.0 ± 0.7	2.0 ± 0.5	0.70 ± 0.20	0.30 ± 0.08
WZ + l – 2j	250 ± 60	5.7 ± 1.6	0.73 ± 0.53	0.31 ± 0.15	0.07 ± 0.06	0.01 ± 0.01
WZ – Other	13 ± 5	1.4 ± 0.4	0.42 ± 0.08	0.2 ± 0.01	0.30 ± 0.05	0.67 ± 0.15
Other VV	6.2 ± 0.6	0.92 ± 0.07	0.02 ± 0.01	0.01 ± 0.01	0.01 ± 0.01	0.01 ± 0.01
ZZ	346 ± 57	19 ± 5	4.3 ± 0.8	2.7 ± 0.5	2.4 ± 0.1	2.1 ± 0.6
t̄W	1.09 ± 0.21	0.2 ± 0.1	0.1 ± 0.1	0.4 ± 0.1	1.5 ± 0.3	0.1 ± 0.2
t̄Z	6.8 ± 1.2	1.4 ± 0.3	1.0 ± 0.2	1.2 ± 0.2	4.4 ± 0.7	3.2 ± 0.5
rare Top	0.14 ± 0.04	0.04 ± 0.02	0.04 ± 0.0	0.1 ± 0.03	0.14 ± 0.04	0.15 ± 0.05
t̄WW	0.04 ± 0.03	0.01 ± 0.02	0.01 ± 0.01	0.01 ± 0.01	0.01 ± 0.02	0.01 ± 0.01
Z + jets	169 ± 37	8.9 ± 1.9	3.7 ± 0.8	3.3 ± 0.7	3.2 ± 0.7	0.8 ± 0.2
W + jets	0.01 ± 0.01					
V + γ	46 ± 28	1.9 ± 2.4	0.1 ± 0.1	0.0 ± 0.2	1.0 ± 0.9	0.0 ± 0.0
tZ	31 ± 4	6.0 ± 1.0	5.3 ± 0.8	7.2 ± 1.0	11.8 ± 1.8	33.9 ± 4.5
tW	1.37 ± 0.82	0.18 ± 0.26	0.01 ± 0.12	0.67 ± 0.64	0.26 ± 0.42	0.39 ± 0.41
WtZ	2.3 ± 1.2	0.6 ± 0.3	0.3 ± 0.2	0.3 ± 0.2	1.1 ± 0.6	0.6 ± 0.3
VVV	12.4 ± 0.4	0.9 ± 0.1	0.4 ± 0.1	0.13 ± 0.02	0.14 ± 0.03	0.02 ± 0.01
VH	40 ± 6	2.6 ± 1.4	0.9 ± 0.8	0.7 ± 0.8	0.4 ± 0.6	0.01 ± 0.01
t̄t	12.1 ± 1.6	2.9 ± 0.6	2.5 ± 0.5	2.8 ± 0.5	11.2 ± 1.5	10.9 ± 1.4
t̄tH	0.24 ± 0.03	0.05 ± 0.01	0.04 ± 0.01	0.06 ± 0.01	0.20 ± 0.03	0.13 ± 0.02
Total	5100 ± 110	227 ± 12	87 ± 6	56.7 ± 4.4	76 ± 9	52.5 ± 4.2

Table 16: Post-fit yields in each of the 1-jet regions.

556 The impact of each NP is calculated by performing the fit with the parameter of interest held
 557 fixed, varied from its fitted value by its uncertainty, and calculating $\Delta\mu$ relative to the baseline
 558 fit. The impact of the most significant sources of systematic uncertainties on WZ + b with one
 559 associated jet is summarized in Table 17.

Uncertainty Source	$\Delta\mu$	
WZ + 1-jet light XS	0.13	-0.18
WZ + charm cross-section	-0.10	0.12
Jet Energy Scale	0.1	-0.13
tZ cross-section	-0.10	0.10
WZ 1-jet/2-jet Migration	0.08	-0.07
Jet Energy Resolution	-0.10	0.10
Luminosity	-0.08	0.09
Other Diboson + b cross-section	-0.07	0.07
Flavor tagging	0.05	0.05
t <bar>t} cross-section</bar>	-0.05	0.05
Total Systematic Uncertainty	0.29	0.34

Table 17: Summary of the most significant sources of systematic uncertainty on the measurement of WZ + b with exactly one associated jet.

560 The ranking and impact of those nuisance parameters with the largest contribution to the overall
561 uncertainty is shown in Figure 34.

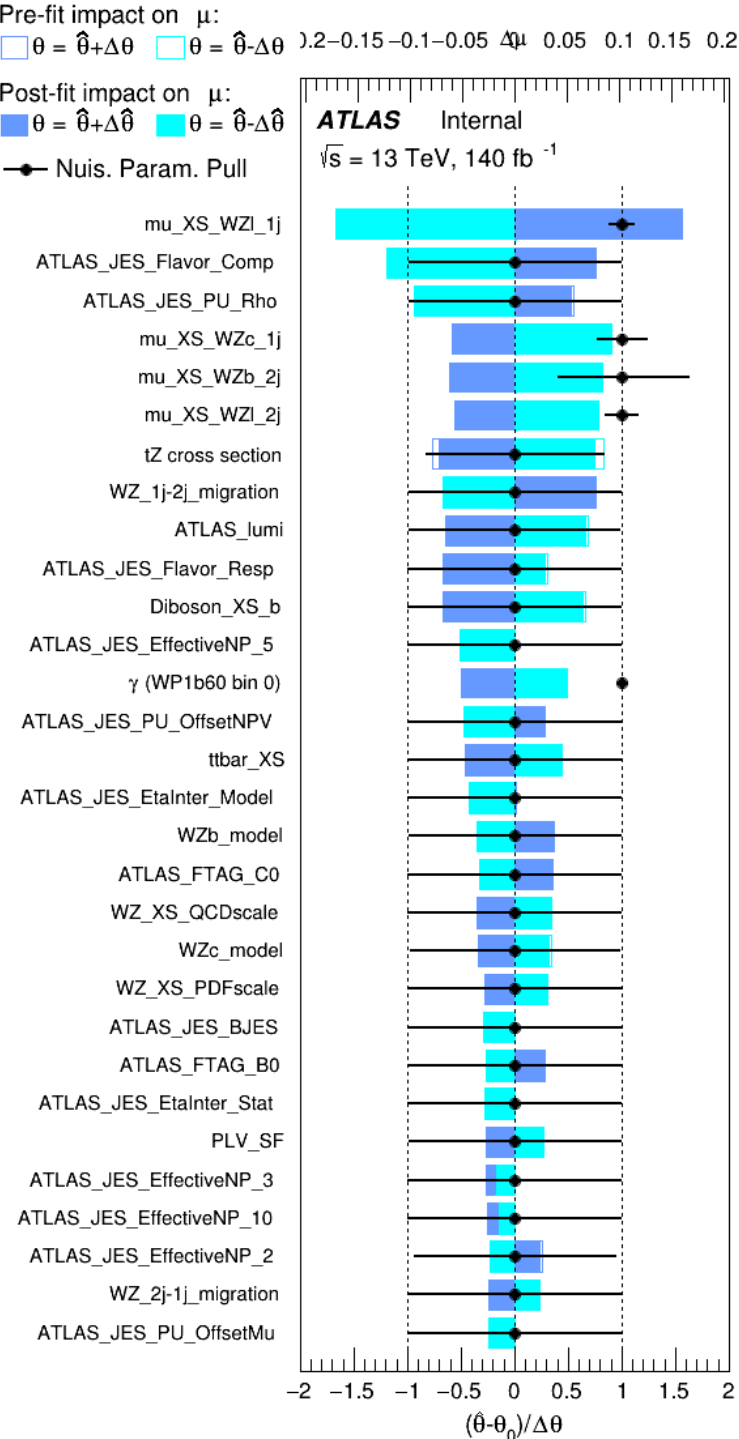


Figure 34: Impact of systematic uncertainties on the signal-strength of $WZ + b$ for events with exactly one jet

⁵⁶² The large impact of the Jet Energy Scale and Jet Flavor Tagging is unsurprising, as the shape of
⁵⁶³ the fit regions depends heavily on the modeling of the jets. The other major sources of uncertainty
⁵⁶⁴ come from background modelling and cross-section uncertainty.

⁵⁶⁵ Pre-fit yields in each of the 2-jet fit are shown in Figure 8.2.

	2j, <85% WP	2j, 77%-85% WP	2j, 70%-77% WP	2j, 60%-70% WP	2j, >60% WP	tZ CR 2j
WZ + b - 2j	3.1 ± 1.6	6.7 ± 0.5	5.6 ± 0.4	8.0 ± 0.6	24 ± 2	5 ± 1
WZ + c - 2j	180 ± 20	54 ± 6	41 ± 3	24 ± 3	17 ± 2	7.0 ± 0.6
WZ + l - 2j	1250 ± 150	90 ± 14	18 ± 3	5.8 ± 1.4	1.4 ± 0.4	0.25 ± 0.15
WZ + b - 1j	3.4 ± 0.6	1.52 ± 0.35	1.58 ± 0.23	1.95 ± 0.39	7.8 ± 1.1	0.8 ± 0.6
WZ + c - 1j	56 ± 14	17.6 ± 4.0	8.6 ± 2.2	6.3 ± 1.8	3.0 ± 0.9	0.7 ± 0.2
WZ + l - 1j	427 ± 120	24 ± 7	4.7 ± 2.3	1.6 ± 0.7	0.3 ± 0.2	0.01 ± 0.01
WZ - Other	129 ± 29	6.1 ± 4.6	1.2 ± 0.3	0.3 ± 0.2	2.9 ± 0.5	3.6 ± 0.6
Other VV	7.63 ± 0.63	0.6 ± 0.5	0.16 ± 0.03	0.01 ± 0.01	0.1 ± 0.1	0.1 ± 0.1
ZZ	135 ± 20	14.1 ± 3.2	4.7 ± 0.8	4.0 ± 0.6	4.1 ± 0.7	3.1 ± 0.5
t̄tW	0.8 ± 0.2	0.4 ± 0.1	0.5 ± 0.1	0.7 ± 0.2	4.3 ± 0.6	3.9 ± 0.6
t̄tZ	14.7 ± 2.2	5.6 ± 0.8	4.5 ± 0.7	6.5 ± 1.1	25.4 ± 4.0	21.9 ± 3.4
rare Top	0.14 ± 0.04	0.07 ± 0.03	0.03 ± 0.02	0.09 ± 0.03	0.37 ± 0.07	0.6 ± 0.1
t̄tWW	0.04 ± 0.03	0.02 ± 0.02	0.01 ± 0.01	0.01 ± 0.00	0.03 ± 0.03	0.01 ± 0.01
Z + jets	110.0 ± 22.9	9.6 ± 2.0	2.1 ± 0.50	1.6 ± 0.4	5.1 ± 1.1	1.5 ± 0.3
W + jets	0.0 ± 0.0	0.0 ± 0.0	0.0 ± 0.0	0.0 ± 0.0	0.0 ± 0.0	0.0 ± 0.0
V + γ	25 ± 18	0.5 ± 0.2	0.1 ± 0.1	0.1 ± 0.1	0.0 ± 0.02	0.05 ± 0.07
tZ	21.9 ± 2.9	9.6 ± 1.3	9.1 ± 1.0	10.0 ± 1.5	14.7 ± 3.2	60 ± 6
tW	0.9 ± 0.7	0.2 ± 0.3	0.0 ± 0.1	0.0 ± 0.0	0.8 ± 0.6	0.2 ± 0.2
WtZ	4.9 ± 2.5	1.5 ± 0.8	1.1 ± 0.6	1.3 ± 0.7	4.6 ± 2.4	3.3 ± 1.7
VVV	7.4 ± 0.3	1.0 ± 0.1	0.4 ± 0.1	0.2 ± 0.1	0.13 ± 0.03	0.04 ± 0.01
VH	19.5 ± 4.2	2.8 ± 1.6	0.7 ± 0.7	0.1 ± 0.2	0.0 ± 0.0	0.0 ± 0.0
t̄t	0.7 ± 0.4	0.1 ± 0.1	0.05 ± 0.06	0.15 ± 0.13	0.8 ± 0.5	2.3 ± 1.2
t̄t	6.8 ± 1.0	2.4 ± 0.5	1.8 ± 0.4	3.3 ± 0.6	8.4 ± 1.2	13.6 ± 1.7
t̄tH	0.4 ± 0.1	0.2 ± 0.1	0.16 ± 0.02	0.23 ± 0.03	0.94 ± 0.11	1.03 ± 0.12
Total	2580 ± 160	229 ± 24	89 ± 13	69 ± 11	120 ± 15	108 ± 11

Table 18: Pre-fit yields in each of the 2-jet regions.

⁵⁶⁶ The post-fit yields in each region are summarized in Figure 8.2.

	2j, <85% WP	2j, 77%-85% WP	2j, 70%-77% WP	2j, 60%-70% WP	2j, >60% WP	tZ CR 2j
WZ + b	13 ± 6	6.7 ± 2.9	5.8 ± 2.5	8.0 ± 3.5	31 ± 13	14 ± 5
WZ + c	260 ± 60	77 ± 15	41 ± 8	26 ± 5	10.9 ± 2.4	4.8 ± 1.1
WZ + l	1860 ± 90	90 ± 12	17.6 ± 2.8	5.8 ± 1.3	1.4 ± 0.4	0.3 ± 0.2
WZ + b - 1j	3.4 ± 0.6	1.52 ± 0.35	1.58 ± 0.23	1.95 ± 0.39	6.7 ± 1.1	1.9 ± 0.6
WZ + c - 1j	56 ± 14	17.6 ± 4.0	8.6 ± 2.2	6.3 ± 1.8	3.0 ± 0.9	0.7 ± 0.2
WZ + l - 1j	427 ± 120	24 ± 7	4.7 ± 2.3	1.6 ± 0.7	0.3 ± 0.2	0.01 ± 0.01
WZ - Other	129 ± 29	6.1 ± 4.6	1.2 ± 0.3	0.3 ± 0.2	2.9 ± 0.5	3.6 ± 0.6
Other VV	7.6 ± 0.6	0.3 ± 0.3	0.3 ± 0.1	0.1 ± 0.06	0.03 ± 0.02	0.1 ± 0.1
ZZ	145 ± 30	11.3 ± 4.4	2.7 ± 1.6	1.0 ± 0.3	4.0 ± 0.1	2.4 ± 0.1
t̄tW	0.8 ± 0.2	0.4 ± 0.1	0.54 ± 0.12	0.74 ± 0.15	4.3 ± 0.6	3.9 ± 0.6
t̄tZ	14.7 ± 2.2	5.6 ± 0.8	4.5 ± 0.7	6.5 ± 1.0	25.4 ± 3.9	21.9 ± 3.3
rare Top	0.14 ± 0.04	0.07 ± 0.03	0.03 ± 0.02	0.09 ± 0.03	0.4 ± 0.1	0.6 ± 0.1
t̄tWW	0.04 ± 0.03	0.02 ± 0.02	0.01 ± 0.01	0.01 ± 0.01	0.03 ± 0.03	0.01 ± 0.01
Z + jets	110 ± 23	9.6 ± 2.0	2.1 ± 0.5	1.6 ± 0.4	5.1 ± 1.1	1.5 ± 0.3
W + jets	0.0 ± 0.0					
V + γ	25 ± 19	0.5 ± 0.2	0.1 ± 0.1	0.13 ± 0.14	0.0 ± 0.02	0.05 ± 0.07
tZ	21.9 ± 2.7	9.6 ± 1.2	7.1 ± 0.9	10.0 ± 1.4	14.7 ± 3.0	60 ± 6
tW	0.1 ± 0.7	0.2 ± 0.3	0.0 ± 0.1	0.0 ± 0.0	0.8 ± 0.6	0.2 ± 0.2
WtZ	4.9 ± 2.5	1.5 ± 0.8	1.1 ± 0.6	1.3 ± 0.7	4.6 ± 2.3	3.3 ± 1.7
VVV	7.4 ± 0.3	1.0 ± 0.1	0.36 ± 0.03	0.19 ± 0.03	0.13 ± 0.03	0.04 ± 0.01
VH	19 ± 4	2.8 ± 1.6	0.7 ± 0.7	0.1 ± 0.2	0.0 ± 0.0	0.0 ± 0.0
t̄t	6.8 ± 1.0	2.4 ± 0.5	1.8 ± 0.4	3.3 ± 0.6	8.4 ± 1.2	13.6 ± 1.7
t̄tH	0.40 ± 0.05	0.19 ± 0.03	0.16 ± 0.02	0.23 ± 0.03	0.94 ± 0.11	1.03 ± 0.11
Total	2580 ± 60	229 ± 11	89 ± 6	69.1 ± 4.1	120 ± 10	108 ± 6

Table 19: Post-fit yields in each of the 2-jet regions.

⁵⁶⁷ The same set of systematic uncertainties consider for the 1-jet fit are included in the 2-jet fit as
⁵⁶⁸ well. The impact of the most significant systematic uncertainties is summarized in Table 20.

Uncertainty Source	$\Delta\mu$	
WZ + c 2-jet cross-section	0.19	0.15
WZ 0-jet, $>=3$ -jet cross-section	0.14	-0.14
Luminosity	-0.11	0.12
tZ cross-section	-0.11	0.11
Jet Energy Scale	-0.11	0.11
ttZ cross-section - QCD scale	-0.08	0.09
WZ + l cross-section	0.08	-0.07
WtZ cross-section	-0.07	0.07
Flavor tagging	0.05	0.05
Other VV + b cross-section	-0.05	0.05
Total	0.32	0.36

Table 20: Summary of the most significant sources of systematic uncertainty on the measurement of WZ + b 2-jet events.

⁵⁶⁹ The ranking and impact of those nuisance parameters with the largest contribution to the overall
⁵⁷⁰ uncertainty is shown in Figure 35.

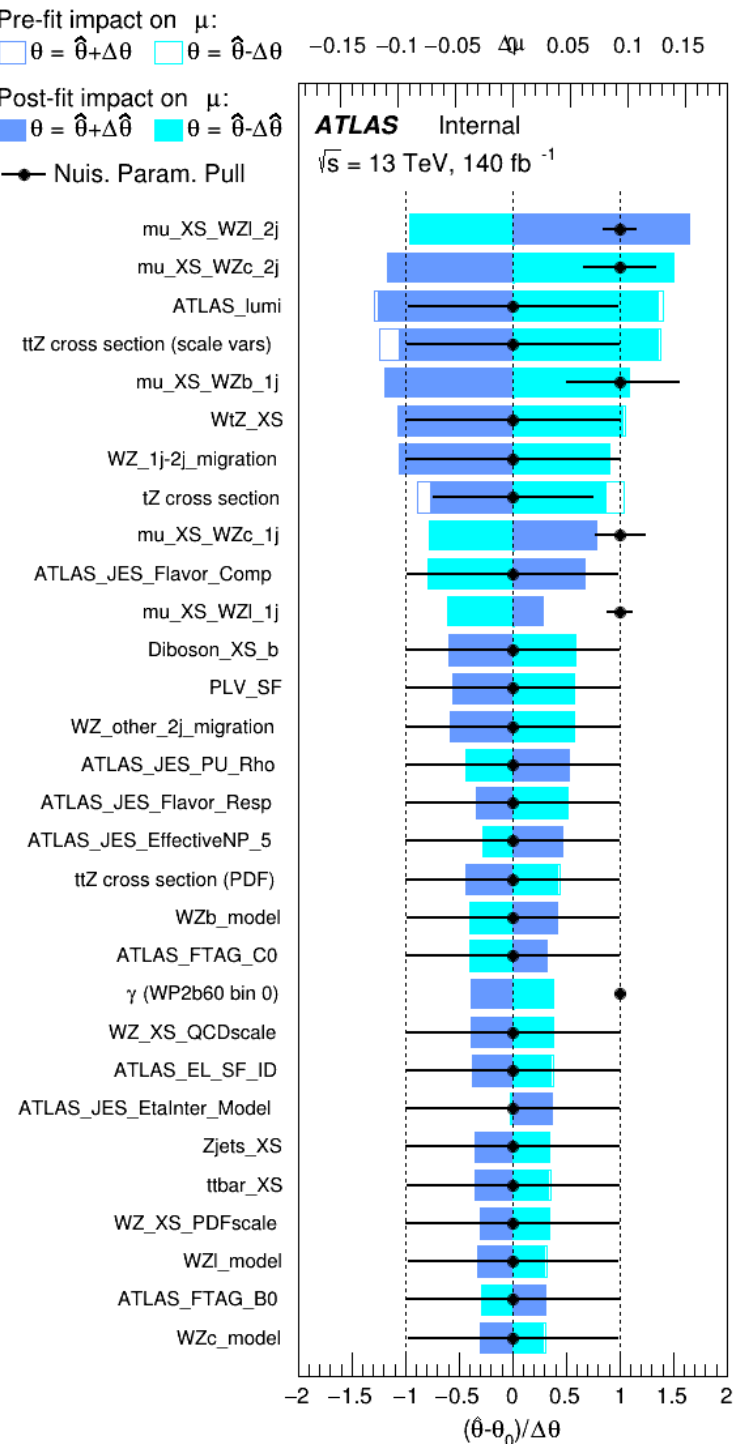


Figure 35: Impact of systematic uncertainties on the signal-strength of $WZ + b$ in 2-jet events.

571 The large impact of the Jet Energy Scale and Jet Flavor Tagging is unsurprising, as the shape of
 572 the fit regions depends heavily on the modeling of the jets. The other major sources of uncertainty
 573 come from background modelling and cross-section uncertainty.

574 9 Conclusion

575 A measurement of $WZ +$ heavy flavor is performed using 140 fb^{-1} of $\sqrt{s} = 13 \text{ TeV}$ proton-
 576 proton collision data collected by the ATLAS detector at the LHC. The expected cross-section
 577 of $WZ+b$ with 1-jet is $1.74^{+0.82}_{-0.75}(\text{stat})^{+0.53}_{-0.48}(\text{sys}) \text{ fb}$, and $14.6 \pm 2.5(\text{stat}) \pm 2.3(\text{sys}) \text{ fb}$ for WZ
 578 + charm, with a correlation of -0.22 between them. An expected significance of 2.0 is observed
 579 for $WZ + b$ in this region.

580 For the 2-jet regions, an expected significance of 1.7 is observed for $WZ + b$, with an ex-
 581 pected cross-section of $2.5^{+1.3}_{-1.3}(\text{stat})^{+0.95}_{-0.83}(\text{sys}) \text{ fb}$. For $WZ +$ charm, a cross-section of
 582 $12.7 \pm 3.2(\text{stat}) \pm 2.7(\text{sys}) \text{ fb}$ is expected for 2-jet events. A correlation of -0.26 is observed
 583 for $WZ+b$ and $WZ +$ charm.

584 **This section will be include final results once unblinded.**

585 References

- 586 [1] M. Aaboud et al. ‘Observation of electroweak $W^\pm Z$ boson pair production in association
 587 with two jets in pp collisions at $\sqrt{s} = 13 \text{ TeV}$ with the ATLAS detector’. In: *Phys.
 588 Lett.* B793 (2019), pp. 469–492. doi: [10.1016/j.physletb.2019.05.012](https://doi.org/10.1016/j.physletb.2019.05.012). arXiv:
 589 [1812.09740 \[hep-ex\]](https://arxiv.org/abs/1812.09740).
- 590 [2] T. Gleisberg et al. ‘Event generation with SHERPA 1.1’. In: *JHEP* 02 (2009), p. 007. doi:
 591 [10.1088/1126-6708/2009/02/007](https://doi.org/10.1088/1126-6708/2009/02/007). arXiv: [0811.4622 \[hep-ph\]](https://arxiv.org/abs/0811.4622).
- 592 [3] R. D. Ball et al. ‘Parton distributions for the LHC Run II’. In: *JHEP* 04 (2015), p. 040.
 593 doi: [10.1007/JHEP04\(2015\)040](https://doi.org/10.1007/JHEP04(2015)040). arXiv: [1410.8849 \[hep-ph\]](https://arxiv.org/abs/1410.8849).
- 594 [4] H.-L. Lai et al. ‘New parton distributions for collider physics’. In: *Phys. Rev. D* 82 (2010),
 595 p. 074024. doi: [10.1103/PhysRevD.82.074024](https://doi.org/10.1103/PhysRevD.82.074024). arXiv: [1007.2241 \[hep-ph\]](https://arxiv.org/abs/1007.2241).
- 596 [5] S. Frixione, G. Ridolfi and P. Nason. ‘A positive-weight next-to-leading-order Monte Carlo
 597 for heavy flavour hadroproduction’. In: *JHEP* 09 (2007), p. 126. doi: [10.1088/1126-6708/2007/09/126](https://doi.org/10.1088/1126-

 598 6708/2007/09/126). arXiv: [0707.3088 \[hep-ph\]](https://arxiv.org/abs/0707.3088).
- 599 [6] E. Re. ‘Single-top Wt-channel production matched with parton showers using the POWHEG
 600 method’. In: *Eur. Phys. J. C* 71 (2011), p. 1547. doi: [10.1140/epjc/s10052-011-1547-z](https://doi.org/10.1140/epjc/s10052-011-

 601 1547-z). arXiv: [1009.2450 \[hep-ph\]](https://arxiv.org/abs/1009.2450).
- 602 [7] ATLAS Collaboration. *Electron efficiency measurements with the ATLAS detector using
 603 the 2015 LHC proton–proton collision data*. ATLAS-CONF-2016-024. 2016. url: <https://cds.cern.ch/record/2157687>.

- 605 [8] ATLAS Collaboration. ‘Measurement of the muon reconstruction performance of the
 606 ATLAS detector using 2011 and 2012 LHC proton–proton collision data’. In: *Eur. Phys.*
 607 *J. C* 74 (2014), p. 3130. doi: [10.1140/epjc/s10052-014-3130-x](https://doi.org/10.1140/epjc/s10052-014-3130-x). arXiv: [1407.3935](https://arxiv.org/abs/1407.3935)
 608 [[hep-ex](#)].
- 609 [9] R. Narayan et al. *Measurement of the total and differential cross sections of a top-quark-*
 610 *antiquark pair in association with a W boson in proton-proton collisions at a centre-of-*
 611 *mass energy of 13 TeV with ATLAS detector at the Large Hadron Collider*. Tech. rep.
 612 ATL-COM-PHYS-2020-217. Geneva: CERN, Mar. 2020. URL: <https://cds.cern.ch/record/2712986>.
- 613 [10] ATLAS Collaboration. *Jet Calibration and Systematic Uncertainties for Jets Reconstruc-*
 614 *ted in the ATLAS Detector at $\sqrt{s} = 13$ TeV*. ATL-PHYS-PUB-2015-015. 2015. URL:
 615 <https://cds.cern.ch/record/2037613>.
- 616 [11] ATLAS Collaboration. *Selection of jets produced in 13 TeV proton–proton collisions with*
 617 *the ATLAS detector*. ATLAS-CONF-2015-029. 2015. URL: <https://cds.cern.ch/record/2037702>.
- 618 [12] ATLAS Collaboration. ‘Performance of pile-up mitigation techniques for jets in pp col-
 619 *lisions at $\sqrt{s} = 8$ TeV using the ATLAS detector*’. In: *Eur. Phys. J. C* 76 (2016), p. 581.
 620 doi: [10.1140/epjc/s10052-016-4395-z](https://doi.org/10.1140/epjc/s10052-016-4395-z). arXiv: [1510.03823](https://arxiv.org/abs/1510.03823) [[hep-ex](#)].
- 621 [13] ATLAS Collaboration. *Performance of missing transverse momentum reconstruction with*
 622 *the ATLAS detector in the first proton–proton collisions at $\sqrt{s} = 13$ TeV*. ATL-PHYS-
 623 PUB-2015-027. 2015. URL: <https://cds.cern.ch/record/2037904>.
- 624 [14] *Evidence for the associated production of the Higgs boson and a top quark pair with the*
 625 *ATLAS detector*. Tech. rep. ATLAS-CONF-2017-077. Geneva: CERN, Nov. 2017. URL:
 626 <https://cds.cern.ch/record/2291405>.
- 627 [15] 2021. URL: https://twiki.cern.ch/twiki/bin/view/AtlasProtected/BTagCalibrationRecommendationsRelease21#Tools_for_Flavor_Tagging_Calibra.
- 628 [16] P. S. A. Hoecker. ‘TMVA 4 Toolkit for Multivariate Data Analysis with ROOT’. In:
 629 *arXiv:physics/0703039* (2013).
- 630 [17] F. Cardillo et al. ‘Measurement of the fiducial and differential cross-section of a top quark
 631 pair in association with a Z boson at 13 TeV with the ATLAS detector’. In: ATL-COM-
 632 PHYS-2019-334 (Apr. 2019). URL: <https://cds.cern.ch/record/2672207>.
- 633 [18] T. Chen and C. Guestrin. ‘XGBoost: A Scalable Tree Boosting System’. In: *Proceedings*
 634 *of the 22nd ACM SIGKDD International Conference on Knowledge Discovery and Data*
 635 *Mining*. KDD ’16. San Francisco, California, USA: ACM, 2016, pp. 785–794. ISBN: 978-
 636 1-4503-4232-2. doi: [10.1145/2939672.2939785](https://doi.org/10.1145/2939672.2939785). URL: <http://doi.acm.org/10.1145/2939672.2939785>.
- 637 [19] ATLAS Collaboration. ‘Luminosity determination in pp collisions at $\sqrt{s} = 7$ TeV using
 638 the ATLAS detector at the LHC’. In: *Eur. Phys. J. C* 71 (2011), p. 1630. doi: [10.1140/epjc/s10052-011-1630-5](https://doi.org/10.1140/epjc/s10052-011-1630-5). arXiv: [1101.2185](https://arxiv.org/abs/1101.2185) [[hep-ex](#)].
- 639

- 645 [20] G. Avoni et al. ‘The new LUCID-2 detector for luminosity measurement and monitoring in
646 ATLAS’. In: *JINST* 13.07 (2018), P07017. doi: [10.1088/1748-0221/13/07/P07017](https://doi.org/10.1088/1748-0221/13/07/P07017).
- 647 [21] G. Aad et al. ‘Jet energy resolution in proton-proton collisions at $\sqrt{s} = 7$ TeV recorded
648 in 2010 with the ATLAS detector’. In: *The European Physical Journal C* 73.3 (Mar.
649 2013), p. 2306. ISSN: 1434-6052. doi: [10.1140/epjc/s10052-013-2306-0](https://doi.org/10.1140/epjc/s10052-013-2306-0). URL:
650 <https://doi.org/10.1140/epjc/s10052-013-2306-0>.
- 651 [22] A. Collaboration. ‘Performance of b -jet identification in the ATLAS experiment’. In:
652 *Journal of Instrumentation* 11.04 (2016), P04008. URL: <http://stacks.iop.org/1748-0221/11/i=04/a=P04008>.
- 653 [23] ‘Observation of the associated production of a top quark and a Z boson at 13 TeV with
654 ATLAS’. In: (July 2020). URL: <https://cds.cern.ch/record/2722504>.

656 **A Appendices**

657 **A.1 Non-prompt lepton MVA**

658 A lepton MVA has been developed to better reject non-prompt leptons than standard cut
 659 based selections based upon impact parameter, isolation and PID. The name of this MVA is
 660 `PromptLeptonIso`. The full set of studies and detailed explanation can be found in [9].

661 The decays of W and Z bosons are commonly selected by the identification of one or two electrons
 662 or muons. The negligible lifetimes of these bosons mean that the leptons produced in the decay
 663 originate from the interaction vertex and are thus labelled “prompt”. Analyses using these
 664 light leptons impose strict reconstruction quality, isolation and impact parameter requirements
 665 to remove “fake” leptons. A significant source of the fake light leptons are non-prompt leptons
 666 produced in decays of hadrons that contain bottom (b) or charm (c) quarks. Such hadrons
 667 typically have microscopically significant lifetimes that can be detected experimentally.

668 These non-prompt leptons can also pass the tight selection criteria. In analyses that involve top (t)
 669 quarks, which decay almost exclusively into a W boson and a b quark, non-prompt leptons from
 670 the semileptonic decay of bottom and charm hadrons can be a significant source of background
 671 events. This is particularly the case in the selection of same-sign dilepton and multilepton final
 672 states.

673 The main idea is to identify non-prompt light leptons using lifetime information associated with a
 674 track jet that matches the selected light lepton. This lifetime information is computed using tracks
 675 contained within the jet. Typically, lepton lifetime is determined using the impact parameter of the
 676 track reconstructed by the inner tracking detector which is matched to the reconstructed lepton.
 677 Using additional reconstructed charged particle tracks increases the precision of identifying the
 678 displaced decay vertex of bottom or charm hadrons that produced a non-prompt light lepton.
 679 The MVA also includes information related to the isolation of the lepton to reject non-prompt
 680 leptons. `PromptLeptonIso` is a gradient boosted BDT. The training of the BDT is performed on
 681 leptons selected from the PowHEG+PYTHIA6 non-allhad t \bar{t} MC sample. Eight variables are used
 682 to train the BDT in order to discriminate between prompt and non-prompt leptons. The track
 683 jets that are matched to the non-prompt leptons correspond to jets initiated by b or c quarks, and
 684 may contain a displaced vertex. Consequently, three of the selected variables are used to identify
 685 b-tag jets by standard ATLAS flavour tagging algorithms. Two variables use the relationship
 686 between the track jet and lepton: the ratio of the lepton p_T with respect to the track jet p_T and
 687 ΔR between the lepton and the track jet axis. Finally three additional variables test whether the
 688 reconstructed lepton is isolated: the number of tracks collected by the track jet and the lepton
 689 track and calorimeter isolation variables. Table 21 describes the variables used to train the BDT
 690 algorithm. The choice of input variables has been extensively discussed with Egamma, Muon,
 691 Tracking, and Flavour Tagging CP groups.

692 The efficiency of the tight `PromptLeptonIso` working point is measured using the tag and probe
 693 method with $Z \rightarrow \ell^+\ell^-$ events. Such calibration are performed by analysers from this analysis
 694 in communication with the Egamma and Muon combined performance groups. The scale factor

Variable	Description
N_{track} in track jet	Number of tracks collected by the track jet
$\text{IP2 log}(P_b/P_{\text{light}})$	Log-likelihood ratio between the b and light jet hypotheses with the IP2D algorithm
$\text{IP3 log}(P_b/P_{\text{light}})$	Log-likelihood ratio between the b and light jet hypotheses with the IP3D algorithm
N_{TrkAtVtx} SV + JF	Number of tracks used in the secondary vertex found by the SV1 algorithm in addition to the number of tracks from secondary vertices found by the JetFitter algorithm with at least two tracks
$p_T^{\text{lepton}}/p_T^{\text{track jet}}$	The ratio of the lepton p_T and the track jet p_T
$\Delta R(\text{lepton}, \text{track jet})$	ΔR between the lepton and the track jet axis
$p_T^{\text{VarCone30}}/p_T$	Lepton track isolation, with track collecting radius of $\Delta R < 0.3$
$E_T^{\text{TopoCone30}}/p_T$	Lepton calorimeter isolation, with topological cluster collecting radius of $\Delta R < 0.3$

Table 21: A table of the variables used in the training of `PromptLeptonIso`.

are approximately 0.92 for $10 < p_T < 15$ GeV, and averaging at 0.98 to 0.99 for higher p_T leptons. An extra systematic is applied to muons within $\Delta R < 0.6$ of a calorimeter jet, since there is a strong dependence on the scale factor due to the presence of these jets. For electrons, the dominant systematics is coming from pile-up dependence. Overall the systematics are a maximum of 3% at low p_T and decreasing at a function of p_T .

700 A.2 Non-prompt CR Modelling

- 701 In order to further validate the modeling in each of the non-prompt CRs, additional kinematic
702 plots are made in the Z+jets CR and $t\bar{t}$ CR in each of the continuous b-tag regions.
- 703 In the case of the Z+jets CR, the p_T spectrum of the lepton originating from the W candidate is
704 shown, as this is the distribution used to extract the scale factor applied to Z+jets. These plots
705 are shown in Figures 36 and 37.

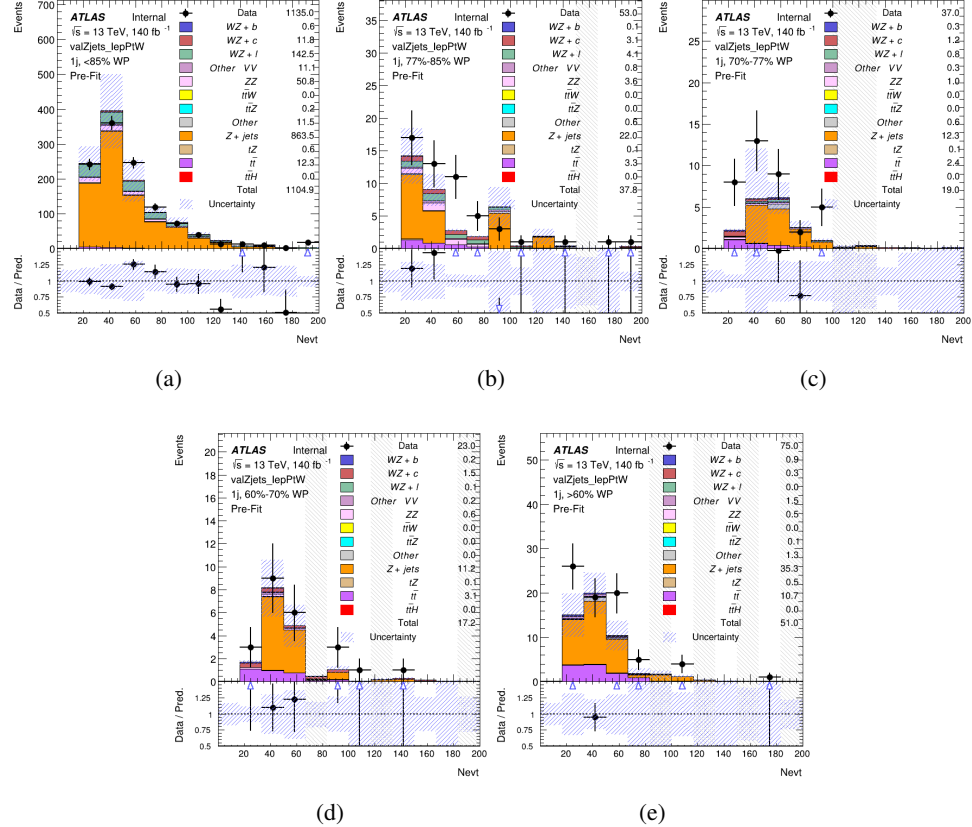


Figure 36: Comparisons between the data and MC distributions in the Z+jets CR for each of the 1-jet b-tag working point regions

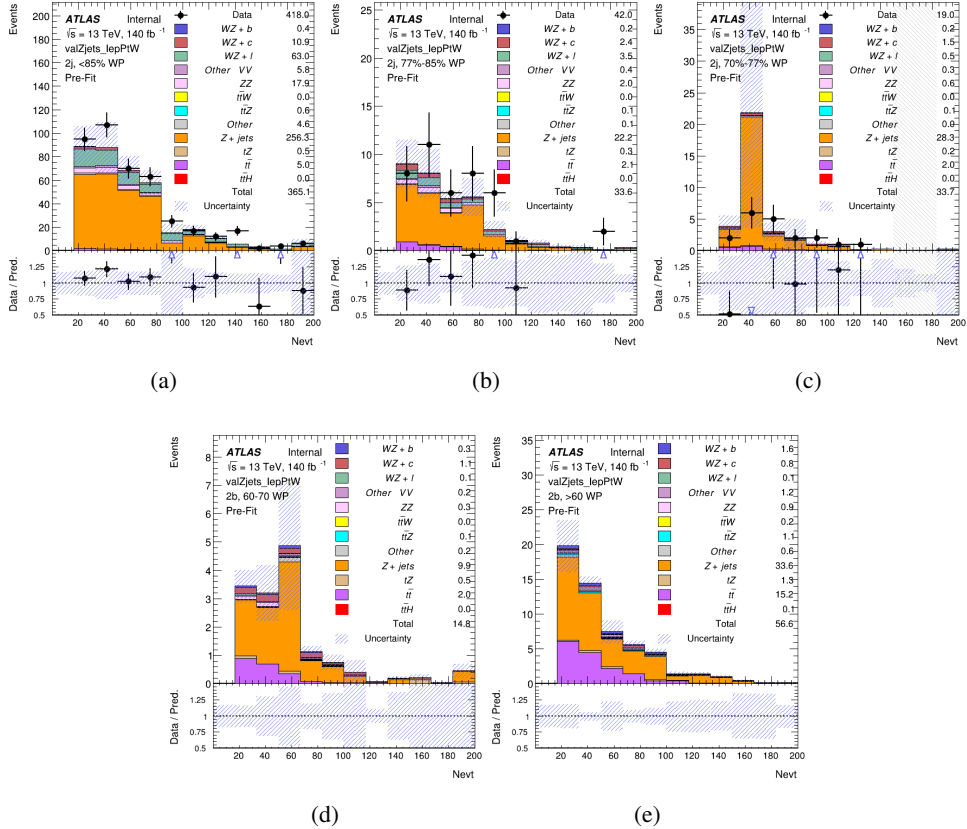


Figure 37: Comparisons between the data and MC distributions in the Z+jets CR for each of the 2-jet b-tag working point regions

706 The same is shown for the $t\bar{t}$ CR, but the p_T of the OS lepton is used instead as a representation
 707 of the modeling, as the lepton from the W is not well defined for $t\bar{t}$ events. These plots are shown
 708 in Figures 38 and 39.

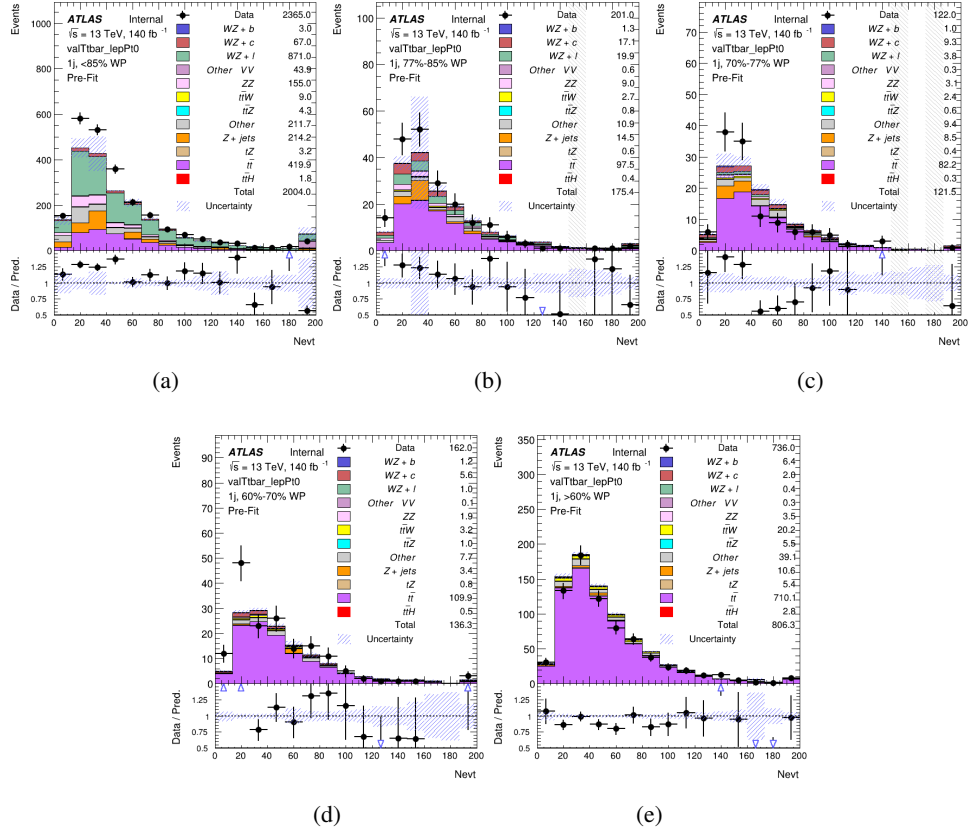


Figure 38: Comparisons between the data and MC distributions in the $t\bar{t}$ CR for each of the 1-jet b-tag working point regions

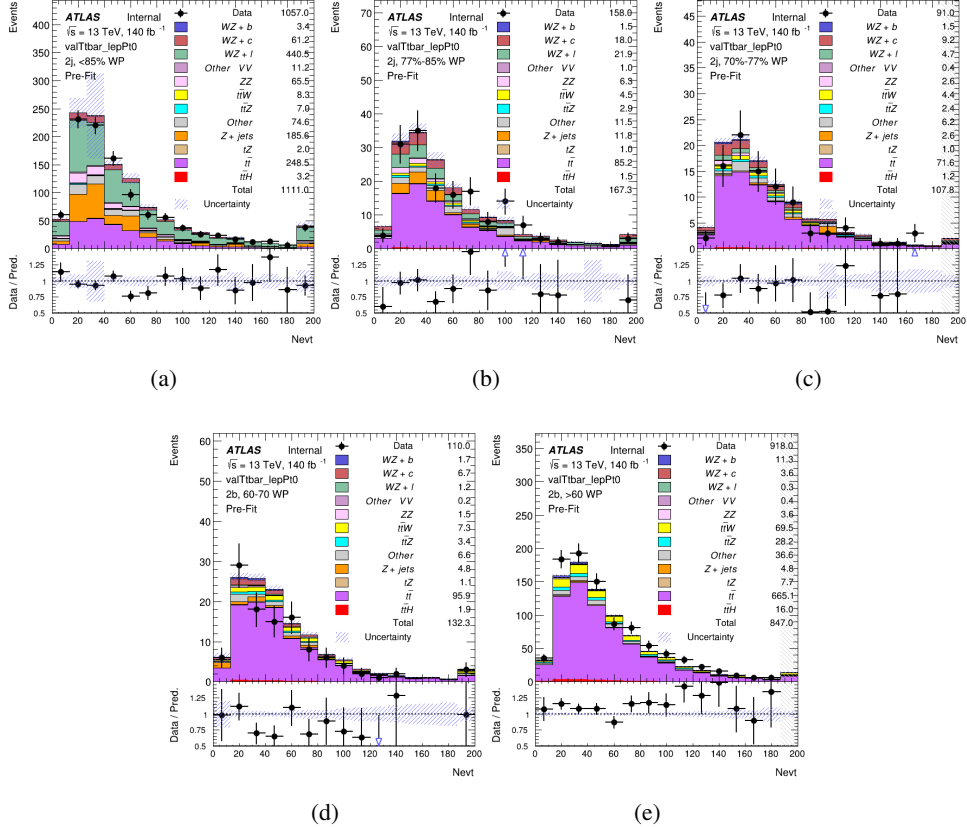


Figure 39: Comparisons between the data and MC distributions in the $t\bar{t}$ CR for each of the 2-jet b-tag working point regions

A.3 tZ Interference Studies

Because it includes an on-shell Z boson as well as a b-jet and W from the top decay, tZ production represents an identical final state to WZ + b-jet. This implies the possibility of matrix level interference between these two processes not accounted for in the Monte Carlo simulations, which consider the two processes independently. Truth level studies are performed in order to estimate the impact of these interference effects.

In order to estimate the matrix level interference effects between tZ and WZ + b-jet, two different sets of simulations are produced using MadGraph 5 [Madgraph] - one which simulates these two processes independently, and another where they are produced simultaneously, such that interference effects are present. These two sets of samples are then compared, and the difference between them can be taken to represent any interference effects.

MadGraph simulations of 10,000 tZ and 10,000 WZ + b-jet events are produced, along with 20,000 events where both are present, in the fiducial region where three leptons and at least one

722 jet are produced.

723 A selection mimicking the preselection used in the main analysis is applied to the samples: The
724 SS leptons are required to have $p_T > 20$ GeV, and > 10 GeV is required for the OS lepton. The
725 associated b-jet is required to have $p_T > 25$ GeV, and all physics objects are required to fall in a
726 range of $|\eta| < 2.5$.

727 The kinematics of these samples after the selection has been applied are shown below:

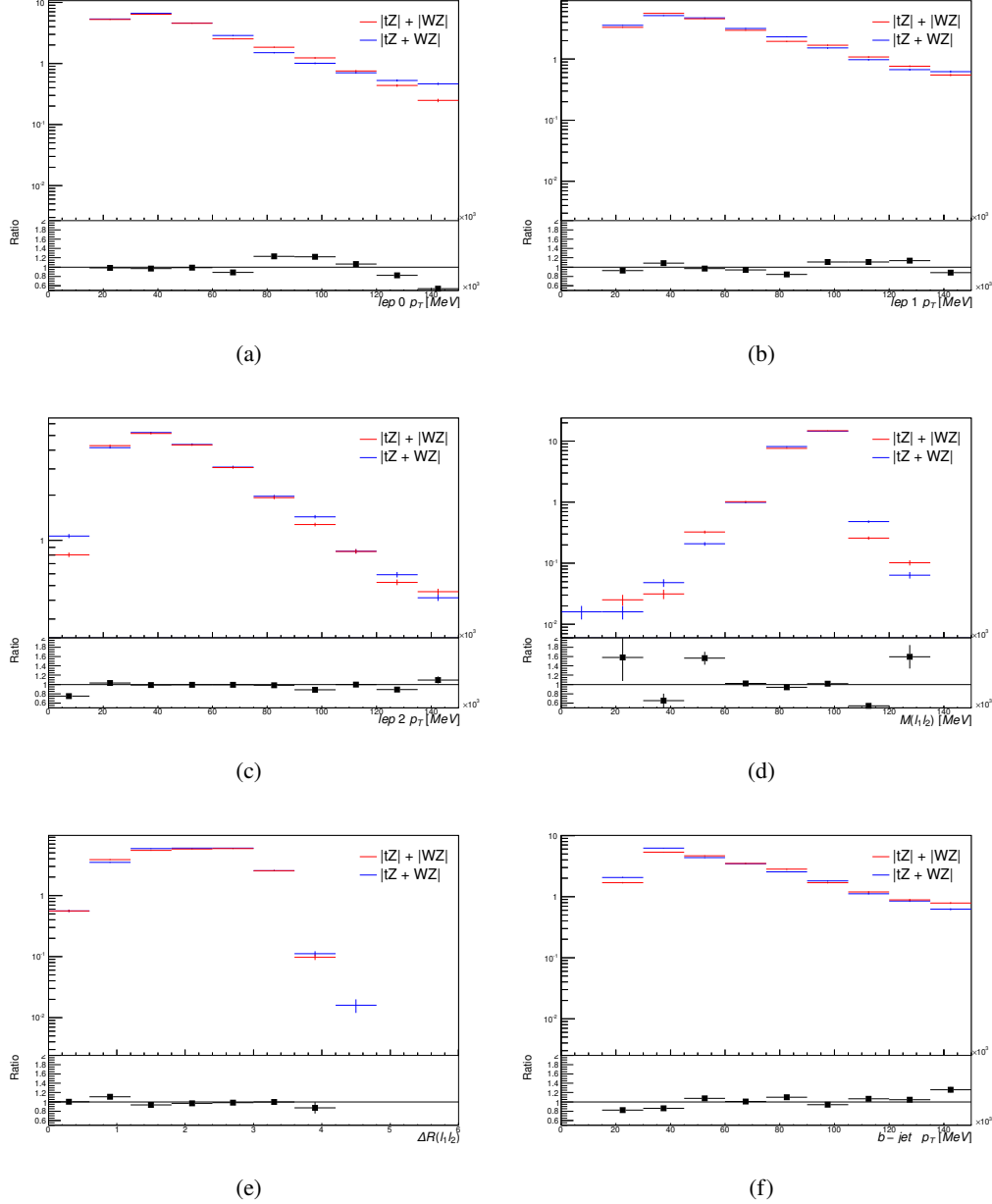


Figure 40: Comparisons between (a) the p_T of the lepton from the W, (b) and (c) show the p_T of the lepton from the Z, (d) the invariant mass of the Z-candidate, (e) ΔR of the leptons from the Z, and (f) the p_T of the b-jet, for WZ and tZ events generated with interference effects (blue) and without interference effects (red).

728 The overall cross-section of the two methods agree within error, and no significant differences
729 in the kinematic distributions are seen. It is therefore concluded that interference effects do not

730 significantly impact the results.

731 A.4 Inclusive 1+2 Jet Cross Check

732 An alternate fit is performed which combines the WZ + 1-jet and WZ + 2-jet samples rather than
 733 fitting them independently. This is done primarily as a cross-check of the nominal analysis, to
 734 see if measuring 1-jet and 2-jet events separately and combining them gives drastically different
 735 results than measuring them together.

736 For this study, three signal templates, WZ + b, WZ + charm and WZ + light, are fit to data, and
 737 the systematics accounting for migrations between 1-jet and 2-jet bins are removed. All other
 738 background and nuisance parameters remain the same as the nominal fit.

739 The measured μ value for WZ + b is $\mu = 1.00^{+0.30}_{-0.29}(\text{stat})^{+0.25}_{-23}(\text{sys})$, with a significance of 2.8σ ,
 740 and the uncertainty on WZ + charm is $\mu = 1.00 \pm 0.12(\text{stat}) \pm 0.13(\text{sys})$. This is compared to
 741 combined uncertainty of $\mu = 1.00^{+0.32}_{-0.30}(\text{stat})^{+0.24}_{-23}(\text{sys})$ for WZ + b when 1-jet and 2-jet events
 742 are measured separately and then combined.

743 A post-fit summary plot of the fit regions is shown in Figure 41:

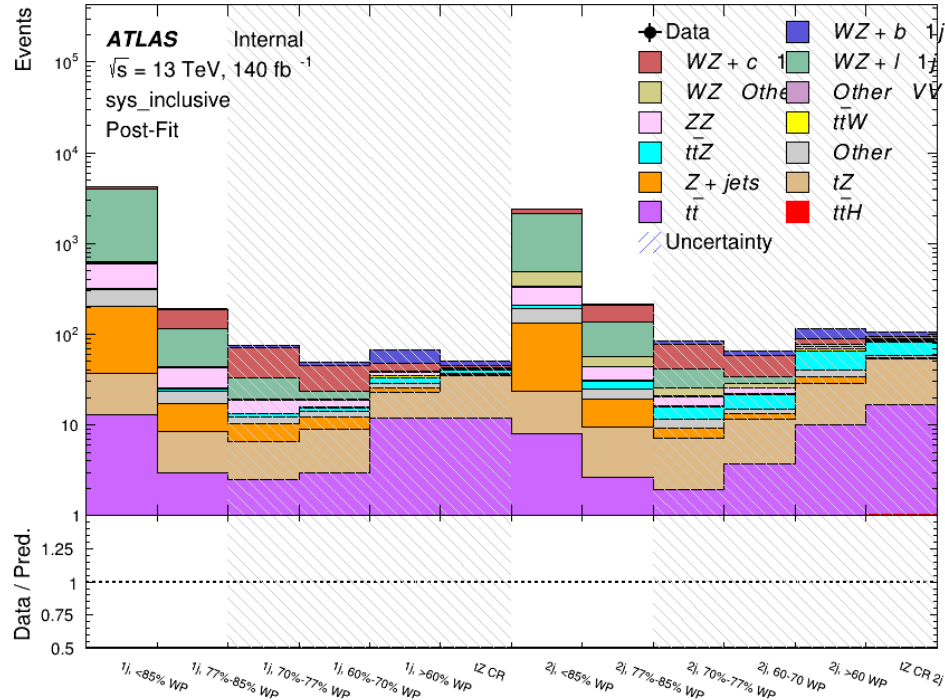


Figure 41: Post-fit summary of the 1-jet fit regions.

⁷⁴⁴ The impact of the most significant sources of systematic uncertainties on the measurement of
⁷⁴⁵ WZ+b is summarized in Table 22.

Uncertainty Source	$\Delta\mu$	
WZ + light cross-section	0.13	-0.12
WZ + charm cross-section	-0.10	0.12
Jet Energy Scale	0.08	0.13
tZ cross-section	-0.10	0.10
Jet Energy Resolution	-0.10	0.10
Luminosity	-0.08	0.09
Other Diboson + b cross-section	-0.07	0.07
Flavor tagging	0.05	0.05
t <bar>t} cross-section</bar>	-0.05	0.05
WZ cross-section - QCD scale	-0.04	0.03
Total Systematic Uncertainty	0.28	0.32

Table 22: Summary of the most significant sources of systematic uncertainty on the measurement of WZ + b with one or two associated jets.

⁷⁴⁶ The ranking and impact of those nuisance parameters with the largest contribution to the overall
⁷⁴⁷ uncertainty is shown in Figure 42.

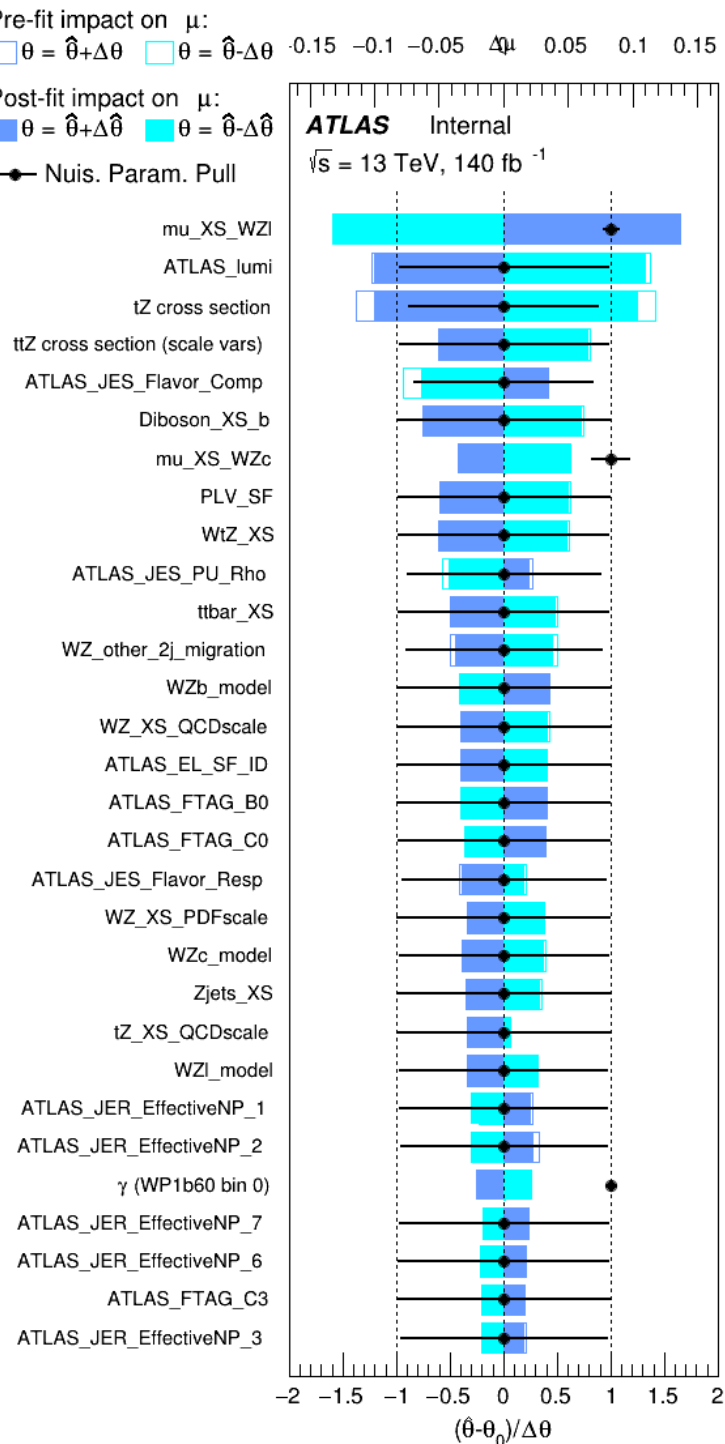


Figure 42: Impact of systematic uncertainties on the signal-strength of $WZ + b$ for events with one or two jets

748 **A.5 Alternate tZ Inclusive Fit**

749 **A.5.1 tZ Inclusive Fit**

750 While tZ is often considered as a distinct process from WZ + b, this could also be considered part
 751 of the signal. Alternate studies are performed where, using the same framework as the nominal
 752 analysis, a measurement of WZ + b is performed that includes tZ as part of WZ+b.

753 Because of this change, the tZ CR is no longer necessary, and only the five pseudo-continuous
 754 b-tag regions are used in the fit. Further, systematics related to the tZ cross-section are removed
 755 from the fit, as they are now encompassed by the normalization measurement of WZ + b. All
 756 other systematic uncertainties are carried over from the nominal analysis.

757 An expected WZ + b cross-section of $4.1^{+0.78}_{-0.74}(\text{stat})^{+0.53}_{-0.52}(\text{sys}) \text{ fb}$ is extracted from the fit, with
 758 an expected significance of 4.0σ .

759 The impact of the predominate systematics are summarized in Table 23.

Uncertainty Source	$\Delta\mu$	
WZ + light cross-section	0.08	-0.08
Jet Energy Scale	-0.06	0.08
Luminosity	-0.05	0.06
WZ + charm cross-section	-0.04	0.05
Other Diboson + b cross-section	-0.04	0.04
WZ cross-section - QCD scale	-0.04	0.03
t̄t cross-section	-0.03	0.03
Jet Energy Resolution	-0.03	0.03
Flavor tagging	-0.03	0.03
Z+jets cross section	-0.02	0.02
Total Systematic Uncertainty	-0.15	0.16

Table 23: Summary of the most significant sources of systematic uncertainty on the measurement of WZ + b with exactly one associated jet.

760 **A.5.2 Floating tZ**

761 In order to quantify the impact of the tZ uncertainty on the fit, an alternate fit strategy is used
 762 where the tZ normalization is allowed to float. This normalization factor replaces the cross-
 763 section uncertainty on tZ, and all other parameters of the fit remain the same.

764 An uncertainty of 17% on the normalization of tZ is extracted from the fit, compared to a theory
 765 uncertainty of 15% applied to the tZ cross-section. The measured uncertainties on WZ remain
 766 the same.

767 **A.6 DSID list**

Data:

```
data15_13TeV.AllYear.physics_Main.PhysCont.DAOD_HIGG8D1.grp15_v01_p4134
data16_13TeV.AllYear.physics_Main.PhysCont.DAOD_HIGG8D1.grp16_v01_p4134
data17_13TeV.AllYear.physics_Main.PhysCont.DAOD_HIGG8D1.grp17_v01_p4134
data18_13TeV.AllYear.physics_Main.PhysCont.DAOD_HIGG8D1.grp18_v01_p4134
```

mc16a:

```
mc16_13TeV.361603.PowhegPy8EG_CT10nloME_AZNLOCTEQ6L1_ZZllll_mll4.deriv.DAOD_HIGG8D1.e4475_s3126_r9364_r9315_p4133
mc16_13TeV.361602.PowhegPy8EG_CT10nloME_AZNLOCTEQ6L1_WZlvvv_mll4.deriv.DAOD_HIGG8D1.e4054_s3126_r9364_r9315_p4133
mc16_13TeV.361604.PowhegPy8EG_CT10nloME_AZNLOCTEQ6L1_ZZvvll_mll4.deriv.DAOD_HIGG8D1.e4475_s3126_r9364_r9315_p4133
mc16_13TeV.361600.PowhegPy8EG_CT10nloME_AZNLOCTEQ6L1_WWllvv.deriv.DAOD_HIGG8D1.e4616_s3126_r9364_r9315_p4133
mc16_13TeV.361605.PowhegPy8EG_CT10nloME_AZNLOCTEQ6L1_ZZvvvv_mll4.deriv.DAOD_HIGG8D1.e4054_s3126_s3136_r9364_r9315_p4133
mc16_13TeV.361601.PowhegPy8EG_CT10nloME_AZNLOCTEQ6L1_WZlvvll_mll4.deriv.DAOD_HIGG8D1.e4475_s3126_r9364_r9315_p4133
mc16_13TeV.364286.Sherpa_222_NNPDF30NNLO_llvj_ss_EW4.deriv.DAOD_HIGG8D1.e6055_e5984_s3126_r9364_r9315_p3983 mc16_13TeV.364285.Sherpa_222_NNPDF30NNLO_llvj_ss_EW4.deriv.DAOD_HIGG8D1.e6055_e5984_s3126_r9364_r9315_p4133
mc16_13TeV.364740.MGPy8EG_NNPDF30NLO_A14NNPDF23LO_lvlljjEW6_OFPlus.deriv.DAOD_HIGG8D1.e7421_e5984_s3126_r9364_r9315_p4133
mc16_13TeV.364742.MGPy8EG_NNPDF30NLO_A14NNPDF23LO_lvlljjEW6_SFPlus.deriv.DAOD_HIGG8D1.e7421_e5984_s3126_r9364_r9315_p4133
mc16_13TeV.364253.Sherpa_222_NNPDF30NNLO_llll.deriv.DAOD_HIGG8D1.e5916_s3126_r9364_r9315_p4133
mc16_13TeV.364250.Sherpa_222_NNPDF30NNLO_llll.deriv.DAOD_HIGG8D1.e5894_s3126_r9364_r9315_p4133
mc16_13TeV.364254.Sherpa_222_NNPDF30NNLO_llvv.deriv.DAOD_HIGG8D1.e5916_s3126_r9364_r9315_p4133
mc16_13TeV.364255.Sherpa_222_NNPDF30NNLO_llvvv.deriv.DAOD_HIGG8D1.e5916_s3126_r9364_r9315_p4133
mc16_13TeV.410155.aMcAtNloPythia8EvtGen_MEN30NLO_A14N23LO_ttW.deriv.DAOD_HIGG8D1.e5070_s3126_r9364_r9315_p4133
mc16_13TeV.410156.aMcAtNloPythia8EvtGen_MEN30NLO_A14N23LO_ttZnunu.deriv.DAOD_HIGG8D1.e5070_s3126_r9364_r9315_p4133
mc16_13TeV.410157.aMcAtNloPythia8EvtGen_MEN30NLO_A14N23LO_ttZqq.deriv.DAOD_HIGG8D1.e5070_s3126_r9364_r9315_p4133
mc16_13TeV.410218.aMcAtNloPythia8EvtGen_MEN30NLO_A14N23LO_ttee.deriv.DAOD_HIGG8D1.e5070_s3126_r9364_r9315_p4133
mc16_13TeV.410219.aMcAtNloPythia8EvtGen_MEN30NLO_A14N23LO_ttmumu.deriv.DAOD_HIGG8D1.e5070_s3126_r9364_r9315_p4133
mc16_13TeV.410220.aMcAtNloPythia8EvtGen_MEN30NLO_A14N23LO_ttautau.deriv.DAOD_HIGG8D1.e5070_s3126_r9364_r9315_p4133
mc16_13TeV.412063.aMcAtNloPythia8EvtGen_tllq_NNPDF30_nf4_A4.deriv.DAOD_TOPQ1.e7054_e5984_s3126_r9364_r9315_p4174
mc16_13TeV.410276.aMcAtNloPythia8EvtGen_MEN30NLO_A14N23LO_ttee_mll_1_5.deriv.DAOD_HIGG8D1.e6087_e5984_s3126_r9364_r9315_p4133
mc16_13TeV.410277.aMcAtNloPythia8EvtGen_MEN30NLO_A14N23LO_ttmumu_mll_1_5.deriv.DAOD_HIGG8D1.e6087_e5984_s3126_r9364_r9315_p4133
mc16_13TeV.410278.aMcAtNloPythia8EvtGen_MEN30NLO_A14N23LO_ttautau_mll_1_5.deriv.DAOD_HIGG8D1.e6087_e5984_s3126_r9364_r9315_p4133
mc16_13TeV.410397.MadGraphPythia8EvtGen_ttbar_wbee_MEN30LO_A14N23LO.deriv.DAOD_HIGG8D1.e6086_e5984_s3126_r9364_r9315_p4133
mc16_13TeV.410398.MadGraphPythia8EvtGen_ttbar_wbmumu_MEN30LO_A14N23LO.deriv.DAOD_HIGG8D1.e6086_e5984_s3126_r9364_r9315_p4133
mc16_13TeV.410399.MadGraphPythia8EvtGen_ttbar_wbtautau_MEN30LO_A14N23LO.deriv.DAOD_HIGG8D1.e6086_e5984_s3126_r9364_r9315_p4133
mc16_13TeV.410658.PhPy8EG_A14_tchan_BW50_lept_top.deriv.DAOD_HIGG8D1.e6671_e5984_s3126_r9364_r9315_p4133
mc16_13TeV.410659.PhPy8EG_A14_tchan_BW50_lept_antitop.deriv.DAOD_HIGG8D1.e6671_e5984_s3126_r9364_r9315_p4133
mc16_13TeV.410644.PowhegPythia8EvtGen_A14_singletop_schan_lept_top.deriv.DAOD_HIGG8D1.e6527_e5984_s3126_r9364_r9315_p4133
mc16_13TeV.410645.PowhegPythia8EvtGen_A14_singletop_schan_lept_antitop.deriv.DAOD_HIGG8D1.e6527_e5984_s3126_r9364_r9315_p4133
mc16_13TeV.304014.MadGraphPythia8EvtGen_A14NNPDF23_3top_SM.deriv.DAOD_HIGG8D1.e4324_s3126_r9364_r9315_p4133
mc16_13TeV.410080.MadGraphPythia8EvtGen_A14NNPDF23_4topSM.deriv.DAOD_HIGG8D1.e4111_s3126_r9364_r9315_p4133
mc16_13TeV.410081.MadGraphPythia8EvtGen_A14NNPDF23_ttbarWW.deriv.DAOD_HIGG8D1.e4111_s3126_r9364_r9315_p4133
mc16_13TeV.364100.Sherpa_221_NNPDF30NNLO_Zmumu_MAXHPTV0_70_CVetoBVeto.deriv.DAOD_HIGG8D1.e5271_s3126_r9364_r9315_p4133
mc16_13TeV.364101.Sherpa_221_NNPDF30NNLO_Zmumu_MAXHPTV0_70_CFilterBVeto.deriv.DAOD_HIGG8D1.e5271_s3126_r9364_r9315_p4133
mc16_13TeV.364102.Sherpa_221_NNPDF30NNLO_Zmumu_MAXHPTV0_70_BFilter.deriv.DAOD_HIGG8D1.e5271_s3126_r9364_r9315_p4133
mc16_13TeV.364103.Sherpa_221_NNPDF30NNLO_Zmumu_MAXHPTV70_140_CVetoBVeto.deriv.DAOD_HIGG8D1.e5271_s3126_r9364_r9315_p4133
mc16_13TeV.364104.Sherpa_221_NNPDF30NNLO_Zmumu_MAXHPTV70_140_CFilterBVeto.deriv.DAOD_HIGG8D1.e5271_s3126_r9364_r9315_p4133
mc16_13TeV.364106.Sherpa_221_NNPDF30NNLO_Zmumu_MAXHPTV140_280_CVetoBVeto.deriv.DAOD_HIGG8D1.e5271_s3126_r9364_r9315_p4133
mc16_13TeV.364107.Sherpa_221_NNPDF30NNLO_Zmumu_MAXHPTV140_280_CFilterBVeto.deriv.DAOD_HIGG8D1.e5271_s3126_r9364_r9315_p4133
mc16_13TeV.364108.Sherpa_221_NNPDF30NNLO_Zmumu_MAXHPTV140_280_BFilter.deriv.DAOD_HIGG8D1.e5271_s3126_r9364_r9315_p4133
mc16_13TeV.364109.Sherpa_221_NNPDF30NNLO_Zmumu_MAXHPTV280_500_CVetoBVeto.deriv.DAOD_HIGG8D1.e5271_s3126_r9364_r9315_p4133
mc16_13TeV.364110.Sherpa_221_NNPDF30NNLO_Zmumu_MAXHPTV280_500_CFilterBVeto.deriv.DAOD_HIGG8D1.e5271_s3126_r9364_r9315_p4133
mc16_13TeV.364111.Sherpa_221_NNPDF30NNLO_Zmumu_MAXHPTV280_500_BFilter.deriv.DAOD_HIGG8D1.e5271_s3126_r9364_r9315_p4133
mc16_13TeV.364111.Sherpa_221_NNPDF30NNLO_Zmumu_MAXHPTV280_500_BFilter.deriv.DAOD_HIGG8D1.e5271_s3126_r9364_r9315_p4133
mc16_13TeV.364112.Sherpa_221_NNPDF30NNLO_Zmumu_MAXHPTV500_1000.deriv.DAOD_HIGG8D1.e5271_s3126_r9364_r9315_p4133
mc16_13TeV.364113.Sherpa_221_NNPDF30NNLO_Zmumu_MAXHPTV1000_E_CMS.deriv.DAOD_HIGG8D1.e5271_s3126_r9364_r9315_p4133
mc16_13TeV.364114.Sherpa_221_NNPDF30NNLO_Zee_MAXHPTV0_70_CVetoBVeto.deriv.DAOD_HIGG8D1.e5299_s3126_r9364_r9315_p4133
mc16_13TeV.364115.Sherpa_221_NNPDF30NNLO_Zee_MAXHPTV0_70_CFilterBVeto.deriv.DAOD_HIGG8D1.e5299_s3126_r9364_r9315_p4133
mc16_13TeV.364116.Sherpa_221_NNPDF30NNLO_Zee_MAXHPTV0_70_BFilter.deriv.DAOD_HIGG8D1.e5299_s3126_r9364_r9315_p4133
mc16_13TeV.364117.Sherpa_221_NNPDF30NNLO_Zee_MAXHPTV70_140_CVetoBVeto.deriv.DAOD_HIGG8D1.e5299_s3126_r9364_r9315_p4133
mc16_13TeV.364118.Sherpa_221_NNPDF30NNLO_Zee_MAXHPTV70_140_CFilterBVeto.deriv.DAOD_HIGG8D1.e5299_s3126_r9364_r9315_p4133
```


mc16_13TeV.364531.Sherpa_222_NNPDF30NNLO_taunugamma_pty_7_15.deriv.DAOD_HIGG8D1.e5928_s3126_r9364_r9315_p4133
 mc16_13TeV.364532.Sherpa_222_NNPDF30NNLO_taunugamma_pty_15_35.deriv.DAOD_HIGG8D1.e5928_s3126_r9364_r9315_p4133
 mc16_13TeV.364533.Sherpa_222_NNPDF30NNLO_taunugamma_pty_35_70.deriv.DAOD_HIGG8D1.e5928_s3126_r9364_r9315_p4133
 mc16_13TeV.364534.Sherpa_222_NNPDF30NNLO_taunugamma_pty_70_140.deriv.DAOD_HIGG8D1.e5928_s3126_r9364_r9315_p4133
 mc16_13TeV.364535.Sherpa_222_NNPDF30NNLO_taunugamma_pty_140_E_CMS.deriv.DAOD_HIGG8D1.e5928_s3126_r9364_r9315_p4133
 mc16_13TeV.364535.Sherpa_222_NNPDF30NNLO_taunugamma_pty_140_E_CMS.deriv.DAOD_HIGG8D1.e5928_s3126_r9364_r9315_p4133
 mc16_13TeV.410560.MadGraphPythia8EvtGen_A14_lZ_4fl_tchan_noAllHad.deriv.DAOD_HIGG8D1.e5803_s3126_r9364_r9315_p4133
 mc16_13TeV.410013.PowhegPythiaEvtGen_P2012_Wt_inclusive_top.deriv.DAOD_HIGG8D1.e3753_s3126_r9364_r9315_p4133
 mc16_13TeV.410014.PowhegPythiaEvtGen_P2012_Wt_inclusive_antitop.deriv.DAOD_HIGG8D1.e3753_s3126_r9364_r9315_p4133
 mc16_13TeV.410408.aMcAtNloPythia8EvtGen_tWZ_Ztoll_minDR1.deriv.DAOD_HIGG8D1.e6423_e5984_s3126_r9364_r9315_p4133
 mc16_13TeV.364242.Sherpa_222_NNPDF30NNLO_WWW_3l3v_EW6.deriv.DAOD_HIGG8D1.e5887_s3126_r9364_r9315_p4133
 mc16_13TeV.364243.Sherpa_222_NNPDF30NNLO_WWZ_4l2v_EW6.deriv.DAOD_HIGG8D1.e5887_s3126_r9364_r9315_p4133
 mc16_13TeV.364244.Sherpa_222_NNPDF30NNLO_WWZ_2l4v_EW6.deriv.DAOD_HIGG8D1.e5887_s3126_r9364_r9315_p4133
 mc16_13TeV.364245.Sherpa_222_NNPDF30NNLO_WZZ_5l1v_EW6.deriv.DAOD_HIGG8D1.e5887_s3126_r9364_r9315_p4133
 mc16_13TeV.364246.Sherpa_222_NNPDF30NNLO_WZZ_3l3v_EW6.deriv.DAOD_HIGG8D1.e5887_s3126_r9364_r9315_p4133
 mc16_13TeV.364247.Sherpa_222_NNPDF30NNLO_ZZZ_6l0v_EW6.deriv.DAOD_HIGG8D1.e5887_s3126_r9364_r9315_p4133
 mc16_13TeV.364248.Sherpa_222_NNPDF30NNLO_ZZZ_4l2v_EW6.deriv.DAOD_HIGG8D1.e5887_s3126_r9364_r9315_p4133
 mc16_13TeV.364249.Sherpa_222_NNPDF30NNLO_ZZZ_2l4v_EW6.deriv.DAOD_HIGG8D1.e5887_s3126_r9364_r9315_p4133
 mc16_13TeV.342284.Pythia8EvtGen_A14NNPDF23LO_WH125_inc.deriv.DAOD_HIGG8D1.e4246_s3126_r9364_r9315_p4133
 mc16_13TeV.342285.Pythia8EvtGen_A14NNPDF23LO_ZH125_inc.deriv.DAOD_HIGG8D1.e4246_s3126_r9364_r9315_p4133
 mc16_13TeV.341998.aMcAtNloHppEG_UEEE5_CTEQ6L1_CT10ME_tWH125_gamgam_yt_plus1.deriv.DAOD_HIGG8D1.e4394_e5984_s3126_r9364_r9315_p4133
 mc16_13TeV.410389.MadGraphPythia8EvtGen_A14NNPDF23_ttgamma_nonallhadronic.deriv.DAOD_HIGG8D1.e6155_e5984_s3126_r9364_r9315_p4133
 mc16_13TeV.410470.PhPy8EG_A14_tbbar_hdamp258p75_nonallhad.deriv.DAOD_HIGG8D1.e6337_e5984_s3126_r9364_r9315_p4133
 mc16_13TeV.410472.PhPy8EG_A14_tbbar_hdamp258p75_dil.deriv.DAOD_HIGG8D1.e6348_e5984_s3126_r9364_r9315_p4133
 mc16_13TeV.346343.PhPy8EG_A14NNPDF23_NNPDF30ME_ttH125_allhad.deriv.DAOD_HIGG8D1.e7148_e5984_s3126_r9364_r9315_p4133
 mc16_13TeV.346344.PhPy8EG_A14NNPDF23_NNPDF30ME_ttH125_semilep.deriv.DAOD_HIGG8D1.e7148_e5984_s3126_r9364_r9315_p4133
 mc16_13TeV.346345.PhPy8EG_A14NNPDF23_NNPDF30ME_ttH125_dilep.deriv.DAOD_HIGG8D1.e7148_e5984_s3126_r9364_r9315_p4133

mc16d:

mc16_13TeV.364253.Sherpa_222_NNPDF30NNLO_llv.deriv.DAOD_HIGG8D1.e5916_e5984_s3126_r10201_r10210_p4133
 mc16_13TeV.364250.Sherpa_222_NNPDF30NNLO_lll.deriv.DAOD_HIGG8D1.e5894_e5984_s3126_r10201_r10210_p4133
 mc16_13TeV.364254.Sherpa_222_NNPDF30NNLO_llv.deriv.DAOD_HIGG8D1.e5916_e5984_s3126_r10201_r10210_p4133
 mc16_13TeV.364255.Sherpa_222_NNPDF30NNLO_llv.deriv.DAOD_HIGG8D1.e5916_e5984_s3126_r10201_r10210_p4133
 mc16_13TeV.410155.aMcAtNloPythia8EvtGen_MEN30NLO_A14N23LO_ttW.deriv.DAOD_HIGG8D1.e5070_e5984_s3126_r10201_r10210_p4133
 mc16_13TeV.410156.aMcAtNloPythia8EvtGen_MEN30NLO_A14N23LO_ttZnunu.deriv.DAOD_HIGG8D1.e5070_e5984_s3126_r10201_r10210_p4133
 mc16_13TeV.410157.aMcAtNloPythia8EvtGen_MEN30NLO_A14N23LO_ttZqq.deriv.DAOD_HIGG8D1.e5070_e5984_s3126_r10201_r10210_p4133
 mc16_13TeV.410218.aMcAtNloPythia8EvtGen_MEN30NLO_A14N23LO_ttee.deriv.DAOD_HIGG8D1.e5070_e5984_s3126_r10201_r10210_p4133
 mc16_13TeV.410219.aMcAtNloPythia8EvtGen_MEN30NLO_A14N23LO_ttmumu.deriv.DAOD_HIGG8D1.e5070_e5984_s3126_r10201_r10210_p4133
 mc16_13TeV.410220.aMcAtNloPythia8EvtGen_MEN30NLO_A14N23LO_ttautau.deriv.DAOD_HIGG8D1.e5070_e5984_s3126_r10201_r10210_p4133
 mc16_13TeV.410276.aMcAtNloPythia8EvtGen_MEN30NLO_A14N23LO_tee_mll_1_5.deriv.DAOD_HIGG8D1.e6087_e5984_s3126_r10201_r10210_p4133
 mc16_13TeV.410277.aMcAtNloPythia8EvtGen_MEN30NLO_A14N23LO_ttmumu_mll_1_5.deriv.DAOD_HIGG8D1.e6087_e5984_s3126_r10201_r10210_p4133
 mc16_13TeV.410278.aMcAtNloPythia8EvtGen_MEN30NLO_A14N23LO_ttautau_mll_1_5.deriv.DAOD_HIGG8D1.e6087_e5984_s3126_r10201_r10210_p4133
 mc16_13TeV.410397.MadGraphPythia8EvtGen_tbbar_wbee_MEN30LO_A14N23LO.deriv.DAOD_HIGG8D1.e6086_e5984_s3126_r10201_r10210_p4133
 mc16_13TeV.410398.MadGraphPythia8EvtGen_tbbar_wbmumu_MEN30LO_A14N23LO.deriv.DAOD_HIGG8D1.e6086_e5984_s3126_r10201_r10210_p4133
 mc16_13TeV.410399.MadGraphPythia8EvtGen_tbbar_wbtautau_MEN30LO_A14N23LO.deriv.DAOD_HIGG8D1.e6086_e5984_s3126_r10201_r10210_p4133
 mc16_13TeV.410658.PhPy8EG_A14_tchan_BW50_lept_top.deriv.DAOD_HIGG8D1.e6671_e5984_s3126_r10201_r10210_p4133
 mc16_13TeV.410659.PhPy8EG_A14_tchan_BW50_lept_antitop.deriv.DAOD_HIGG8D1.e6671_e5984_s3126_r10201_r10210_p4133
 mc16_13TeV.410644.PowhegPythia8EvtGen_A14_singletop_schan_lept_top.deriv.DAOD_HIGG8D1.e6527_e5984_s3126_r10201_r10210_p4133
 mc16_13TeV.410645.PowhegPythia8EvtGen_A14_singletop_schan_lept_antitop.deriv.DAOD_HIGG8D1.e6527_s3126_r10201_r10210_p4133
 mc16_13TeV.412063.aMcAtNloPythia8EvtGen_tllq_NNPDF30_nf4_A14.deriv.DAOD_TOPQ1.e7054_e5984_s3126_r10201_r10210_p4174
 mc16_13TeV.304014.MadGraphPythia8EvtGen_A14NNPDF23_3top_SM.deriv.DAOD_HIGG8D1.e4324_e5984_s3126_r10201_r10210_p4133
 mc16_13TeV.410080.MadGraphPythia8EvtGen_A14NNPDF23_4topSM.deriv.DAOD_HIGG8D1.e4111_e5984_s3126_r10201_r10210_p4133
 mc16_13TeV.410081.MadGraphPythia8EvtGen_A14NNPDF23_tbbarWW.deriv.DAOD_HIGG8D1.e4111_e5984_s3126_r10201_r10210_p4133
 mc16_13TeV.364100.Sherpa_221_NNPDF30NNLO_Zmumu_MAXHTPTV0_70_CVetoBVeto.deriv.DAOD_HIGG8D1.e5271_s3126_r10201_r10210_p4133
 mc16_13TeV.364101.Sherpa_221_NNPDF30NNLO_Zmumu_MAXHTPTV0_70_CFilterBVeto.deriv.DAOD_HIGG8D1.e5271_s3126_r10201_r10210_p4133
 mc16_13TeV.364101.Sherpa_221_NNPDF30NNLO_Zmumu_MAXHTPTV0_70_CFilterBVeto.deriv.DAOD_HIGG8D1.e5271_e5984_s3126_r10201_r10210_p4133
 mc16_13TeV.364102.Sherpa_221_NNPDF30NNLO_Zmumu_MAXHTPTV0_70_BFilter.deriv.DAOD_HIGG8D1.e5271_s3126_r10201_r10210_p4133
 mc16_13TeV.364103.Sherpa_221_NNPDF30NNLO_Zmumu_MAXHTPTV0_70_CFilterBVeto.deriv.DAOD_HIGG8D1.e5271_s3126_r10201_r10210_p4133
 mc16_13TeV.364104.Sherpa_221_NNPDF30NNLO_Zmumu_MAXHTPTV0_70_CFilterBVeto.deriv.DAOD_HIGG8D1.e5271_s3126_r10201_r10210_p4133
 mc16_13TeV.364106.Sherpa_221_NNPDF30NNLO_Zmumu_MAXHTPTV0_70_CVetoBVeto.deriv.DAOD_HIGG8D1.e5271_s3126_r10201_r10210_p4133
 mc16_13TeV.364107.Sherpa_221_NNPDF30NNLO_Zmumu_MAXHTPTV0_70_CFilterBVeto.deriv.DAOD_HIGG8D1.e5271_s3126_r10201_r10210_p4133
 mc16_13TeV.364108.Sherpa_221_NNPDF30NNLO_Zmumu_MAXHTPTV0_70_BFilter.deriv.DAOD_HIGG8D1.e5271_s3126_r10201_r10210_p4133

mc16_13TeV.364189.Sherpa_221_NNPDF30NNLO_Wtaunu_MAXHTPTV70_140_BFilter.deriv.DAOD_HIGG8D1.e5340_e5984_s3126_r10201_r10210_p4133
 mc16_13TeV.364190.Sherpa_221_NNPDF30NNLO_Wtaunu_MAXHTPTV140_280_CVetoBVeto.deriv.DAOD_HIGG8D1.e5340_s3126_r10201_r10210_p4133
 mc16_13TeV.364190.Sherpa_221_NNPDF30NNLO_Wtaunu_MAXHTPTV140_280_CVetoBVeto.deriv.DAOD_HIGG8D1.e5340_e5984_s3126_s3136_r10201_r10210_p4133
 mc16_13TeV.364191.Sherpa_221_NNPDF30NNLO_Wtaunu_MAXHTPTV140_280_CFilterBVeto.deriv.DAOD_HIGG8D1.e5340_e5984_s3126_s3136_r10201_r10210_p4133
 mc16_13TeV.364191.Sherpa_221_NNPDF30NNLO_Wtaunu_MAXHTPTV140_280_CFilterBVeto.deriv.DAOD_HIGG8D1.e5340_s3126_r10201_r10210_p4133
 mc16_13TeV.364192.Sherpa_221_NNPDF30NNLO_Wtaunu_MAXHTPTV140_280_BFilter.deriv.DAOD_HIGG8D1.e5340_e5984_s3126_r10201_r10210_p4133
 mc16_13TeV.364193.Sherpa_221_NNPDF30NNLO_Wtaunu_MAXHTPTV280_500_CVetoBVeto.deriv.DAOD_HIGG8D1.e5340_e5984_s3126_r10201_r10210_p4133
 mc16_13TeV.364193.Sherpa_221_NNPDF30NNLO_Wtaunu_MAXHTPTV280_500_CVetoBVeto.deriv.DAOD_HIGG8D1.e5340_s3126_s3136_r10201_r10210_p4133
 mc16_13TeV.364194.Sherpa_221_NNPDF30NNLO_Wtaunu_MAXHTPTV280_500_CFilterBVeto.deriv.DAOD_HIGG8D1.e5340_e5984_s3126_r10201_r10210_p4133
 mc16_13TeV.364194.Sherpa_221_NNPDF30NNLO_Wtaunu_MAXHTPTV280_500_CFilterBVeto.deriv.DAOD_HIGG8D1.e5340_e5984_s3126_s3136_r10201_r10210_p4133
 mc16_13TeV.364195.Sherpa_221_NNPDF30NNLO_Wtaunu_MAXHTPTV280_500_BFilter.deriv.DAOD_HIGG8D1.e5340_e5984_s3126_r10201_r10210_p4133
 mc16_13TeV.364195.Sherpa_221_NNPDF30NNLO_Wtaunu_MAXHTPTV280_500_BFilter.deriv.DAOD_HIGG8D1.e5340_s3126_r10201_r10210_p4133
 mc16_13TeV.364196.Sherpa_221_NNPDF30NNLO_Wtaunu_MAXHTPTV500_1000.deriv.DAOD_HIGG8D1.e5340_e5984_s3126_s3136_r10201_r10210_p4133
 mc16_13TeV.364196.Sherpa_221_NNPDF30NNLO_Wtaunu_MAXHTPTV500_1000.deriv.DAOD_HIGG8D1.e5340_s3126_r10201_r10210_p4133
 mc16_13TeV.364197.Sherpa_221_NNPDF30NNLO_Wtaunu_MAXHTPTV1000_E_CMS.deriv.DAOD_HIGG8D1.e5340_e5984_s3126_r10201_r10210_p4133
 mc16_13TeV.364500.Sherpa_222_NNPDF30NNLO_eegamma_pty_7_15.deriv.DAOD_HIGG8D1.e5928_e5984_s3126_r10201_r10210_p4133
 mc16_13TeV.364501.Sherpa_222_NNPDF30NNLO_eegamma_pty_15_35.deriv.DAOD_HIGG8D1.e5928_e5984_s3126_r10201_r10210_p4133
 mc16_13TeV.364502.Sherpa_222_NNPDF30NNLO_eegamma_pty_35_70.deriv.DAOD_HIGG8D1.e5928_e5984_s3126_r10201_r10210_p4133
 mc16_13TeV.364503.Sherpa_222_NNPDF30NNLO_eegamma_pty_70_140.deriv.DAOD_HIGG8D1.e5928_e5984_s3126_r10201_r10210_p4133
 mc16_13TeV.364504.Sherpa_222_NNPDF30NNLO_eegamma_pty_140_E_CMS.deriv.DAOD_HIGG8D1.e5928_e5984_s3126_r10201_r10210_p4133
 mc16_13TeV.364505.Sherpa_222_NNPDF30NNLO_mumugamma_pty_7_15.deriv.DAOD_HIGG8D1.e5928_e5984_s3126_r10201_r10210_p4133
 mc16_13TeV.364506.Sherpa_222_NNPDF30NNLO_mumugamma_pty_15_35.deriv.DAOD_HIGG8D1.e5928_e5984_s3126_r10201_r10210_p4133
 mc16_13TeV.364507.Sherpa_222_NNPDF30NNLO_mumugamma_pty_35_70.deriv.DAOD_HIGG8D1.e5928_e5984_s3126_r10201_r10210_p4133
 mc16_13TeV.364508.Sherpa_222_NNPDF30NNLO_mumugamma_pty_70_140.deriv.DAOD_HIGG8D1.e5928_e5984_s3126_r10201_r10210_p4133
 mc16_13TeV.364509.Sherpa_222_NNPDF30NNLO_mumugamma_pty_140_E_CMS.deriv.DAOD_HIGG8D1.e5928_e5984_s3126_r10201_r10210_p4133
 mc16_13TeV.364510.Sherpa_222_NNPDF30NNLO_tautaugamma_pty_7_15.deriv.DAOD_HIGG8D1.e5928_e5984_s3126_r10201_r10210_p4133
 mc16_13TeV.364511.Sherpa_222_NNPDF30NNLO_tautaugamma_pty_15_35.deriv.DAOD_HIGG8D1.e5928_e5984_s3126_r10201_r10210_p4133
 mc16_13TeV.364512.Sherpa_222_NNPDF30NNLO_tautaugamma_pty_35_70.deriv.DAOD_HIGG8D1.e5928_e5984_s3126_r10201_r10210_p4133
 mc16_13TeV.364513.Sherpa_222_NNPDF30NNLO_tautaugamma_pty_70_140.deriv.DAOD_HIGG8D1.e5928_e5984_s3126_r10201_r10210_p4133
 mc16_13TeV.364513.Sherpa_222_NNPDF30NNLO_tautaugamma_pty_70_140.deriv.DAOD_HIGG8D1.e5928_e5984_s3126_r10201_r10210_p4133
 mc16_13TeV.364514.Sherpa_222_NNPDF30NNLO_tautaugamma_pty_140_E_CMS.deriv.DAOD_HIGG8D1.e5928_e5984_s3126_r10201_r10210_p4133
 mc16_13TeV.364521.Sherpa_222_NNPDF30NNLO_enugamma_pty_7_15.deriv.DAOD_HIGG8D1.e5928_e5984_s3126_r10201_r10210_p4133
 mc16_13TeV.364522.Sherpa_222_NNPDF30NNLO_enugamma_pty_15_35.deriv.DAOD_HIGG8D1.e5928_e5984_s3126_r10201_r10210_p4133
 mc16_13TeV.364523.Sherpa_222_NNPDF30NNLO_enugamma_pty_35_70.deriv.DAOD_HIGG8D1.e5928_e5984_s3126_r10201_r10210_p4133
 mc16_13TeV.364524.Sherpa_222_NNPDF30NNLO_enugamma_pty_70_140.deriv.DAOD_HIGG8D1.e5928_e5984_s3126_r10201_r10210_p4133
 mc16_13TeV.364525.Sherpa_222_NNPDF30NNLO_enugamma_pty_140_E_CMS.deriv.DAOD_HIGG8D1.e5928_e5984_s3126_r10201_r10210_p4133
 mc16_13TeV.364526.Sherpa_222_NNPDF30NNLO_munugamma_pty_7_15.deriv.DAOD_HIGG8D1.e5928_e5984_s3126_r10201_r10210_p4133
 mc16_13TeV.364527.Sherpa_222_NNPDF30NNLO_munugamma_pty_15_35.deriv.DAOD_HIGG8D1.e5928_e5984_s3126_r10201_r10210_p4133
 mc16_13TeV.364528.Sherpa_222_NNPDF30NNLO_munugamma_pty_35_70.deriv.DAOD_HIGG8D1.e5928_e5984_s3126_r10201_r10210_p4133
 mc16_13TeV.364529.Sherpa_222_NNPDF30NNLO_munugamma_pty_70_140.deriv.DAOD_HIGG8D1.e5928_e5984_s3126_r10201_r10210_p4133
 mc16_13TeV.364531.Sherpa_222_NNPDF30NNLO_taunugamma_pty_7_15.deriv.DAOD_HIGG8D1.e5928_e5984_s3126_r10201_r10210_p4133
 mc16_13TeV.364532.Sherpa_222_NNPDF30NNLO_taunugamma_pty_15_35.deriv.DAOD_HIGG8D1.e5928_e5984_s3126_r10201_r10210_p4133
 mc16_13TeV.364533.Sherpa_222_NNPDF30NNLO_taunugamma_pty_35_70.deriv.DAOD_HIGG8D1.e5928_e5984_s3126_r10201_r10210_p4133
 mc16_13TeV.364534.Sherpa_222_NNPDF30NNLO_taunugamma_pty_70_140.deriv.DAOD_HIGG8D1.e5928_e5984_s3126_r10201_r10210_p4133
 mc16_13TeV.364535.Sherpa_222_NNPDF30NNLO_taunugamma_pty_140_E_CMS.deriv.DAOD_HIGG8D1.e5928_e5984_s3126_r10201_r10210_p4133
 mc16_13TeV.410560.MadGraphPythia8EvtGen_A14_tZ_4fl_tchan_noAllHad.deriv.DAOD_HIGG8D1.e5803_e5984_s3126_r10201_r10210_p4133
 mc16_13TeV.410013.PowhegPythiaEvtGen_P2012_Wt_inclusive_top.deriv.DAOD_HIGG8D1.e3753_s3126_r10201_r10210_p4133
 mc16_13TeV.410014.PowhegPythiaEvtGen_P2012_Wt_inclusive_antitop.deriv.DAOD_HIGG8D1.e3753_s3126_r10201_r10210_p4133
 mc16_13TeV.410408.aMcAtNloPythia8EvtGen_tWZ_Tzoll_minDR1.deriv.DAOD_HIGG8D1.e6423_e5984_s3126_r10201_r10210_p4133
 mc16_13TeV.364242.Sherpa_222_NNPDF30NNLO_WWW_313v_EW6.deriv.DAOD_HIGG8D1.e5887_e5984_s3126_r10201_r10210_p4133
 mc16_13TeV.364243.Sherpa_222_NNPDF30NNLO_WWZ_412v_EW6.deriv.DAOD_HIGG8D1.e5887_e5984_s3126_r10201_r10210_p4133
 mc16_13TeV.364244.Sherpa_222_NNPDF30NNLO_WWZ_214v_EW6.deriv.DAOD_HIGG8D1.e5887_e5984_s3126_r10201_r10210_p4133
 mc16_13TeV.364245.Sherpa_222_NNPDF30NNLO_WZZ_511v_EW6.deriv.DAOD_HIGG8D1.e5887_e5984_s3126_r10201_r10210_p4133
 mc16_13TeV.364246.Sherpa_222_NNPDF30NNLO_WZZ_313v_EW6.deriv.DAOD_HIGG8D1.e5887_e5984_s3126_r10201_r10210_p4133
 mc16_13TeV.364247.Sherpa_222_NNPDF30NNLO_ZZZ_610v_EW6.deriv.DAOD_HIGG8D1.e5887_e5984_s3126_r10201_r10210_p4133
 mc16_13TeV.364248.Sherpa_222_NNPDF30NNLO_ZZZ_412v_EW6.deriv.DAOD_HIGG8D1.e5887_e5984_s3126_r10201_r10210_p4133
 mc16_13TeV.364249.Sherpa_222_NNPDF30NNLO_ZZZ_214v_EW6.deriv.DAOD_HIGG8D1.e5887_e5984_s3126_r10201_r10210_p4133
 mc16_13TeV.342284.Pythia8EvtGen_A14NNPDF23LO_WH125_inc.deriv.DAOD_HIGG8D1.e4246_e5984_s3126_r10201_r10210_p4133
 mc16_13TeV.342285.Pythia8EvtGen_A14NNPDF23LO_ZH125_inc.deriv.DAOD_HIGG8D1.e4246_e5984_s3126_r10201_r10210_p4133
 mc16_13TeV.341998.aMcAtNloHppEG_UEEE5_CTEQ6L1_CT10ME_tWH125_gamgam_yt_plus1.deriv.DAOD_HIGG8D1.e4394_e5984_s3126_r10201_r10210_p4133

mc16_13TeV.410470.PhPy8EG_A14_ttbar_hdamp258p75_nonallhad.deriv.DAOD_HIGG8D1.e6337_e5984_s3126_r10201_r10210_p4133
mc16_13TeV.410472.PhPy8EG_A14_ttbar_hdamp258p75_dil.deriv.DAOD_HIGG8D1.e6348_e5984_s3126_r10201_r10210_p4133
mc16_13TeV.346343.PhPy8EG_A14NNPDF23_NNPDF30ME_ttH125_allhad.deriv.DAOD_HIGG8D1.e7148_e5984_s3126_r10201_r10210_p4133
mc16_13TeV.346344.PhPy8EG_A14NNPDF23_NNPDF30ME_ttH125_semilep.deriv.DAOD_HIGG8D1.e7148_e5984_a875_r10201_r10210_p4133
mc16_13TeV.346345.PhPy8EG_A14NNPDF23_NNPDF30ME_ttH125_dilep.deriv.DAOD_HIGG8D1.e7148_e5984_a875_r10201_r10210_p4133

mc16e:
mc16_13TeV.361605.PowhegPy8EG_CT10nloME_AZNLOCTEQ6L1_ZZvvvv_mll4.deriv.DAOD_HIGG8D1.e4054_e5984_s3126_r10724_r10726_p4133
mc16_13TeV.361602.PowhegPy8EG_CT10nloME_AZNLOCTEQ6L1_WZlvvv_mll4.deriv.DAOD_HIGG8D1.e4054_e5984_s3126_r10724_r10726_p4133
mc16_13TeV.361601.PowhegPy8EG_CT10nloME_AZNLOCTEQ6L1_WZlvl_mll4.deriv.DAOD_HIGG8D1.e4475_e5984_s3126_r10724_r10726_p4133
mc16_13TeV.361600.PowhegPy8EG_CT10nloME_AZNLOCTEQ6L1_WWlqlv.deriv.DAOD_HIGG8D1.e4616_e5984_s3126_r10724_r10726_p4133
mc16_13TeV.361603.PowhegPy8EG_CT10nloME_AZNLOCTEQ6L1_ZZlIII_mll4.deriv.DAOD_HIGG8D1.e4475_e5984_s3126_r10724_r10726_p4133
mc16_13TeV.361604.PowhegPy8EG_CT10nloME_AZNLOCTEQ6L1_ZZvvll_mll4.deriv.DAOD_HIGG8D1.e4475_e5984_s3126_r10724_r10726_p4133
mc16_13TeV.364288.Sherpa_222_NNPDF30NNLO_llll_lowMllPtComplement.deriv.DAOD_HIGG8D1.e6096_s3126_r10724_p3983 mc16_13TeV.364287.Sherpa_222_NNPDF30NNLO_llvv_llvvjj_EW6.deriv.DAOD_HIGG8D1.e6055_e5984_s3126_r10724_r10726_p3983
mc16_13TeV.364285.Sherpa_222_NNPDF30NNLO_llvvjj_EW6.deriv.DAOD_HIGG8D1.e6055_s3126_r10724_r10726_p3983
mc16_13TeV.364284.Sherpa_222_NNPDF30NNLO_llvvjj_EW6.deriv.DAOD_HIGG8D1.e6055_s3126_r10724_p3983
mc16_13TeV.364283.Sherpa_222_NNPDF30NNLO_lllljj_EW6.deriv.DAOD_HIGG8D1.e6055_s3126_r10724_p3983
mc16_13TeV.364739.MGPy8EG_NNPDF30NLO_A14NNPDF23LO_lvlljjEW6_OFMinus.deriv.DAOD_HIGG8D1.e7421_e5984_s3126_r10724_r10726_p4133
mc16_13TeV.364742.MGPy8EG_NNPDF30NLO_A14NNPDF23LO_lvlljjEW6_SFPlus.deriv.DAOD_HIGG8D1.e7421_e5984_s3126_r10724_r10726_p4133
mc16_13TeV.364740.MGPy8EG_NNPDF30NLO_A14NNPDF23LO_lvlljjEW6_OFPlus.deriv.DAOD_HIGG8D1.e7421_e5984_s3126_r10724_r10726_p4133
mc16_13TeV.364741.MGPy8EG_NNPDF30NLO_A14NNPDF23LO_lvlljjEW6_SFMinus.deriv.DAOD_HIGG8D1.e7421_e5984_s3126_r10724_r10726_p4133
mc16_13TeV.364253.Sherpa_222_NNPDF30NNLO_llll.deriv.DAOD_HIGG8D1.e5916_e5984_s3126_r10724_r10726_p4133
mc16_13TeV.364250.Sherpa_222_NNPDF30NNLO_llll.deriv.DAOD_HIGG8D1.e5984_s3126_r10724_r10726_p4133
mc16_13TeV.364254.Sherpa_222_NNPDF30NNLO_llvv.deriv.DAOD_HIGG8D1.e5916_e5984_s3126_r10724_r10726_p4133
mc16_13TeV.364255.Sherpa_222_NNPDF30NNLO_lvvv.deriv.DAOD_HIGG8D1.e5916_e5984_s3126_r10724_r10726_p4133
mc16_13TeV.410155.aMcAtNloPythia8EvtGen_MEN30NLO_A14N23LO_ttW.deriv.DAOD_HIGG8D1.e5070_e5984_s3126_r10724_r10726_p4133
mc16_13TeV.410156.aMcAtNloPythia8EvtGen_MEN30NLO_A14N23LO_ttZnunu.deriv.DAOD_HIGG8D1.e5070_e5984_s3126_r10724_r10726_p4133
mc16_13TeV.410157.aMcAtNloPythia8EvtGen_MEN30NLO_A14N23LO_ttZqq.deriv.DAOD_HIGG8D1.e5070_e5984_s3126_r10724_r10726_p4133
mc16_13TeV.410218.aMcAtNloPythia8EvtGen_MEN30NLO_A14N23LO_ttee.deriv.DAOD_HIGG8D1.e5070_e5984_s3126_r10724_r10726_p4133
mc16_13TeV.410219.aMcAtNloPythia8EvtGen_MEN30NLO_A14N23LO_ttmumu.deriv.DAOD_HIGG8D1.e5070_e5984_s3126_r10724_r10726_p4133
mc16_13TeV.410220.aMcAtNloPythia8EvtGen_MEN30NLO_A14N23LO_ttautau.deriv.DAOD_HIGG8D1.e5070_e5984_s3126_r10724_r10726_p4133
mc16_13TeV.410276.aMcAtNloPythia8EvtGen_MEN30NLO_A14N23LO_ttee_mll_1_5.deriv.DAOD_HIGG8D1.e6087_e5984_s3126_r10724_r10726_p4133
mc16_13TeV.410277.aMcAtNloPythia8EvtGen_MEN30NLO_A14N23LO_ttmumu_mll_1_5.deriv.DAOD_HIGG8D1.e6087_e5984_s3126_r10724_r10726_p4133
mc16_13TeV.410278.aMcAtNloPythia8EvtGen_MEN30NLO_A14N23LO_ttautau_mll_1_5.deriv.DAOD_HIGG8D1.e6087_e5984_s3126_r10724_r10726_p4133
mc16_13TeV.410397.MadGraphPythia8EvtGen_ttbar_wbee_MEN30LO_A14N23LO.deriv.DAOD_HIGG8D1.e6086_e5984_s3126_r10724_r10726_p4133
mc16_13TeV.410398.MadGraphPythia8EvtGen_ttbar_wbmumu_MEN30LO_A14N23LO.deriv.DAOD_HIGG8D1.e6086_e5984_s3126_r10724_r10726_p4133
mc16_13TeV.410399.MadGraphPythia8EvtGen_ttbar_wbtautau_MEN30LO_A14N23LO.deriv.DAOD_HIGG8D1.e6086_e5984_s3126_r10724_r10726_p4133
mc16_13TeV.410658.PhPy8EG_A14_tchan_BW50_lept_top.deriv.DAOD_HIGG8D1.e6671_e5984_s3126_s3136_r10724_r10726_p4133
mc16_13TeV.410659.PhPy8EG_A14_tchan_BW50_lept_antitop.deriv.DAOD_HIGG8D1.e6671_e5984_s3126_s3136_r10724_r10726_p4133
mc16_13TeV.410644.PowhegPythia8EvtGen_A14_singletop_schan_lept_top.deriv.DAOD_HIGG8D1.e6527_e5984_s3126_r10724_r10726_p4133
mc16_13TeV.410645.PowhegPythia8EvtGen_A14_singletop_schan_lept_antitop.deriv.DAOD_HIGG8D1.e6527_e5984_s3126_r10724_r10726_p4133
mc16_13TeV.412063.aMcAtNloPythia8EvtGen_tllq_NNPDF30_nf4_A14.deriv.DAOD_TOPQ1.e7054_e5984_s3126_r10724_r10726_p4174
mc16_13TeV.304014.MadGraphPythia8EvtGen_A14NNPDF23_3top_SM.deriv.DAOD_HIGG8D1.e4324_e5984_s3126_r10724_r10726_p4133
mc16_13TeV.410080.MadGraphPythia8EvtGen_A14NNPDF23_4topSM.deriv.DAOD_HIGG8D1.e4111_e5984_s3126_r10724_r10726_p4133
mc16_13TeV.410081.MadGraphPythia8EvtGen_A14NNPDF23_ttbarWW.deriv.DAOD_HIGG8D1.e4111_e5984_s3126_r10724_r10726_p4133
mc16_13TeV.364100.Sherpa_221_NNPDF30NNLO_Zmumu_MAXHTPTV0_70_CVetoBVeto.deriv.DAOD_HIGG8D1.e5271_e5984_s3126_s3136_r10724_r10726_p4133
mc16_13TeV.364100.Sherpa_221_NNPDF30NNLO_Zmumu_MAXHTPTV0_70_CVetoBVeto.deriv.DAOD_HIGG8D1.e5271_e5984_s3126_r10724_r10726_p4133
mc16_13TeV.364101.Sherpa_221_NNPDF30NNLO_Zmumu_MAXHTPTV0_70_CFilterBVeto.deriv.DAOD_HIGG8D1.e5271_e5984_s3126_r10724_r10726_p4133
mc16_13TeV.364102.Sherpa_221_NNPDF30NNLO_Zmumu_MAXHTPTV0_70_BFilter.deriv.DAOD_HIGG8D1.e5271_e5984_s3126_s3136_r10724_r10726_p4133
mc16_13TeV.364102.Sherpa_221_NNPDF30NNLO_Zmumu_MAXHTPTV0_70_BFilter.deriv.DAOD_HIGG8D1.e5271_e5984_s3126_r10724_r10726_p4133
mc16_13TeV.364103.Sherpa_221_NNPDF30NNLO_Zmumu_MAXHTPTV70_140_CVetoBVeto.deriv.DAOD_HIGG8D1.e5271_e5984_s3126_r10724_r10726_p4133
mc16_13TeV.364103.Sherpa_221_NNPDF30NNLO_Zmumu_MAXHTPTV70_140_CVetoBVeto.deriv.DAOD_HIGG8D1.e5271_e5984_s3126_s3136_r10724_r10726_p4133
mc16_13TeV.364104.Sherpa_221_NNPDF30NNLO_Zmumu_MAXHTPTV70_140_CFilterBVeto.deriv.DAOD_HIGG8D1.e5271_e5984_s3126_r10724_r10726_p4133
mc16_13TeV.364104.Sherpa_221_NNPDF30NNLO_Zmumu_MAXHTPTV70_140_CFilterBVeto.deriv.DAOD_HIGG8D1.e5271_e5984_s3126_r10724_r10726_p4133
mc16_13TeV.364106.Sherpa_221_NNPDF30NNLO_Zmumu_MAXHTPTV140_280_CVetoBVeto.deriv.DAOD_HIGG8D1.e5271_e5984_s3126_s3136_r10724_r10726_p4133
mc16_13TeV.364106.Sherpa_221_NNPDF30NNLO_Zmumu_MAXHTPTV140_280_CVetoBVeto.deriv.DAOD_HIGG8D1.e5271_e5984_s3126_r10724_r10726_p4133
mc16_13TeV.364107.Sherpa_221_NNPDF30NNLO_Zmumu_MAXHTPTV140_280_CFilterBVeto.deriv.DAOD_HIGG8D1.e5271_e5984_s3126_r10724_r10726_p4133
mc16_13TeV.364107.Sherpa_221_NNPDF30NNLO_Zmumu_MAXHTPTV140_280_CFilterBVeto.deriv.DAOD_HIGG8D1.e5271_e5984_s3126_s3136_r10724_r10726_p4133
mc16_13TeV.364108.Sherpa_221_NNPDF30NNLO_Zmumu_MAXHTPTV140_280_BFilter.deriv.DAOD_HIGG8D1.e5271_e5984_s3126_r10724_r10726_p4133
mc16_13TeV.364109.Sherpa_221_NNPDF30NNLO_Zmumu_MAXHTPTV280_500_CVetoBVeto.deriv.DAOD_HIGG8D1.e5271_e5984_s3126_r10724_r10726_p4133
mc16_13TeV.364110.Sherpa_221_NNPDF30NNLO_Zmumu_MAXHTPTV280_500_CFilterBVeto.deriv.DAOD_HIGG8D1.e5271_e5984_s3126_r10724_r10726_p4133
mc16_13TeV.364110.Sherpa_221_NNPDF30NNLO_Zmumu_MAXHTPTV280_500_CFilterBVeto.deriv.DAOD_HIGG8D1.e5271_e5984_s3126_r10724_r10726_p4133

mc16_13TeV.364193.Sherpa_221_NNPDF30NNLO_Wtaunu_MAXHTPTV280_500_CVetoBVeto.deriv.DAOD_HIGG8D1.e5340_e5984_s3126_r10724_r10726_p4133
 mc16_13TeV.364193.Sherpa_221_NNPDF30NNLO_Wtaunu_MAXHTPTV280_500_CVetoBVeto.deriv.DAOD_HIGG8D1.e5340_e5984_s3126_s3136_r10724_r10726_p4133
 mc16_13TeV.364194.Sherpa_221_NNPDF30NNLO_Wtaunu_MAXHTPTV280_500_CFilterBVeto.deriv.DAOD_HIGG8D1.e5340_e5984_s3126_s3136_r10724_r10726_p4133
 mc16_13TeV.364194.Sherpa_221_NNPDF30NNLO_Wtaunu_MAXHTPTV280_500_CFilterBVeto.deriv.DAOD_HIGG8D1.e5340_e5984_s3126_r10724_r10726_p4133
 mc16_13TeV.364195.Sherpa_221_NNPDF30NNLO_Wtaunu_MAXHTPTV280_500_BFilter.deriv.DAOD_HIGG8D1.e5340_e5984_s3126_s3136_r10724_r10726_p4133
 mc16_13TeV.364195.Sherpa_221_NNPDF30NNLO_Wtaunu_MAXHTPTV280_500_BFilter.deriv.DAOD_HIGG8D1.e5340_e5984_s3126_r10724_r10726_p4133
 mc16_13TeV.364196.Sherpa_221_NNPDF30NNLO_Wtaunu_MAXHTPTV500_1000.deriv.DAOD_HIGG8D1.e5340_e5984_s3126_s3136_r10724_r10726_p4133
 mc16_13TeV.364196.Sherpa_221_NNPDF30NNLO_Wtaunu_MAXHTPTV500_1000.deriv.DAOD_HIGG8D1.e5340_e5984_s3126_r10724_r10726_p4133
 mc16_13TeV.364197.Sherpa_221_NNPDF30NNLO_Wtaunu_MAXHTPTV1000_E_CMS.deriv.DAOD_HIGG8D1.e5340_e5984_s3126_s3136_r10724_r10726_p4133
 mc16_13TeV.364197.Sherpa_221_NNPDF30NNLO_Wtaunu_MAXHTPTV1000_E_CMS.deriv.DAOD_HIGG8D1.e5340_e5984_s3126_r10724_r10726_p4133
 mc16_13TeV.364500.Sherpa_222_NNPDF30NNLO_eegamma_pty_7_15.deriv.DAOD_HIGG8D1.e5928_e5984_s3126_r10724_r10726_p4133
 mc16_13TeV.364501.Sherpa_222_NNPDF30NNLO_eegamma_pty_15_35.deriv.DAOD_HIGG8D1.e5928_e5984_s3126_r10724_r10726_p4133
 mc16_13TeV.364502.Sherpa_222_NNPDF30NNLO_eegamma_pty_35_70.deriv.DAOD_HIGG8D1.e5928_e5984_s3126_r10724_r10726_p4133
 mc16_13TeV.364503.Sherpa_222_NNPDF30NNLO_eegamma_pty_70_140.deriv.DAOD_HIGG8D1.e5928_e5984_s3126_r10724_r10726_p4133
 mc16_13TeV.364504.Sherpa_222_NNPDF30NNLO_eegamma_pty_140_E_CMS.deriv.DAOD_HIGG8D1.e5928_e5984_s3126_r10724_r10726_p4133
 mc16_13TeV.364505.Sherpa_222_NNPDF30NNLO_mumugamma_pty_7_15.deriv.DAOD_HIGG8D1.e5928_e5984_s3126_r10724_r10726_p4133
 mc16_13TeV.364506.Sherpa_222_NNPDF30NNLO_mumugamma_pty_15_35.deriv.DAOD_HIGG8D1.e5928_e5984_s3126_r10724_r10726_p4133
 mc16_13TeV.364507.Sherpa_222_NNPDF30NNLO_mumugamma_pty_35_70.deriv.DAOD_HIGG8D1.e5928_e5984_s3126_r10724_r10726_p4133
 mc16_13TeV.364508.Sherpa_222_NNPDF30NNLO_mumugamma_pty_70_140.deriv.DAOD_HIGG8D1.e5928_e5984_s3126_r10724_r10726_p4133
 mc16_13TeV.364509.Sherpa_222_NNPDF30NNLO_mumugamma_pty_140_E_CMS.deriv.DAOD_HIGG8D1.e5928_e5984_s3126_r10724_r10726_p4133
 mc16_13TeV.364511.Sherpa_222_NNPDF30NNLO_tautaugamma_pty_15_35.deriv.DAOD_HIGG8D1.e5928_e5984_s3126_r10724_r10726_p4133
 mc16_13TeV.364512.Sherpa_222_NNPDF30NNLO_tautaugamma_pty_35_70.deriv.DAOD_HIGG8D1.e5928_e5984_s3126_r10724_r10726_p4133
 mc16_13TeV.364513.Sherpa_222_NNPDF30NNLO_tautaugamma_pty_70_140.deriv.DAOD_HIGG8D1.e5928_e5984_s3126_r10724_r10726_p4133
 mc16_13TeV.364514.Sherpa_222_NNPDF30NNLO_tautaugamma_pty_140_E_CMS.deriv.DAOD_HIGG8D1.e5928_e5984_s3126_r10724_r10726_p4133
 mc16_13TeV.364522.Sherpa_222_NNPDF30NNLO_enugamma_pty_15_35.deriv.DAOD_HIGG8D1.e5928_e5984_s3126_r10724_r10726_p4133
 mc16_13TeV.364523.Sherpa_222_NNPDF30NNLO_enugamma_pty_35_70.deriv.DAOD_HIGG8D1.e5928_e5984_s3126_r10724_r10726_p4133
 mc16_13TeV.364524.Sherpa_222_NNPDF30NNLO_enugamma_pty_70_140.deriv.DAOD_HIGG8D1.e5928_e5984_s3126_r10724_r10726_p4133
 mc16_13TeV.364525.Sherpa_222_NNPDF30NNLO_enugamma_pty_140_E_CMS.deriv.DAOD_HIGG8D1.e5928_e5984_s3126_r10724_r10726_p4133
 mc16_13TeV.364527.Sherpa_222_NNPDF30NNLO_munugamma_pty_15_35.deriv.DAOD_HIGG8D1.e5928_e5984_s3126_r10724_r10726_p4133
 mc16_13TeV.364529.Sherpa_222_NNPDF30NNLO_munugamma_pty_70_140.deriv.DAOD_HIGG8D1.e5928_e5984_s3126_r10724_r10726_p4133
 mc16_13TeV.364530.Sherpa_222_NNPDF30NNLO_munugamma_pty_140_E_CMS.deriv.DAOD_HIGG8D1.e5928_e5984_s3126_r10724_r10726_p4133
 mc16_13TeV.364532.Sherpa_222_NNPDF30NNLO_taunugamma_pty_15_35.deriv.DAOD_HIGG8D1.e5928_e5984_s3126_r10724_r10726_p4133
 mc16_13TeV.364533.Sherpa_222_NNPDF30NNLO_taunugamma_pty_35_70.deriv.DAOD_HIGG8D1.e5928_e5984_s3126_r10724_r10726_p4133
 mc16_13TeV.364534.Sherpa_222_NNPDF30NNLO_taunugamma_pty_70_140.deriv.DAOD_HIGG8D1.e5928_e5984_s3126_r10724_r10726_p4133
 mc16_13TeV.364535.Sherpa_222_NNPDF30NNLO_taunugamma_pty_140_E_CMS.deriv.DAOD_HIGG8D1.e5928_e5984_s3126_r10724_r10726_p4133
 mc16_13TeV.410560.MadGraphPythia8EvtGen_A14_IZ_4fl_tchan_noAllHad.deriv.DAOD_HIGG8D1.e5803_e5984_s3126_r10724_r10726_p4133
 mc16_13TeV.410408.aMcAtNloPythia8EvtGen_tWZ_Ztoll_minDR1.deriv.DAOD_HIGG8D1.e6423_e5984_s3126_r10724_r10726_p4133
 mc16_13TeV.364242.Sherpa_222_NNPDF30NNLO_WWW_313v_EW6.deriv.DAOD_HIGG8D1.e5887_e5984_s3126_r10724_r10726_p4133
 mc16_13TeV.364243.Sherpa_222_NNPDF30NNLO_WWZ_412v_EW6.deriv.DAOD_HIGG8D1.e5887_e5984_s3126_r10724_r10726_p4133
 mc16_13TeV.364244.Sherpa_222_NNPDF30NNLO_WWZ_214v_EW6.deriv.DAOD_HIGG8D1.e5887_e5984_s3126_r10724_r10726_p4133
 mc16_13TeV.364245.Sherpa_222_NNPDF30NNLO_WZZ_511v_EW6.deriv.DAOD_HIGG8D1.e5887_e5984_s3126_r10724_r10726_p4133
 mc16_13TeV.364246.Sherpa_222_NNPDF30NNLO_WZZ_313v_EW6.deriv.DAOD_HIGG8D1.e5887_e5984_s3126_r10724_r10726_p4133
 mc16_13TeV.364247.Sherpa_222_NNPDF30NNLO_ZZZ_610v_EW6.deriv.DAOD_HIGG8D1.e5887_e5984_s3126_r10724_r10726_p4133
 mc16_13TeV.364248.Sherpa_222_NNPDF30NNLO_ZZZ_412v_EW6.deriv.DAOD_HIGG8D1.e5887_e5984_s3126_r10724_r10726_p4133
 mc16_13TeV.364249.Sherpa_222_NNPDF30NNLO_ZZZ_214v_EW6.deriv.DAOD_HIGG8D1.e5887_e5984_s3126_r10724_r10726_p4133
 mc16_13TeV.342284.Pythia8EvtGen_A14NNPDF23LO_WH125_inc.deriv.DAOD_HIGG8D1.e4246_e5984_s3126_r10724_r10726_p4133
 mc16_13TeV.342285.Pythia8EvtGen_A14NNPDF23LO_ZH125_inc.deriv.DAOD_HIGG8D1.e4246_e5984_s3126_r10724_r10726_p4133
 mc16_13TeV.341998.aMcAtNloHppEG_UEEE5_CTEQ6L1_CT10ME_tWH125_gamgam_yt_plus1.deriv.DAOD_HIGG8D1.e4394_e5984_s3126_r10724_r10726_p4133
 mc16_13TeV.410389.MadGraphPythia8EvtGen_A14NNPDF23_ttgamma_nonallhadronic.deriv.DAOD_HIGG8D1.e6155_e5984_s3126_r10724_r10726_p4133
 mc16_13TeV.410470.PhPy8EG_A14_tbbar_hdamp258p75_nonallhad.deriv.DAOD_HIGG8D1.e6337_e5984_s3126_r10724_r10726_p4133
 mc16_13TeV.410472.PhPy8EG_A14_tbbar_hdamp258p75_dil.deriv.DAOD_HIGG8D1.e6348_e5984_s3126_r10724_r10726_p4133
 mc16_13TeV.346343.PhPy8EG_A14NNPDF23_NNPDF30ME_ttH125_allhad.deriv.DAOD_HIGG8D1.e7148_e5984_s3126_r10724_r10726_p4133
 mc16_13TeV.346343.PhPy8EG_A14NNPDF23_NNPDF30ME_ttH125_allhad.deriv.DAOD_HIGG8D1.e7148_e5984_a875_r10724_r10726_p4133
 mc16_13TeV.346344.PhPy8EG_A14NNPDF23_NNPDF30ME_ttH125_semilep.deriv.DAOD_HIGG8D1.e7148_e5984_a875_r10724_r10726_p4133
 mc16_13TeV.346344.PhPy8EG_A14NNPDF23_NNPDF30ME_ttH125_semilep.deriv.DAOD_HIGG8D1.e7148_e5984_s3126_r10724_r10726_p4133
 mc16_13TeV.346345.PhPy8EG_A14NNPDF23_NNPDF30ME_ttH125_dilep.deriv.DAOD_HIGG8D1.e7148_e5984_a875_r10724_r10726_p4133
 mc16_13TeV.346345.PhPy8EG_A14NNPDF23_NNPDF30ME_ttH125_dilep.deriv.DAOD_HIGG8D1.e7148_e5984_s3126_r10724_r10726_p4133